

DESIGN AND EXPERIMENTAL EVALUATION OF
AN ENERGY HARVESTING SYSTEM TO POWER THE CONTROL SYSTEM OF LOWER
LIMB PROSTHESES



JURRIËN SMITS



DELFT UNIVERSITY OF TECHNOLOGY

MASTER THESIS

**Design and experimental evaluation of
an energy harvesting system to power the
control system of lower limb prostheses**

Jurriën Smits (4583590)

to obtain the degree of Master of Science at the Delft University of Technology,
to be defended publicly on February 29th, 2024.

Project duration: June 1, 2023 - February 29, 2024

Thesis committee:

Ir. B. van der Windt, supervisor, TU Delft

Dr. Ir. G. Smit, Chair, supervisor, TU Delft

Dr. Ir. A. Stienen, TU Delft

MECHANICAL, MARITIME AND MATERIALS ENGINEERING (3ME)
DEPARTMENT OF BIOMECHANICAL DESIGN

PREFACE

This thesis is the result of work in the time period between June 2023 and March 2024. This period has been a somewhat challenging journey for me, as during the bulk of the time period I was recovering from a serious concussion. Where after months of just sitting at home and not being able to do any study related work, I could finally start my thesis and gradually build up the workload. Saying that I found pleasure in doing study work again is an understatement, as I really enjoyed being able to be productive again and work on such an interesting topic. For that opportunity I am grateful and would like to express my sincere gratitude towards Gerwin Smit and Bob van der Windt. They not only guided me through this process, but also followed my recovery and checked up regularly. This made it easier for me to take a step back now and then when necessary or step on the gas pedal. Finding back the pleasure and motivation in study work is also due to them. I have learned a lot, not only concerning this topic but about myself as well. Where I'd say my personality is quite diligent, eager to learn and get things done, I had to learn to take a step back now and then and not overdo it to focus on my health. I can say that I am very pleased and proud with the result of my thesis.

I have gained a lot of knowledge during this period and found great satisfaction in collaborating with everyone in the lab. I would also like to express my gratitude towards Jacques Brenkman from the measurement shop, who not only patiently addressed all my questions regarding circuit design but also provided guidance in steering me toward the successful creation of a vibration shaker table.

*Jurriën Smits
February 2024*

ABSTRACT

Energy harvesting has gained lots of interest over the past few decades. This study explores the application of energy harvesting in lower limb prosthetic devices. The control system of a lower limb prosthesis includes sensors, wireless systems and other active components which all require battery power. In order to save some of this battery power, reduce weight, and have the devices have a longer runtime, a form of energy regeneration is desired. Therefore the goal of this study is to design and experimentally evaluate an energy harvesting system to power the control system of lower limb prostheses. The final prototype is designed following the process of setting up functional requirements, constraints and wishes. This leads to three derived concepts. After an evaluation against performance criteria and an in-depth evaluation concerning the power output, the compliant spring design is chosen to be worked out further and evaluated with a newly designed vibration shaker table. The relevant findings are laid out in the results. From these findings, interpretations and implications are discussed further, concerning advantages and limitations of the energy harvesters and the experiment. Results from the conducted experiment show a peak power output of 25.8 mW at an input amplitude of 12 mm and a frequency of 9 Hz. A power mass ratio of 0.21 W/kg is achieved. The design meets the power demand requirements to power microprocessors and sensors of the control system of a lower limb prosthesis and extends runtime with 15.7%. However it is still important to investigate the power requirements for state of the art lower limb prostheses. Furthermore, it is recommended to improve overall efficiency in future studies, compare the results with state of the art energy harvesters based on vibrations, and execute a gait test for further design validation. The results from this study demonstrate comparable data and present the innovations possible in prosthesis design and the advancements in utilizing ambient power sources for energy harvesting. Enhancing the overall efficiency of this design, and promoting comparable results to other designs in the existing literature, could emphasize on the potential of energy harvesting applications.

Index terms - Lower limb prosthesis; Prosthetic device; Energy harvesting; Vibration energy; Human gait energy harvesting; Biomechanical energy harvesting.

CONTENTS

1	Introduction	5
1.1	Background	5
1.2	State of the art and problem analysis	6
1.3	Goal	6
1.4	Paper structure	7
2	Design method	7
2.1	Design requirements and strategy	7
2.2	Concept solutions	8
2.2.1	Concept 1 - The levitated magnet	8
2.2.2	Concept 2 - The rack and pinion	8
2.2.3	Concept 3 - The compliant spring	9
2.3	Concept selection	10
2.3.1	Concept assessment	10
2.3.2	Preliminary power calculations	11
2.3.3	Prototypes	11
2.3.4	Preliminary power output results and discussion	12
3	Evaluation method	15
3.1	Evaluation strategy	15
3.2	Test bench design	15
3.3	Evaluation protocol and preliminary discussion	16
3.4	Data processing and evaluation	17
4	Design results	19
4.1	Final design	19
4.2	Electrical design	20
5	Evaluation results	21
5.1	Overview	21
5.2	Output results	22
5.2.1	Clutch dynamics	22
5.3	Input results	24
5.4	State of the art comparison	25
6	Discussion	26
6.1	Design advantages and limitations	26
6.1.1	Design characteristics and integration	26
6.1.2	Clutch dynamics and energy impulses	26
6.1.3	Power supply and demand	26
6.1.4	Rectifying circuit	27
6.1.5	Durability	27
6.1.6	Efficiency	28
6.2	Prosthesis battery comparison	28
6.3	3D-printer materials	28
6.3.1	Form flexible 80A	28
6.3.2	Form elastic 50A	28
6.3.3	TPU	29
6.4	Recommendations	29
6.4.1	Gait test	29
6.4.2	Efficiency	29
6.5	Limitations	29
6.5.1	State of the art data	29
6.5.2	Force sensor sampling	29
6.6	Other applications	29
7	Conclusion	30
	References	31

	4
Appendix A: Design strategy	33
A.1 Concept generation	33
A.1.1 Determine energy source	33
A.1.2 Convert energy into electricity	34
A.1.3 Convert linear movement	34
A.1.4 Amplify vibrational input	34
A.1.5 Store electricity	34
A.1.6 Assign position	35
A.2 Performance criteria	35
A.3 Concept selection - detailed explanation	35
A.3.1 Weight	35
A.3.2 Size	36
A.3.3 Potential power output	36
A.3.4 Feasibility	36
A.3.5 Interoperability	36
A.4 Prototyping - detailed explanation	37
A.4.1 The levitated magnet prototype	37
A.4.2 The compliant spring prototype	38
A.5 The compliant spring - final design	38
A.5.1 Compliant component material	38
A.5.2 Clutch mechanism	39
A.6 Circuit design - detailed explanation	39
Appendix B: Calculation description	41
B.1 EMF and power calculations	41
Appendix C: Additional prototype results	43
C.1 Prototype oscilloscope recordings - full results	43
Appendix D: Additional evaluation results	44
D.1 Experiment results overview	44
Appendix E: Extended discussion	46
E.1 Power demand	46
E.2 Rectifying circuit - extended discussion	46
Appendix F: Component worksheets	48
Appendix G: Matlab scripts	60
G.1 Concept 1 - the levitated magnet emf and power output calculations	60
G.2 Concept 2 - the rack and pinion emf and power output calculations	61
G.3 Concept 3 - the compliant spring emf and power output calculations	62
Appendix H: Arduino sketch	65
H.1 Nema 23 stepper motor control sketch	65
H.2 Durability test sketch	65
Appendix I: Literature review	67

1 INTRODUCTION

1.1 Background

When someone loses a limb, they require a prosthesis that substitutes the absent body part. This can be either an upper or lower body limb. Prosthetic devices are part of the science of integrating human body parts with mechanical parts to facilitate this loss in motor control. These 'mechanical limbs' are needed for not only facilitating this loss in motor control, but to present options for people with illness, casualties or inborn deformities [1]. Throughout the last decades there has been an explosion in options for people who are born with or have come across limb deficiencies [1]. These can either assist (exoskeletons) or replace a limb (prostheses). Utilizing a prosthesis to replace a limb not only affects motor control but also influences the communication between the brain and muscles.

The human body contains a complex neural network [2]. Brain and muscles communicate constantly to control limb movement. From the brain information travels through the spinal cord to the leg muscles and back [2]. This is an automated function. In addition, the human body is equipped with numerous sensors which provide feedback about the progression of the movement and the success of taking a step during normal walking motion [2]. Muscle activity and nerve stimulation are continuously interacting and so this information is fed back to the brain [2]. This occurs many times each second.

When someone loses a limb, that specific person also loses the neural network from the brain towards this specific limb. So replacing a lower limb with a mechanical or a robotic limb is not just facilitating the user with a missing limb, but also replacing these sensors and filling in the gap of information exchange between brain and muscles. Since many of these sensors, muscles and neural networks are missing after an amputation. When designing a leg prosthesis it is important to take this into account to approximate the human gait as close as possible. Modern prosthetic devices therefore contain microprocessing units and sensors to replace this loss of information exchange [3]. This does however also require a battery to power the control system.

The C-leg (Ottobock) and the Rheo knee (Össur) [4] [5] are two examples of state-of-the-art leg prostheses. Both these systems contain microprocessors which actively monitor data fed by sensors in the knee. Based on this data the hydraulics in these prosthetic devices are controlled in real-time [4] [5]. The sensors provide information to the microprocessor about the progress of the step. With this information, the microprocessor adjusts the resistance in the hydraulics such that the user has proper support during the stance phase [4] [5]. Also it analyses an optimal release point for the knee to begin the swing phase and to provide proper foot clearance [4] [5]. These sensors and microprocessors are powered by a battery.



(a) The C-leg prosthesis [4]



(b) The Rheo knee prosthesis [5]

Fig. 1: The C-leg (a) and the Rheo knee (b). State of the art lower limb prostheses. These prosthetic devices are designed to approximate the human gait as close as possible. Sensors in the knee and ankle provide information to a microprocessing unit [4], which controls the hydraulics inside the prosthesis in real time to assist in proper gait. The required power is supplied by an integrated battery [4] [5].

Batteries however need to be recharged and unfortunately some of the energy in these systems is lost during use as well. The hydraulic cylinder inside the prosthesis also acts as a shock damper, dampening the impact forces during gait. This may introduce vibrations or heat. Healthy subjects utilise muscles and joints to absorb these impact forces. In addition to recharging the battery being time costly, they also add weight to the prosthesis. So to save energy, weight,

reduce charging time, and make the devices have a longer runtime a form of energy regeneration is desired. Energy regeneration in general or energy harvesting is a concept well known and has been widely investigated in the past few decades [6]. This includes energy harvesting from biomechanical energy, such as limb movement [7]. The human gait is composed of periodic motions, where mechanical vibrations exist inevitably [7]. Capturing this movement can be useful to produce power and charge a battery. Laschowski et al. [8] conducted a study to assess the biomechanical energy available for electrical regeneration during sit-to-stand movement. Joint biomechanical powers were numerically determined. The hip generated the largest maximum negative biomechanical power (1.8 ± 0.5 W/kg), followed by the knee joint (0.8 ± 0.3 W/kg) and ankle joint (0.2 ± 0.1 W/kg) [8]. For walking at 3 km/h the biomechanical powers generated are slightly lower; for the hip (0.2 ± 0.1 W/kg, knee (0.1 ± 0.1 W/kg) and ankle (0.2 ± 0.1 W/kg).

1.2 State of the art and problem analysis

When considering energy harvesting from biomechanical energy, there are numerous studies on energy harvesting exoskeletons already conducted [6]. The idea of this is to capture kinetic energy and convert this into electricity. This kinetic energy is otherwise dissipated to the ambience [3]. The electromagnetic induction principle, the piezoelectric effect, or hydraulic energy harvesting are three main types of energy harvesting from biomechanical vibrations [6]. Prior to this study, a literature study was conducted which describes these types of energy harvesting mechanisms based on human and vehicular induced vibrations [6] (Appendix I). For instance, harvesting energy from the knee, where flexion and extension applies torque to a generator to generate electricity [7]. Another study poses a method where piezoelectric elements are integrated in the sole of the shoe [7]. As stated earlier, the human gait is composed of periodic motions. The reciprocating movement of the human body also poses as a viable energy source, and can be harvested with a backpack suspending a load which undergoes vertical deviation [7]. However, the studies which describe energy harvesters based on human vibrations describe systems for subjects who have not undergone amputation and wear a prosthesis. So here the challenge lies in investigating a method for energy harvesting for users who for instance do not have a knee, proper heel-toe gait, or are able to suspend a loaded backpack [9]. These people should not be strained any further. People with losses in lower extremity can benefit from lower limb prostheses which also have integrated energy harvesting capabilities. They can have a longer runtime or compensate for any energy losses during use.

Jia et al. conducted a numerical feasibility study [3], where the response of a lower leg prosthetic system is numerically computed to determine potential recoverable electrical energy in lower limb prostheses. Analytical equations of force and motion are derived to mathematically describe the dynamics of a prosthetic device while subjected to external acceleration loading while walking and running [3]. The measured gait data is then used to numerically compute and predict the potential recoverable power [3]. This study concludes that the recovered power level during walking at 3 km/h (45 mW) [3] is sufficient to continuously sustain smart electronic microsystems, which include wireless systems, microprocessing units and sensors. This also accounts for losses in power conditioning and parasitic losses. Component specific power requirements are listed in Table 1. Still, different leg prostheses each have their own control system and power requirements which must be investigated.

TABLE 1: Typical power requirements of selected components in bionics smart prosthetic devices [3]

Nr.	Device	Power requirement [mW]
1	Microprocessing unit (MPU)	0,36
2	MEMS 9DOF motion sensor	0,05
3	MEMS pressure sensor	0,2
4	Servo motor	9000
5	Bluetooth 5 +RF chip	27
6	DC Motor	4500
7	Power conditioning circuit	0,5
8	32-bit ARM Cortex	0,002
9	MEMS strain gauge + ASIC	0,2

1.3 Goal

The main goal of this study is to harvest energy and compensate for some of the (otherwise) lost energy in the prosthesis. Extending the device's runtime beyond the original duration and compensating heavy battery weight. In addition, the energy harvesting device is experimentally evaluated and compared to other designs in literature. This system is designed such that it can capture the lost energy, regenerate this to electricity and store it in an energy storage medium. The next step is to directly power the control system of the lower limb prosthesis. Therefore the goal is stated as follows:

Design and experimentally evaluate an energy harvesting system to power the control system of a microprocessor controlled lower limb prostheses.

1.4 Paper structure

Section 2 describes the design method. Section 3 describes how the evaluation method is set up. Section 4 presents the results from the design method. Section 5 presents the results from the evaluation method. Section 6 discusses all relevant interpretations, limitations and recommendations. Section 7 presents the conclusion.

2 DESIGN METHOD

2.1 Design requirements and strategy

The entire design process is described in this section, together with the underlying thoughts. The process started off with an introduction to lower limb prostheses. In order to ensure a good fit between prosthetic device and energy harvesting system it is vital to understand what is expected. From this a list of functional requirements, constraints and wishes is set up:

Functional requirements

- The device harvests energy to essentially power (part of) a lower limb prosthesis' control system (45 mW). This includes microprocessing units, sensors, wireless systems, and valves.
- The harvesting can be done during walking at 3 km/h (step frequency of 1-2 Hz).
- The system regenerates energy provided by the human body.
- The device stores at least 70% of the harvested energy in a power storage medium.
- The device is durable and has a life expectancy of at least one year.

Constraints

- The weight remains below 1 Kg.
- The device must be less than 50 mm in diameter (when added to the cylinder).
- The device must not hinder, restrict or negatively influence normal gait with a leg prosthesis.

Wishes

- The device fits inside the cylinder/prosthetic system.
- The device or most parts of the device can be 3D printed.
- The device can directly supply power to the control system of the leg prosthesis.
- The device contributes to the functioning of the leg prostheses (multi functionality) in a certain way.

From this multiple subproblems are defined, which lead to a morphological chart (Figure 2). The morphological chart helps to generate concepts which fulfill all the required functions the design must have. 3 design routes (Figure 25) are taken which lead to 3 concepts. These concepts are evaluated and weighted against each other with the use of a Harris profile and performance criteria (Table 2). From these 3 concepts one is chosen and worked out further into a final design. The final design is fabricated and tested if it suffices to power the control system of a lower leg prosthesis.

TABLE 2: Performance criteria

Criteria	Description	Assessment
Weight	This criteria assesses the total mass of the design.	Assess weight using Solidworks.
Size	This criteria assesses the total volume of the design.	Assess volume using Solidworks.
Potential power output	This criteria estimates the potential power generation capabilities.	Perform numerical power prediction in Matlab.
Feasibility	This criteria assesses if the design can be built and operated using available technologies, materials, and engineering principles. Design complexity is a part of this criteria.	Determine the amount of moving parts and interconnections and assess possible fabrication and assembly strategy.
Cost of materials	This criteria assesses the predicted costs of the materials used.	Create a bill of materials.
Interoperability	This criteria assesses the operational feasibility. So if the system can be smoothly integrated and how well it interacts with the leg prosthesis.	Evaluate how the design is integrated and interacts with a lower limb prosthesis. Assess any possible challenges that are faced.

2.2 Concept solutions

The following concept solutions are derived from the morphological chart, depicted in Figure 2. The first column in the morphological chart describes functions that help generate a concept design. Each corresponding row displays partial solutions to the function. How the concepts are derived from this morphological chart is depicted and explained in appendix subsection A.1. This includes an elaborate discussion on every partial solution and reasoning for choosing a certain path.




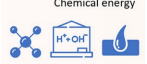
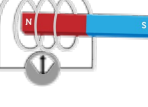
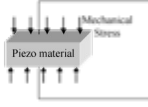
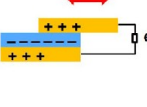


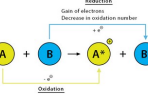
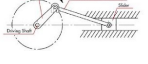



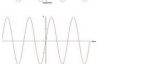



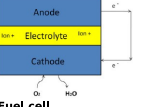
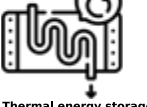





Function	Partial solutions per function					
Provide energy	 Kinetic energy	 Potential energy	 Thermal energy	 BioChemical energy		
Convert energy into electricity	 Electromagnetic induction	 Piezoelectric effect	 Triboelectric effect	 Hydraulic	 Thermoelectric effect	 Chemical reaction
Convert linear movement	 Linear movement to rotary movement	 Linear movement to bending	 No conversion			
Amplify vibration input	 Frequency amplification	 Amplitude amplification	 No increase			
Store electricity	 Battery	 Supercapacitor	 Fuel cell	 Thermal energy storage medium		
Assign position	 Inside the cylinder/system	 Around the cylinder	 Around the knee	 In/around the foot	 At the end of piston/shaft	

Fig. 2: Morphological chart. The first column describes all functions. Partial solutions to the functions are depicted in the corresponding rows. From this chart three paths are taken to form three concepts.

2.2.1 Concept 1 - The levitated magnet

The first concept uses the electromagnetic induction principle with kinetic energy as its energy source. When a magnet moves past or through a coil of wire, electricity is generated [10]. With this idea in mind, the first concept contains 3 sets of magnets and coil windings. The magnets are placed inside cylindrical shaped housing. The coil windings are on the outside of the housing. The system is placed inside the hydraulic cylinder, connected to the piston shaft. The system can also be placed below or on top of the cylinder if necessary. The orientation of the magnets is based on magnetic repulsion. There are magnets on the top and on the bottom which each repel the magnet in the center. When the piston shaft starts to reciprocate linearly, the magnet in the center collides with the top and bottom magnet. This introduces vibrations since the top and bottom magnets are placed on top of compression springs. So the vibration frequency is converted to a higher frequency which increases the change in magnetic flux with respect to time. This results in an increase in the induced voltage by the magnets and generates a higher power output. The voltage is stored in a supercapacitor. The concept is depicted in Figure 3. The image shows a cross sectional view of a hydraulic cylinder with the harvesting system inside.

2.2.2 Concept 2 - The rack and pinion

The second concept uses the electromagnetic induction principle as well with kinetic energy as its energy source. This concept is composed of a rack and pinion, three bevel gears, two one way bearings and a generator. The two bevel gears on the shaft contain one-way bearings. The system is placed at the end of the piston shaft. When the system moves up or down, the rack and pinion introduce rotation in the shaft and bevel gears. When the rack moves down, the first bevel gear is engaged and the second bevel gear has free rotation. This results in clockwise rotation of the generator. When the rack moves up, the second bevel gear is engaged and the first is disengaged. This results in the same clockwise rotation of the generator shaft, meaning this system drives the generator unidirectionally. Rotation of the generator shaft produces power, which is stored in a supercapacitor. The design is depicted in Figure 4.

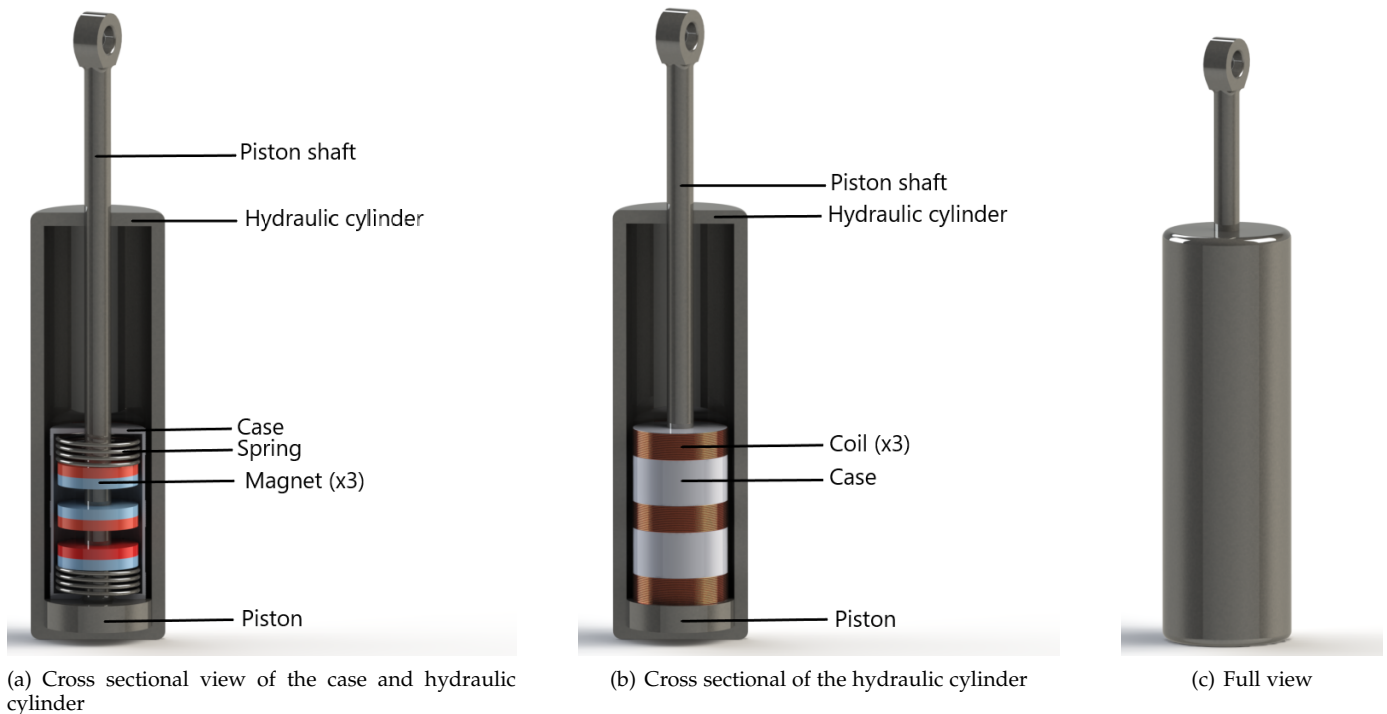


Fig. 3: Concept 1 - The levitated magnet. Cross sectional view of the harvesting system inside the hydraulic cylinder and surrounding case (a). Cross sectional view of the hydraulic cylinder, showing the enclosed casing with surrounding coils (b). Hydraulic cylinder from the outside (c). Reciprocating linear motion results in movement of the magnets inside the coils and generates a voltage.

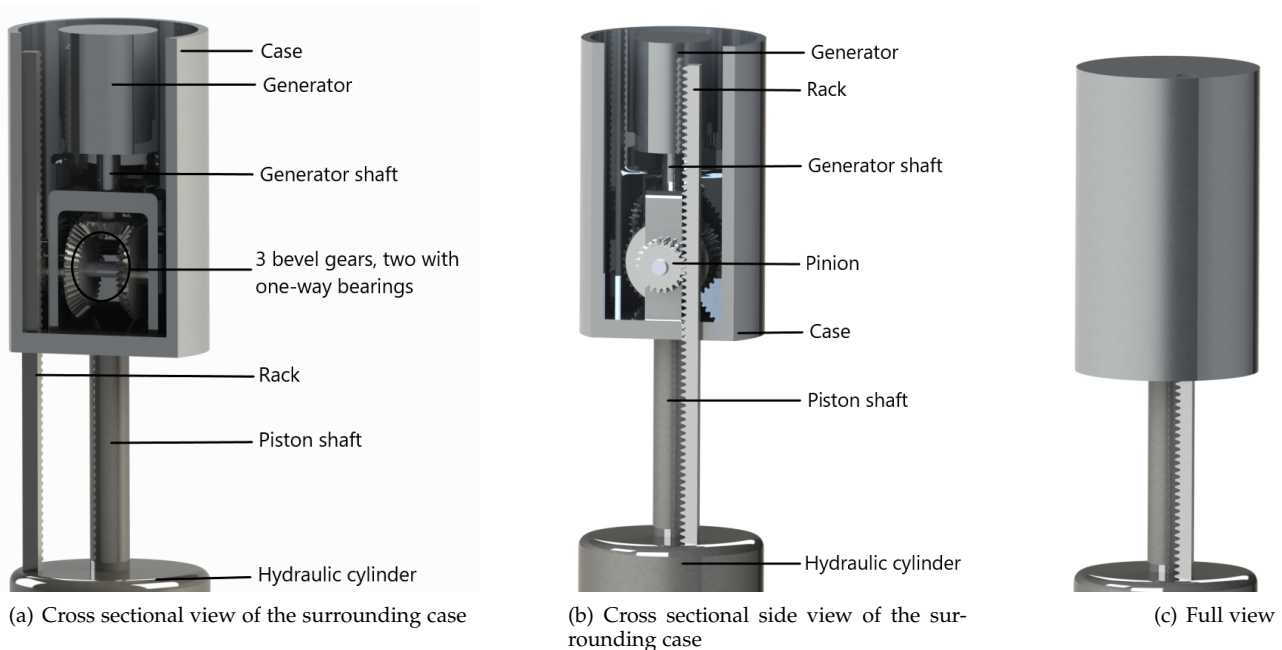


Fig. 4: Concept 2 - The rack and pinion. Cross sectional view of the surrounding case, showing the energy harvesting system from the inside (a). Cross sectional view from the side to highlight the rack and pinion mechanism (b). Harvesting system enclosed (c). Reciprocating linear motion results in a unidirectional rotation of the generator shaft and generates electricity.

2.2.3 Concept 3 - The compliant spring

This concept converts kinetic energy into electricity. The concept's main element is a compliant component which surrounds the piston shaft of the hydraulic cylinder. The idea of this is that when the part is pressed down on top, the sides deform and expand outwards. This part therefore acts like a spring. The system is placed on top of the cylinder. On the inside of this compliant component there are a few elements: a helix screw, a helix nut surrounded by a case and a ball bearing. Inside the casing there are 5 magnets and 5 coils in a circular line up. When the compliant component is pressed down,

the helix screw moves down as well. As the helix screw moves in the nut, the nut rotates. As for the helix nut and case, a one-way rotation of the case is realised with a clutch mechanism. When the nut moves down it is engaged with the case and when it moves up it is disengaged. This rotates the case unidirectionally and introduces rotation of the magnets past the coils, which generates a voltage. So this concept generates electricity via the electromagnetic induction principle. The voltage is stored in a supercapacitor. The concept is depicted in Figure 5.

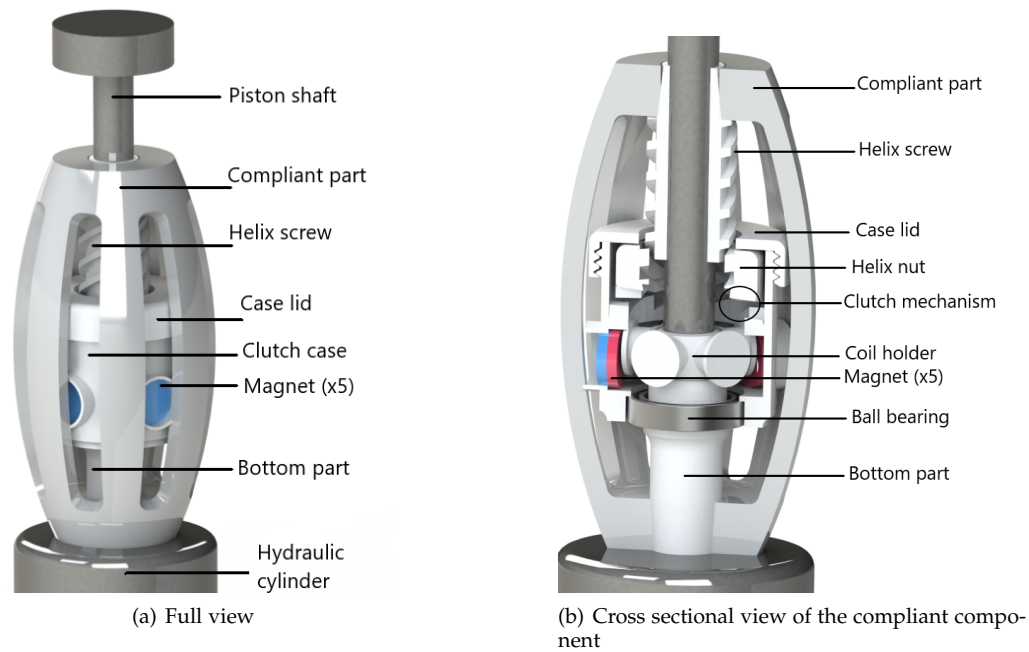


Fig. 5: Concept 3 - The compliant spring. depiction of the whole harvesting system (a). Cross sectional view of the harvesting system (b). Reciprocating linear movement results in a one way rotation of the magnets past the coils and generates a voltage.

2.3 Concept selection

2.3.1 Concept assessment

Each concept has its strengths and weaknesses. To make a good evaluation and to distinguish the concepts, they are assessed against performance criteria to determine its viability. The performance criteria are weighted against each other concerning their independent relevance to this study. This process is discussed in the appendix (subsection A.2). Weight is the most important criteria, followed by size, potential power output, feasibility and interoperability, respectively. The 'Cost of materials' criteria scored zero points and is therefore not included in the concept assessment. The weighted criteria are depicted in Table 3. Table 2 also describes how the assessment of each performance criteria is executed. The concepts are weighted against each other with the use of a Harris profile. A more in-depth description regarding the concept assessment and why a certain amount of points are allocated to a concept can be found in the appendix as well (subsection A.3). Concept 1 (the levitated magnet) and concept 3 (the compliant spring) nearly score the same amount of points, with concept 2 (the rack and pinion) scoring the worst.

TABLE 3: Weighted criteria

	Weight	Size	Potential power output	Feasibility	Interoperability	Cost of materials	Score	Total factor
Weight		1	1	1	1	1	5	5
Size	0		1	1	1	1	4	4
Potential power output	0	0		1	1	1	3	3
Feasibility	0	0	0		1	1	2	2
Interoperability	0	0	0	0		1	1	1
Cost of materials	0	0	0	0	0		0	0

2.3.2 Preliminary power calculations

Considering the potential power output, the predicted wattage of both concepts lies very close to each other (the levitated magnet around 0.7 mW and the compliant spring around 0.6 mW (Figure 8)). How this is calculated is explained in the appendix (subsection B.1). To calculate the power output a step by step approach is taken. The calculations are based on Faraday's law of electromagnetic induction. The first step is to calculate the magnetic field strength. This is determined with the formula:

$$B = \frac{\mu_0 m}{2\pi(z^2 + r^2)^{3/2}}$$

Where:

B = the magnetic field strength [T]

$\mu_0 = 4\pi * 10^{-7}$. The permeability of free space [N/A²].

m = Magnetic moment [Am²].

z = Distance from the magnet to the coil [m].

r = Magnet radius [m].

Then the magnetic flux is calculated. The magnetic flux through the coil is determined with the formula:

$$\Phi = BA \cos(\theta)$$

Where:

Φ = the magnetic flux at the coil [Wb]

B = The magnetic field strength [T].

A = The area of the coil [m²].

θ = The angle between the normal of the coil and the normal of the magnet [deg].

From this the rate of change of the magnetic flux is calculated by taking the derivative of the magnetic flux, i.e. $\frac{d\Phi}{dt}$

The next step is to calculate the induced emf (electromotive force) with the formula:

$$\epsilon = N \frac{d\Phi}{dt}$$

Where:

ϵ = the induced voltage [V]

N = the amount of coil windings.

$\frac{d\Phi}{dt}$ = the magnetic flux change with respect to time.

Finally the predicted power output is determined with the formula:

$$P = \frac{\epsilon^2}{R}$$

Where:

P = the output power [W].

ϵ = the induced emf voltage [V].

R = the load resistance [Ω].

Full detailed description, assumptions and simplifications are explained in appendix subsection B.1.

2.3.3 Prototypes

The results of the calculations can distinguish the better concept, given the similar scores between the two designs. This criteria is essentially the main goal. To verify the calculations a small study on the induced voltage of both concepts is conducted. This is done with the use of 2 proof of concept models. Both concept designs are 3D printed and assembled to determine what voltage the concepts potentially generate before developing one further into a final design. Detailed descriptions of the prototypes can be found in the appendix (subsection A.4). This includes iterations made and challenges faced during fabrication and assembly. The predicted power output is calculated in MATLAB. The scripts can be seen in the appendix as well (Appendix G).

Predicting the behavior of both concepts, it is expected that the compliant spring performs better than the levitated magnet. This is based on the expected spinning effect of the compliant spring where energy harvesting is more continuous than in the levitated magnet. This is however difficult to model in MATLAB and is therefore investigated experimentally. For both the calculated power output and the experimentally determined power output, a load resistance of 100 Ω is applied. The designed prototypes are depicted in Figure 6 and Figure 7. The levitated magnet needed some design changes in order to be built, since testing is done without a hydraulic cylinder. The compliant spring did not need any alterations.

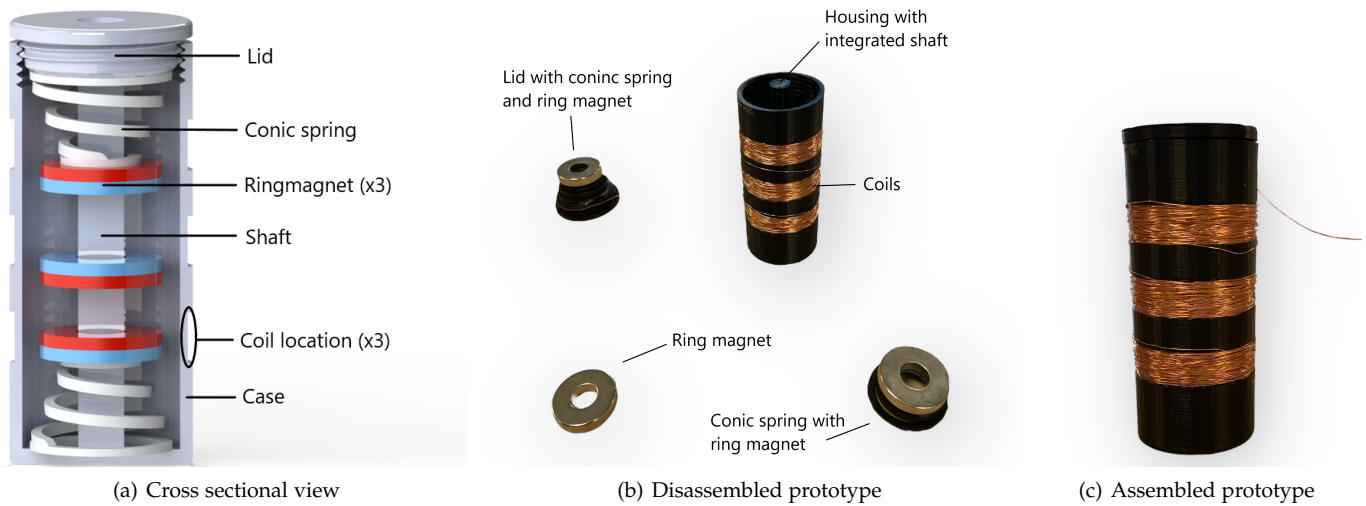


Fig. 6: The levitated magnet - prototype design. The hydraulic piston shaft is replaced by a 3D printed axis. This prevents the magnets to flip inside the housing. The steel springs are replaced by 3D printed conic springs, since the steel windings of a normal spring are attracted by the magnets. Copper wire is wound around the housing to form 3 coils. Each coil contains 100 windings. The images from left to right show a cross sectional view of the design (a), a disassembled view (b) and an assembled view (c).

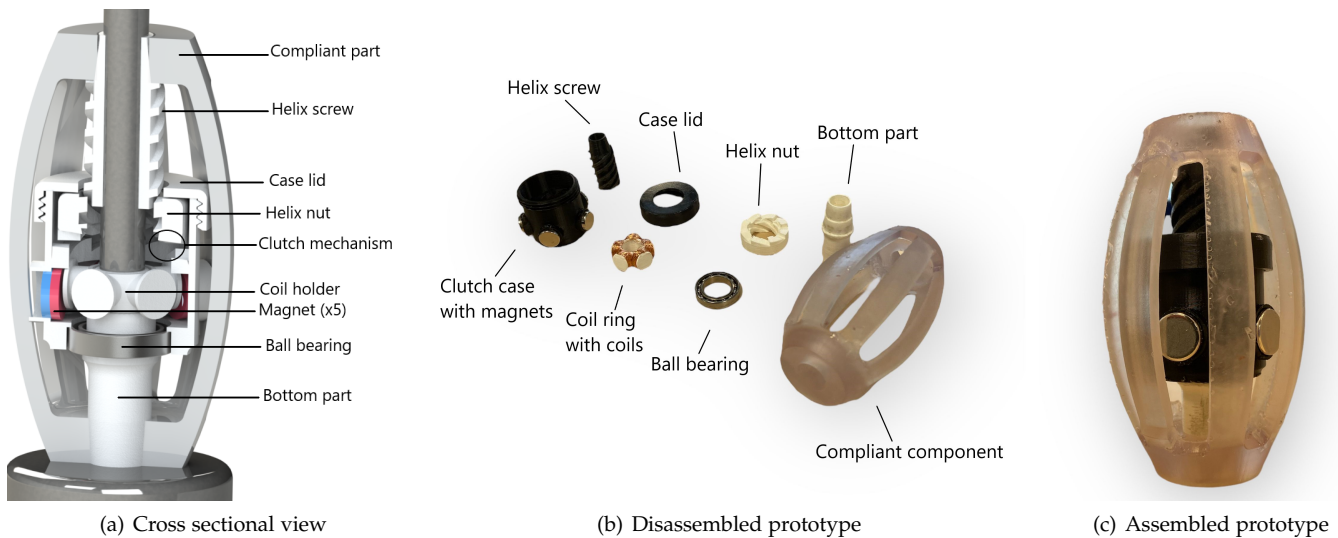
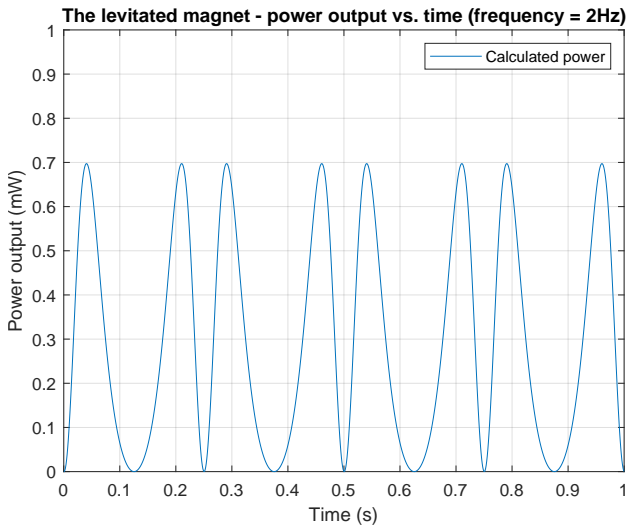


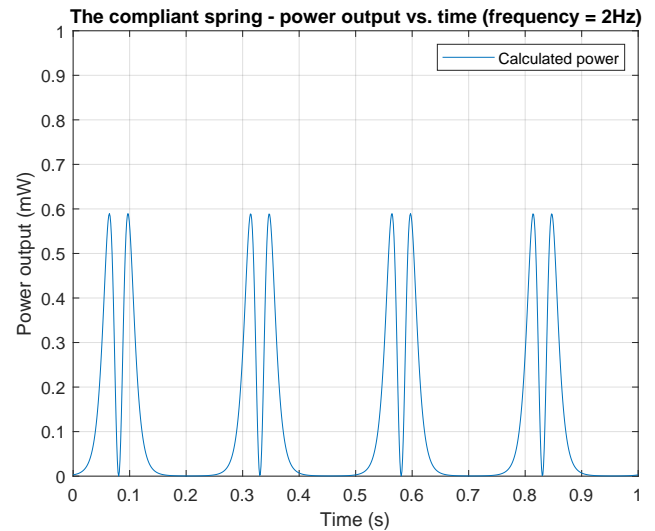
Fig. 7: The compliant spring - prototype design. The prototype is built and does not need the piston shaft or an additional axis. Each coil has 100 windings. The images from left to right show a cross sectional view of the design (a), a disassembled view (b) and an assembled view (c).

2.3.4 Preliminary power output results and discussion

Prior calculations are executed for a simplified setup. The emf and power output are calculated for a situation where a magnet moves through a coil considering the levitated magnet concept. For the compliant spring the emf and power output is calculated for a magnet rotating around a coil. Since the power calculations are simplified to a setup containing one magnet in each concept, the results are multiplied with the amount of magnets and coils used in the prototypes. Keep in mind that the output is not directly proportional to the amount of magnets but gives a good indication of the output. It is dependent on other factors as well, for instance the rotational/vibrational speed and duration, the magnetic field strength, and the volume of the magnets. The magnetic field strength does not increase linearly with the amount of magnets [11]. This is because the magnetic field of the magnets influence each other and determine the overall size and strength of the field [11]. When adding magnets, at some instance the magnetic field increase becomes negligible [11]. For now, the frequency is set on 2 Hz (frequency of walking at normal speed). The voltage measurements are examined for 1-3 Hz (appendix section C.1). This is achieved by applying perturbations within a second for both concepts. This is done by hand in an iterative manner to find the ideal conditions for each concept to work properly. The results of the power calculations as well as the measured voltage and power of the prototypes are depicted in figures 8 - 11.

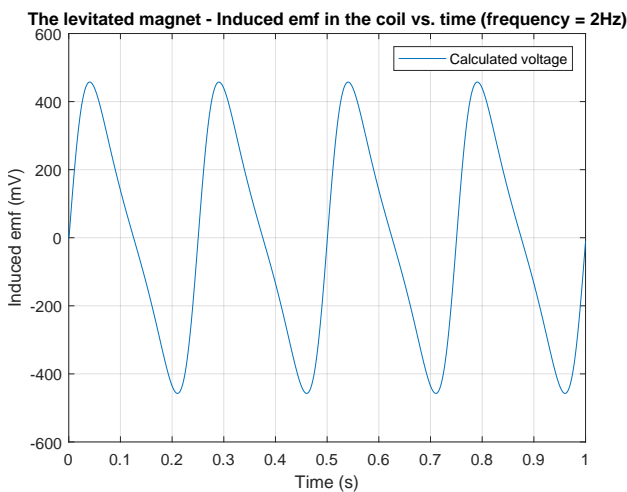


(a) Prior calculated power output of the levitated magnet

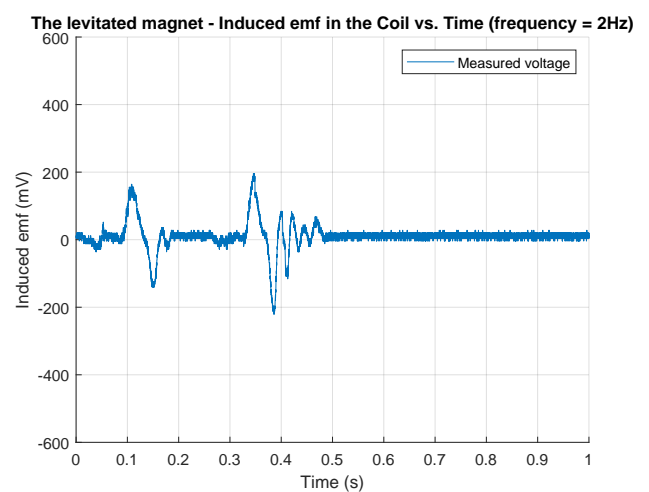


(b) Prior calculated power output of the compliant spring

Fig. 8: The levitated magnet (a) and the compliant spring (b) the calculated power output at 2 Hz. As can be seen the power output of both concepts differ 0.1 mW. Therefore for both concepts prototypes are built in order to verify the calculations. How these values are derived is explained in appendix subsection B.1. For both concepts the resistance ($R = 100 \Omega$) and number of coil windings ($N = 100$) are kept the same to make results comparable.



(a) Prior calculated emf of the levitated magnet

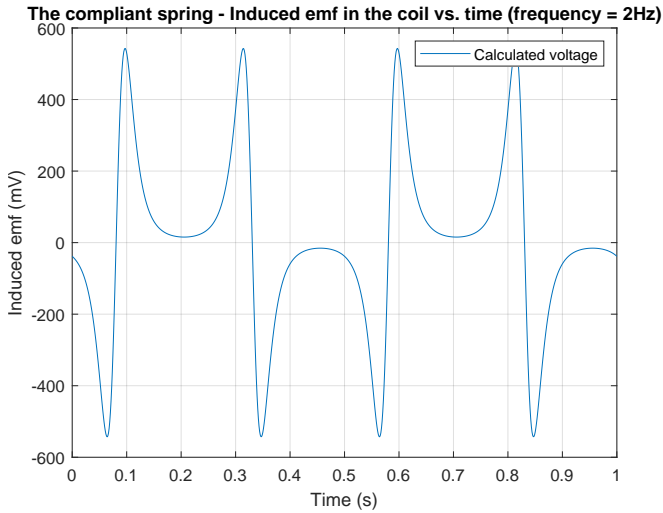


(b) Oscilloscope emf reading of the levitated magnet

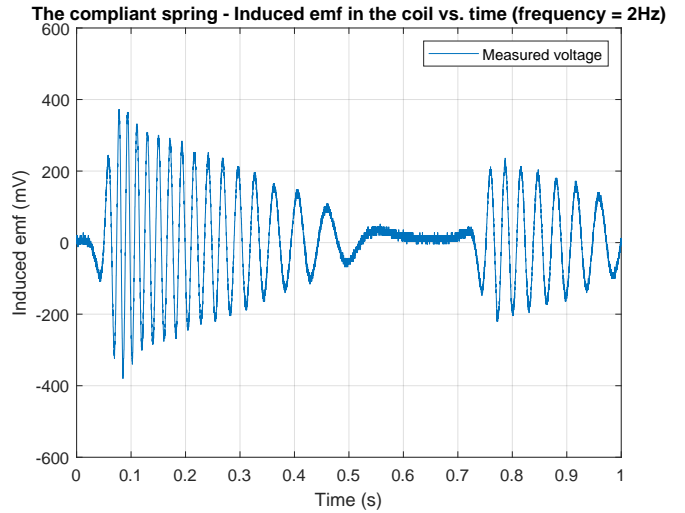
Fig. 9: The levitated magnet (concept 1) voltage calculations (a) versus measurements (b). The measurements with the oscilloscope show the voltage for a frequency of 2 Hz. The predicted peak voltage is higher than what is measured on the oscilloscope. The magnetic forces dampen the vibrations more than expected. Therefore the amplitude is lower and oscillation occurs less. This results in lower voltage measurements.

What can be concluded from the preliminary power output results is that the voltage output of the compliant spring (Figure 10) is higher than that of the levitated magnet (Figure 9). The peaks are higher and oscillation occurs more and longer than in the levitated magnet concept. This is due to the fact that the magnets repulsive forces dampen the vibrations (the levitated magnet concept). Therefore the amplitude of the vibrations in the levitated magnet concept is lower than expected as well as oscillation. Therefore the induced voltage is lower than expected for the levitated magnet concept. Due to the spinning factor of the compliant spring concept, energy conversion is smoother and more continuous compared to the levitated magnet, as it keeps rotating after input. Still, the output voltage is a bit lower than calculated. Another factor which must be considered here for both concepts is that the magnetic field strength does not increase linearly with the amount of magnets, as stated earlier. This predicts the induced emf higher than actually measured as well.

Peak voltage of the levitated magnet at 2 Hz is calculated at 457 mV. The peak voltage shown on the oscilloscope is 212 mV (Figure 9). For the compliant spring the peak voltage is calculated at 542 mV. The peak voltage shown on the oscilloscope is 380 mV (Figure 10). The power output shows more significant differences (Figure 11). What can be concluded from these results is that the total harvested energy from the compliant spring concept is higher than the levitated magnet



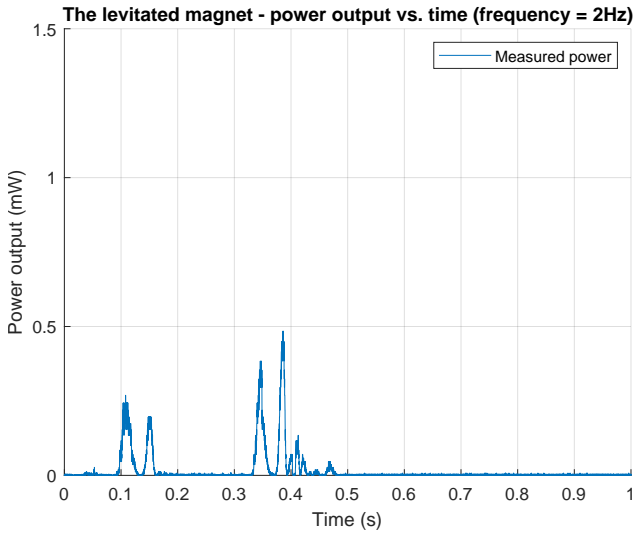
(a) Prior calculated emf of the compliant spring



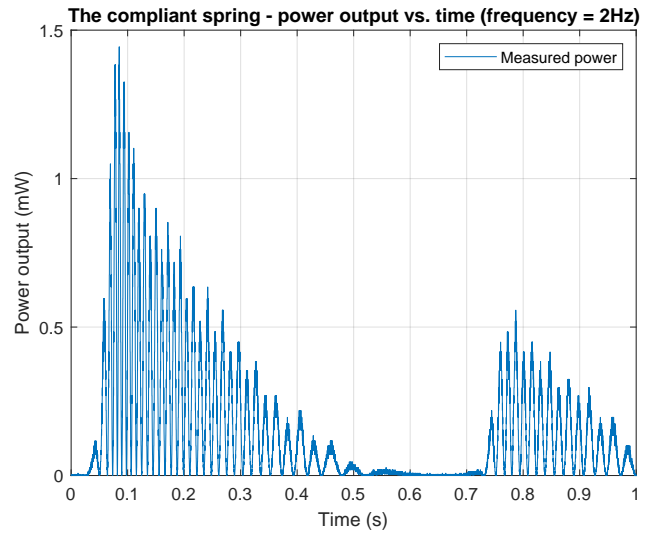
(b) Oscilloscope emf reading of the compliant spring

Fig. 10: The compliant spring (concept 3) voltage calculations (a) versus measurements (b). The measurements with the oscilloscope show the voltage for a frequency of 2Hz. Due to the spinning factor energy conversion is more smooth and continuous than in the levitated magnet. Therefore more energy per second is generated than in the levitated magnet. The measured peak voltage is lower than calculated. This is due to the fact that increasing the amount of magnets to increase voltage is not a linear relation. At some instance the magnetic field increase becomes negligible.

concept. With peak power output of the compliant spring being almost three times the value of the levitated magnet (0.48 mW vs 1.44 mW, both at a load resistance of 100 Ω). The calculated power/mass ratio's for both concepts also show clear differences. The levitated magnet weighs 85 g and has a power/mass ratio of 0.0059 W/kg. The compliant spring weighs 101 g and has a power/mass ratio of 0.015 W/kg. Therefore the compliant spring concept is worked out further into a final design.



(a) Power output of the levitated magnet prototype



(b) Power output of the compliant spring prototype

Fig. 11: Power output calculated from the oscilloscope measurements at a frequency of 2 Hz. The levitated magnet (a) versus the compliant spring (b). What can be seen is that the peak power output of the compliant spring is nearly three times higher than the peak power output of the levitated magnet. Also more energy per second is generated in the compliant spring due to the spinning effect. Therefore concept 3 is worked out further into a final design.

3 EVALUATION METHOD

3.1 Evaluation strategy

The functioning of the prototype can be evaluated in multiple ways. Concluding from the prior conducted literature review [6], a quantitative evaluation can be made with a vibration shaker table. During human gait vibrations exist inevitably and so they can be simulated as well. In addition to the frequency and amplitude controlled shaker table, an oscilloscope is used to measure the voltage output. These output results are compared to other energy harvesters found in literature [6].

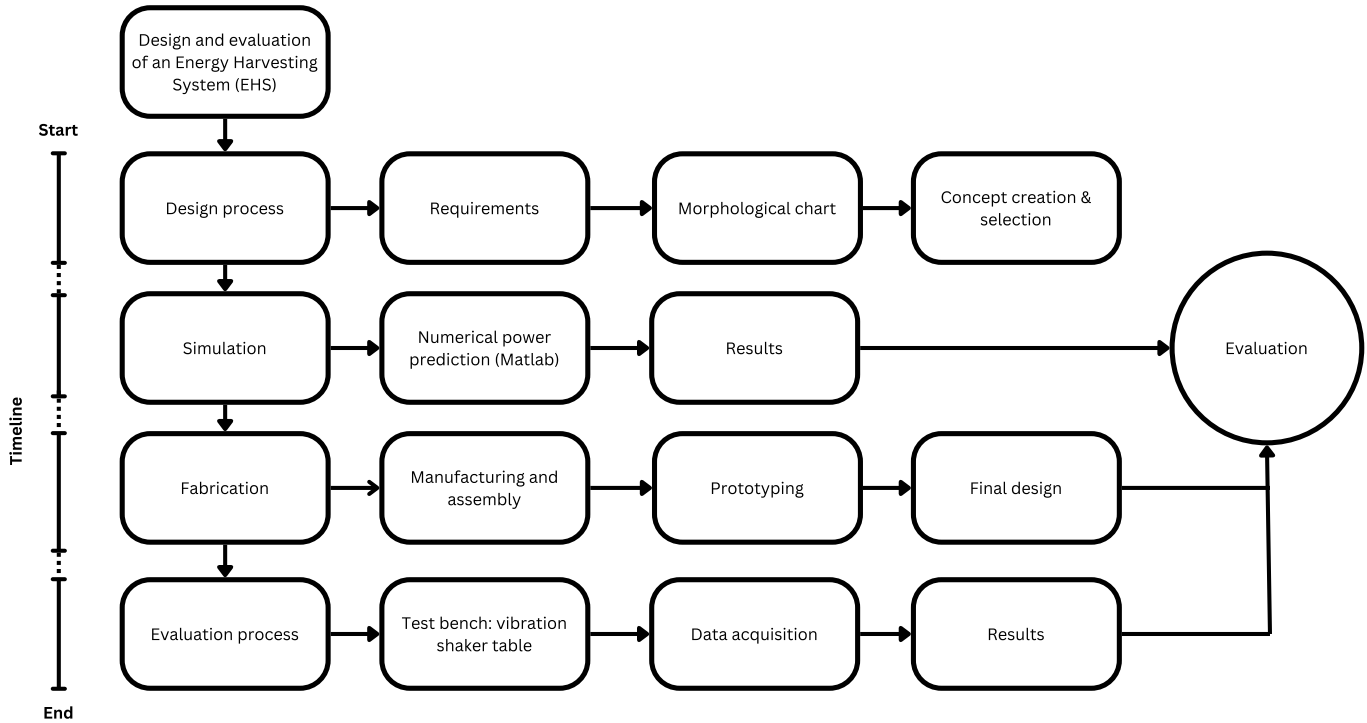


Fig. 12: Evaluation method structure of this study. Split up in 4 parts, namely design, simulation, fabrication and evaluation. The latter three parts lead to evaluation of an energy harvesting system (EHS).

3.2 Test bench design

For the experiment a vibration shaker table is designed. This setup is made such that the frequency and amplitude input can be altered. The setup design is depicted in Figure 13 and Figure 14. The included components are listed in Table 4. The disk included in the setup has multiple holes, each at a different radius. This ensures that the displacement of the linear guide and vibrational force press can be changed and therefore the amplitude of the input vibration can be altered. The frequency of the input can be altered by providing the desired rpm as serial input to the Arduino (arduino sketch can be found in the appendix at subsection H.1). The driver sets the input current to the stepper motor to 3 A (maximum of the Nema 23 stepper motor). As the introduced rotation is transferred to translation, the vibrational force press exerts a linear force on top of the energy harvester. The force sensor integrated in the vibrational force press records the force value. The oscilloscope connected to the energy harvester records the induced voltage. The whole system is mounted on aluminum profiles. All data is fed back to the laptop for processing.

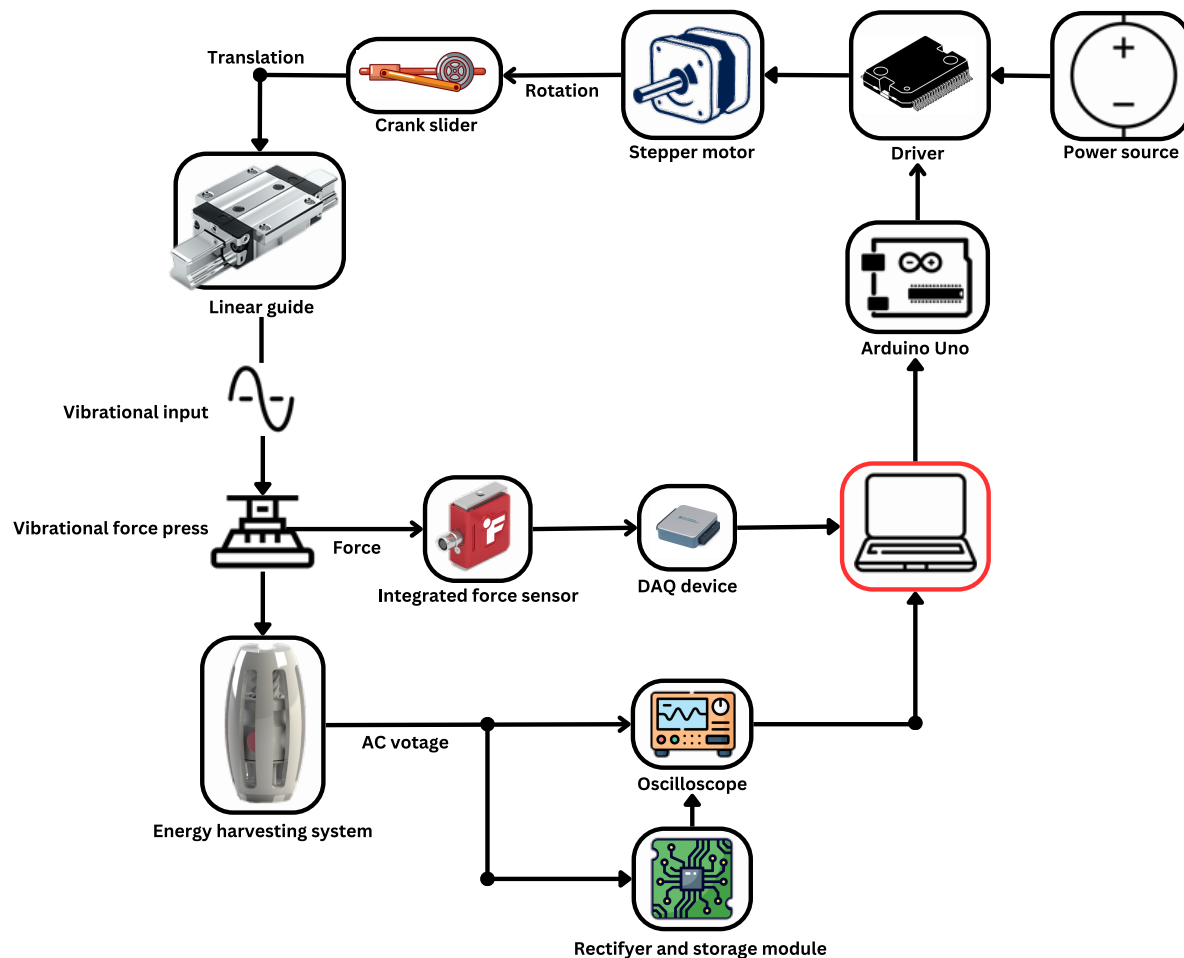


Fig. 13: Experiment schematic (a). Everything starts and ends at the laptop. The stepper motor is controlled by the arduino and driver which are powered by a DC power source. Rotation is turned into translation by means of a crank slider mechanism with linear guide. From this the vibrational force press reciprocates up and down, acting as a vibrational input. The vibrational force press (with force sensor) presses down on the energy harvester. The energy harvester induces an AC voltage which can either be rectified or directly read and recorded on the oscilloscope. The data from the force sensor is read by a DAQ system and recorded in excel. The next step is processing all data.

3.3 Evaluation protocol and preliminary discussion

Before testing begins it is vital to consider what must be recorded. For a certain amplitude and frequency input the following parameters are recorded:

- Peak output voltages [mV],
- Peak input forces [N],
- Charged output voltage in the capacitors [mV],
- Mass [kg],
- Volume [cm³].

From these parameters the input power, output power, power/mass ratio, power density, and efficiency are determined.

What must also be investigated is the frequency sweep and amplitude range. For every amplitude a frequency sweep of 1-10 Hz is executed. This is due to the fact that after 10 Hz the induced emf does not increase anymore and a maximum is reached. This is investigated experimentally by tracking the induced emf voltage on the oscilloscope and see if there is an increase in voltage as the frequency is increased. This is done for amplitude values of 9 - 12 mm. 9 mm is the minimum amplitude input required for the design to start rotating and function properly. 12 mm is the maximum amplitude before the design is damaged. This is investigated experimentally as well, by providing an amplitude input ranging from 1 - 14 mm. The amplitude where the harvester starts rotating properly is set as the minimum amplitude. The amplitude value where the force sensor records a sudden large increase of input force is considered to be a too large amplitude as the design's screw hit the coils inside.

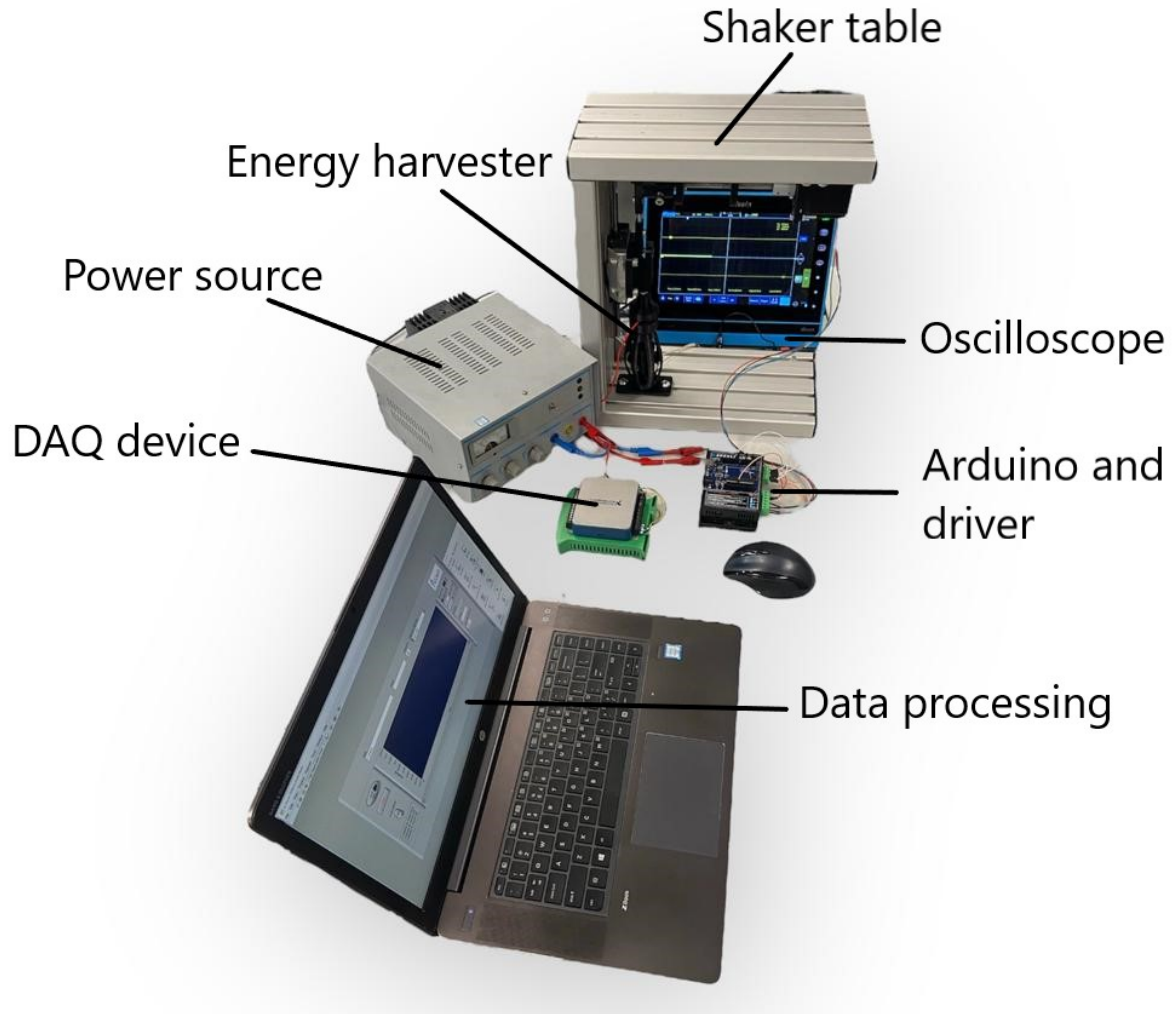


Fig. 14: Experiment setup. Just as explained in Figure 13, only this figure depicts the actual setup. This includes the designed vibration shaker table with all its components, this study's design, oscilloscope, power source, force sensor and data acquisition device, arduino and driver, and the laptop at which all the data is processed.

To start the experiment, the desired rpm is entered at the serial monitor. The harvester starts to generate a voltage from the input force. The force sensor and oscilloscope readings are recorded three times for 10 seconds for a certain amplitude and frequency. Only after the full frequency sweep the amplitude is changed. To assess the durability, the amount of cycles the final prototype undergoes is tracked as well. The charged voltage level in the capacitors is determined by charging the capacitors for 30 seconds for a particular input amplitude and frequency. The voltage level is recorded and the next input setting is applied.

3.4 Data processing and evaluation

After all the data is gathered it is stored for evaluation. In MATLAB all stored data is analysed and plotted into corresponding graphs. The peak output power is calculated with the formula $P = \frac{V^2}{R}$ with a load resistance of $R = 10 \Omega$. The input power is determined by finding the peak input force values and calculating the mechanical work. A peak force value is multiplied with the corresponding amplitude. To calculate the input power, the work done is divided by the time duration the force press pushes on the energy harvester, which is frequency dependent ($T = \frac{1}{f}$). The power mass ratio is determined by dividing the power output by the mass of the energy harvester. The efficiency η is calculated with $\eta = \frac{P_{out}}{P_{in}} * 100\%$. All outcomes are assessed with respect to the goal of this study.

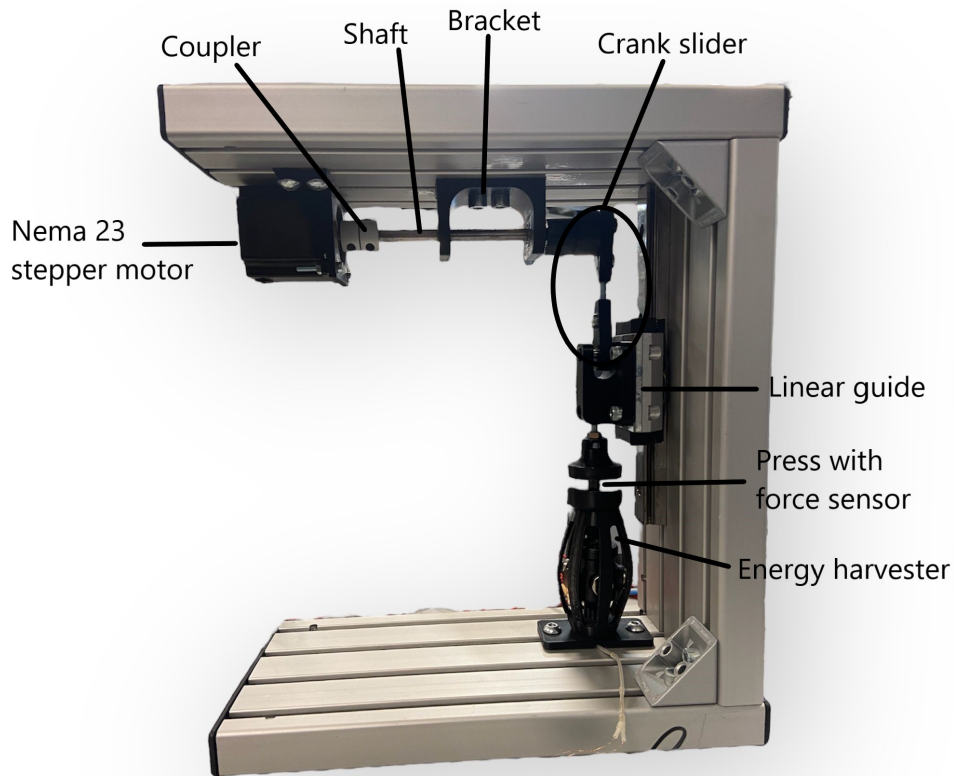


Fig. 15: Vibration shaker table. This shaker table is first designed in Solidworks. After fabrication and assembly of this test bench, the whole experiment setup (Figure 14) is tested before actually conducting the experiment. The testing is executed to ensure proper functioning of the shaker table design and interaction with the energy harvester and data acquisition devices.

TABLE 4: Component list

Nr.	Component	Component details, manufacturing or brands
1	Stepper motor	Nema 23
2	Arduino	Arduino Uno
3	Stepper motor driver	Shenli SL2690A
4	Shaft coupler	6 mm - 8 mm diameter
5	Shaft	8 mm diameter
6	Guiding bracket with ball bearings	3D printed bracket (black tough PLA), steel ball bearings
7	Crank slider mechanism composed of a disk and linear guide	3D printed disk (black tough PLA), linear guide from Item
8	Vibrational force press with integrated force sensor	FUTEK miniature force sensor, 3D printed press (black tough PLA)
9	DAQ device	National instruments
10	Energy harvester	This study's design
11	Oscilloscope	Micsig tablet oscilloscope
12	Rectifying circuit, composed of capacitors and diodes	Schottky (BAT 43) diodes, Kemet 6.3 V 820 μ F capacitors
13	DC power source	Input set to 20 V
14	Aluminum profiles	Item Profile 12/8 240x40 (3x)

4 DESIGN RESULTS

4.1 Final design

The compliant spring is worked out further into a final design. Since the prototype is already built, further iterations are executed quickly for the parts that need improving. The improvements are based on realising a smaller volume while trying to effectively increase the power output. This is achieved by influencing the strength of the magnetic field and therefore the change in flux through the coil windings. The amount of coil windings also play a role in determining the power output of the prototype. Several adjustments are made to the compliant spring (section 2.2.3) to form the final design:

- The volume of the clutch case (incl. lid) is decreased to allow for easier placement in the compliant element (from 11.19 cm^3 to 9.21 cm^3).
- The pitch of the helix screw is decreased such that it introduces more rotations towards the clutch case. The pitch is decreased from 50 mm to 30 mm.
- The diameter of the helix nut is decreased from 28.5 mm to 25 mm. The thickness is decreased as well to make space for bigger magnets. The thickness is decreased from 15 mm to 9.5 mm.
- The volume of the magnets is increased in order to increase the magnetic moment (from $m = 0.89$ to $m = 1.38$). The magnets used are now 15 mm in diameter and 8 mm thick (originally 12 mm in diameter and 8 mm thick).
- The coil windings are increased from $N = 100$ to $N = 150$ windings.
- Placing the coil ring inside the clutch case was a challenge due to the small tolerances between these two parts. Assembly for this is made easier by introducing a bottom lid which holds the ball bearing. The coils can now easily be placed inside and closed with the lid.
- The magnetic field is orientated such that the highest concentration of magnetic field lines pass through the coils. The north pole of each magnet points towards the center (radial direction). For a more elaborate explanation and depiction consider appendix section A.4.2.
- The compliant spring component is printed from TPU to ensure more springback. This part was initially printed from form flexible 80A resin. The thickness is decreased from 4 mm to 2 mm and now ensures more springback. In addition to form flexible and TPU, form elastic resin is tested as well (appendix, Figure 29). All materials are printed with different thicknesses and the best material is chosen. This is based on the compliant component providing enough springback while also being stiff and stable. For a more elaborate explanation consider appendix section A.5.
- All parts are 3D printed from tough PLA to achieve a more durable end product. Only the compliant component is composed of TPU.

These are all the iterations made during prototyping and developing the final design. The final design is depicted in Figure 16. The final prototype with its dynamics are depicted in Figure 17. The clutch mechanism is highlighted in Figure 16. The green parts introduce rotation towards the yellow parts. The parts that are grey do not spin. For a more elaborate explanation concerning the working of this clutch mechanism, consider appendix section A.5.2. Detailed dimensions can be found in Appendix F.

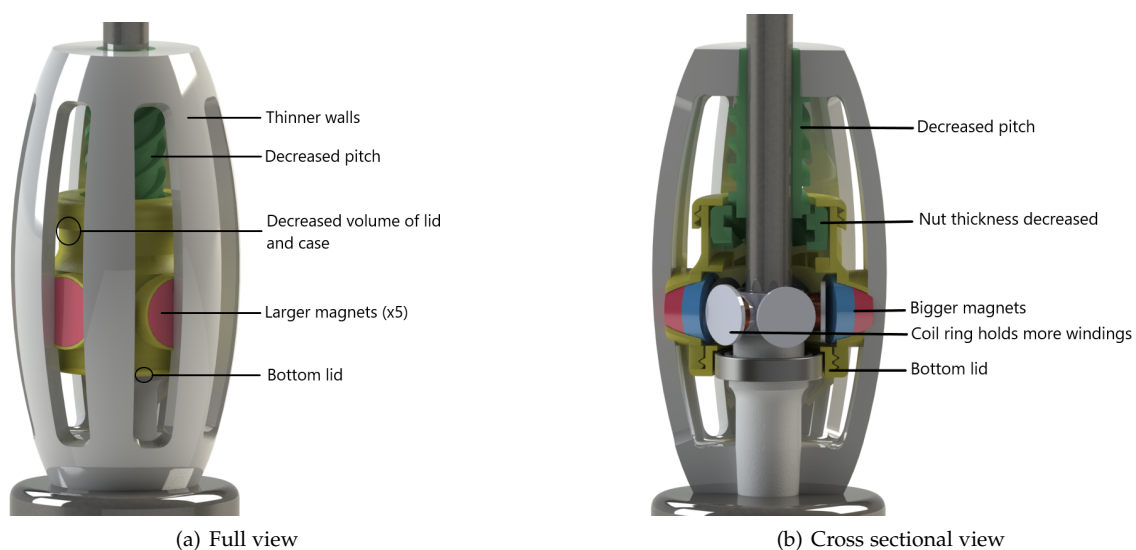


Fig. 16: Final design (a) with highlighted improvements. The cross sectional view (b) shows highlighted improvements as well, with colored parts. The colored parts are to emphasize upon the clutch mechanism. The green parts introduce rotation towards the yellow parts. The parts that are grey do not rotate. The design improvements are based realising a smaller volume while increasing the power output. The design is made from 3D printed parts. All parts except for the compliant spring element are made from 'tough PLA'. The compliant component is printed from TPU.

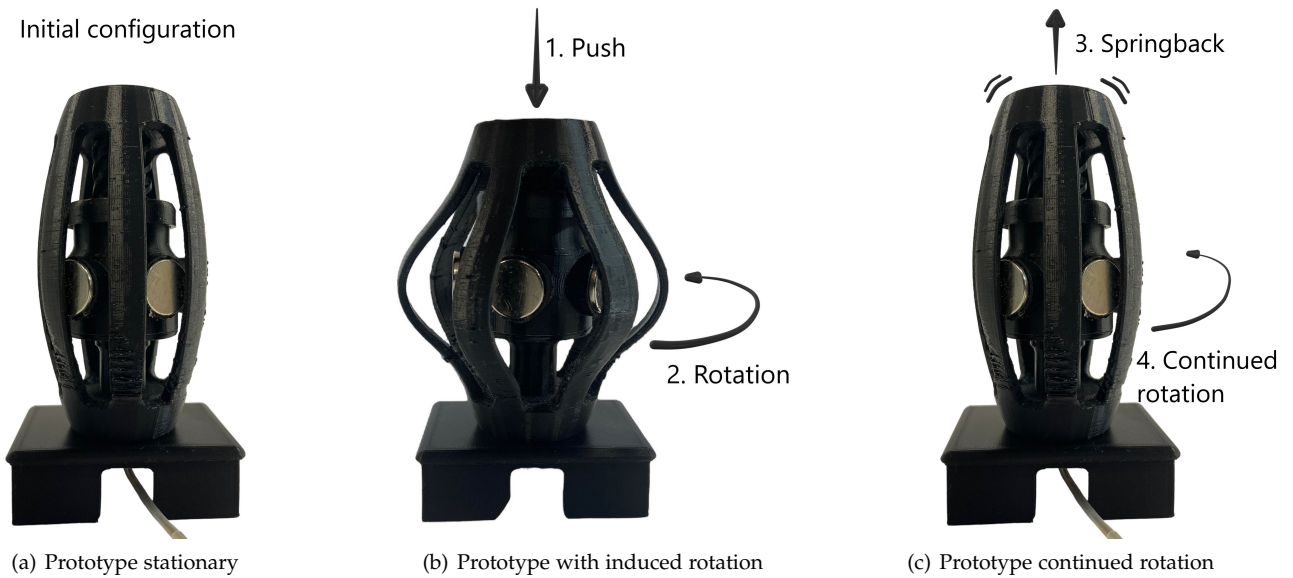


Fig. 17: Final prototype dynamics. In the figure on the left (a) the design is stationary. As the compliant element is pushed down (1.), rotation is induced (2.). As the applied force to the compliant element released, the compliant element springs back to its original state (3.). The inside case keeps on rotating (4.) and gradually comes to a stop. This process can be repeated step by step.

4.2 Electrical design

Developing a suitable electrical circuit is essential to store the harvested electricity. A supercapacitor is chosen (Kemet 6.3 V, 820 μF) as an energy storage module. For the required application, quick charge and discharge is needed to power control systems or supply part of the required energy. Supercapacitors have quick charge and discharge cycles and long lifetime cycles [12]. Using a battery in this case, which has limited charging and discharging, is not suitable [12]. After this limit is reached their capacity degrades significantly [12]. Batteries do however have high energy densities. Since the harvested energy is not that high, supercapacitors are a good fit.

A voltage multiplier circuit is built. This functions to double the voltage and convert the AC input into a pulsating DC output. So actually rectifying the alternating current. The circuit makes use of diodes and capacitors, allowing the current to travel in one direction and blocking it in the other. What must be taken into account is that at the diodes a voltage drop is experienced. The drop depends on the characteristics of the diodes used. The diodes used in this circuit (Schottky diodes) experience a voltage drop of about 0.2 - 0.3 V (a more elaborate explanation regarding this voltage drop can be found in Appendix E). During the cycle, the capacitors are accumulating charge. The charging can be separated in two half cycles where the voltage switches from positive to negative (AC). This determines the current flow, which is influenced by the diodes. The circuit is depicted in Figure 18. For a more elaborate explanation concerning the half cycles in the circuit, consider appendix section A.6.

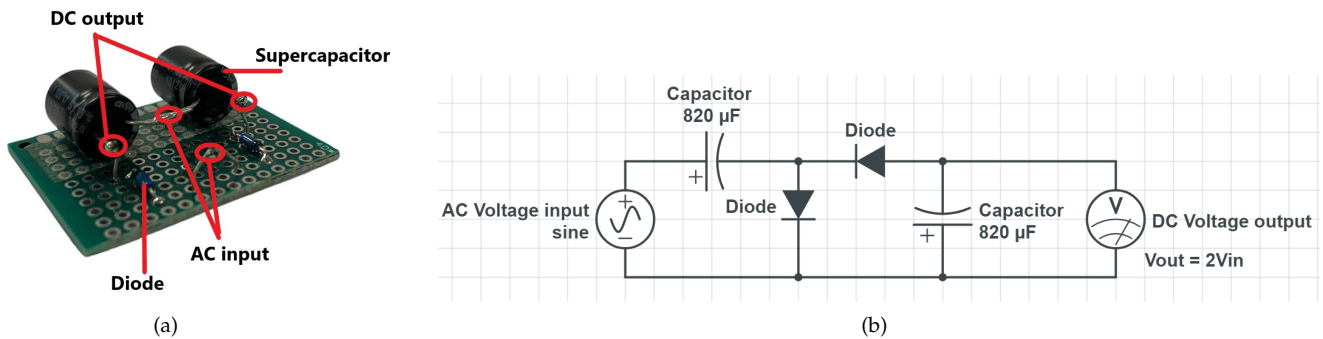


Fig. 18: Assembled energy harvesting circuit (a) and schematic (b). This circuit functions to double the voltage output and convert the AC input into a pulsating DC output.

5 EVALUATION RESULTS

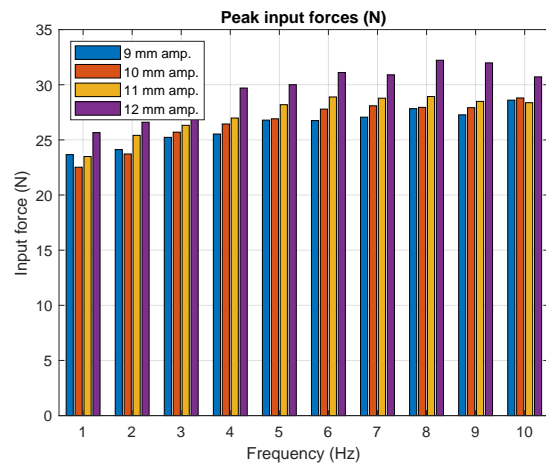
The highlights and most important findings are displayed in this section, which are discussed in the next section (section 6). For an overview of all the amplitude and frequency data consider appendix section D.1.

5.1 Overview

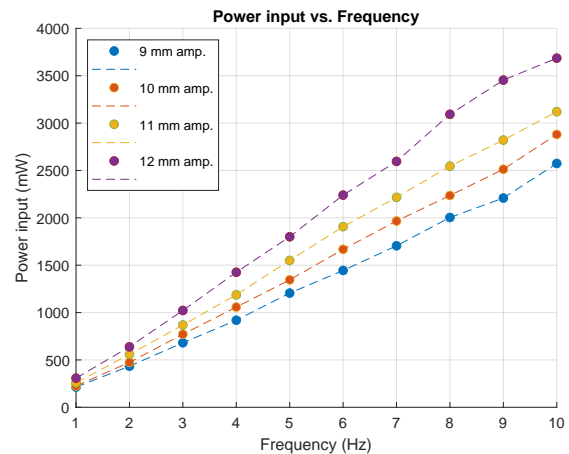
Table 6 shows the highlights of the conducted experiment in an overview. All this data is based on a frequency sweep for an amplitude of 12 mm. This is the amplitude at which the design performs best, which is emphasized upon in Figure 19. For a more detailed overview concerning input and output behavior for all amplitudes, consider appendix section D.1 (Table 10). Table 5 shows for a 12 mm amplitude and frequency sweep the following parameters:

- Peak induced voltage [mV]
- Peak input force [N]
- Peak input power [mW]
- Peak output power [mW]
- Power mass ratio [mW/g]
- Charged voltage in the capacitors [mV]
- Efficiency [%]

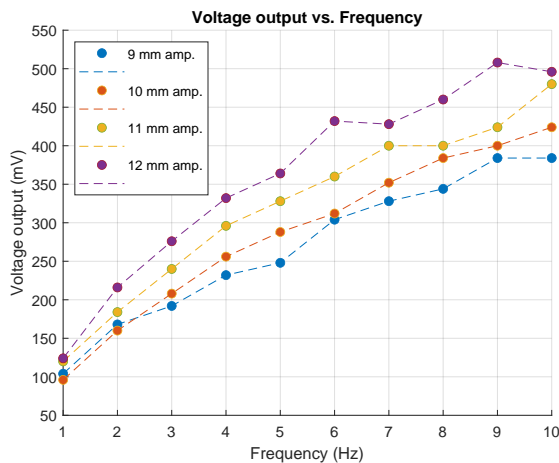
The peak induced voltage is the highest voltage value that is reached during recording time (10 sec) for a certain input. The same is done for the peak input force, input power, output power and charged voltage. From the input and output power the efficiency is calculated.



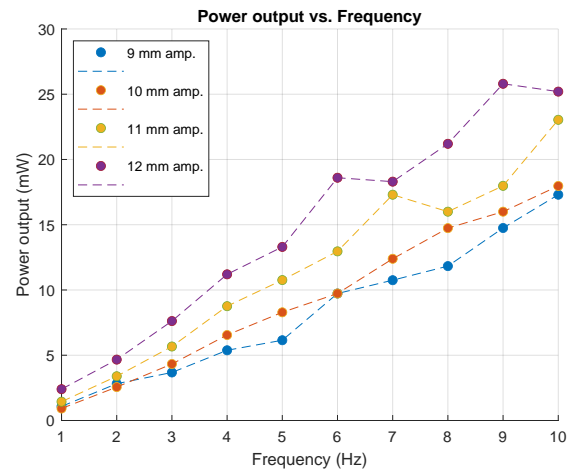
(a) Peak input forces vs. frequency for all amplitudes



(b) Power input values for all amplitudes



(c) Voltage output values for all amplitudes



(d) Power output values for all amplitudes

Fig. 19: Experiment input and output results. The figures display results for a frequency sweep from 1 - 10 Hz with an amplitude of 9 - 12 mm.

TABLE 5: Results for 12 mm amplitude

Amplitude [mm]	Frequency [Hz]	Peak Voltage [mV]	Peak input force [N]	Peak input power [mW]	Peak output power [mW]	Power mass [mW/g]	Charged voltage [mV]	Efficiency [%]
12	1	124	25,66	307,9	2,4	0,020	48	0,779
12	2	216	26,6	638,4	4,665	0,038	92	0,73
12	3	276	28,4	1022,4	7,62	0,062	164	0,75
12	4	332	29,7	1425,6	11,2	0,092	224	0,79
12	5	364	30	1800,0	13,3	0,109	280	0,74
12	6	432	31,11	2239,9	18,6	0,152	320	0,83
12	7	428	30,9	2595,6	18,3	0,150	352	0,71
12	8	460	32,22	3093,1	21,2	0,174	396	0,69
12	9	508	31,98	3453,8	25,8	0,211	408	0,75
12	10	496	30,711	3685,3	25,2	0,207	444	0,68

The highlights in Table 6 are taken from Table 5 and Figure 19. It shows for every parameter the highest achieved values during the experiment. Every results is coupled to a frequency and amplitude input, except for the volume, mass, and durability of the design.

TABLE 6: Highlights of the conducted experiment

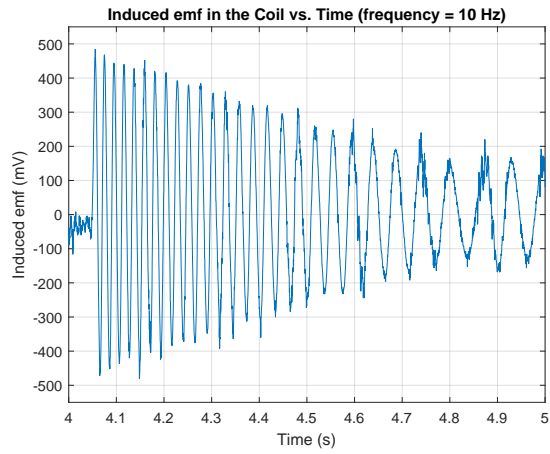
Parameter	Value	Amplitude	Frequency
Voltage output	508 mV	12 mm	9 Hz
Power output (peak)	25,8 mW	12 mm	9 Hz
Power output (average)	9,54 mW	12 mm	10 Hz
Charged voltage	444 mV	12 mm	10 Hz
Efficiency	0,83%	12 mm	6 Hz
Force input	32,22 N	12 mm	8 Hz
Power input	3685,3 mW	12 mm	10 Hz
Power/mass ratio	0,211 W/kg	12 mm	9 Hz
Power density	187 $\mu\text{W}/\text{cm}^3$	12 mm	9 Hz
Volume	138 cm^3	-	-
Mass	122 g	-	-
Durability	59400 cycles	-	-

5.2 Output results

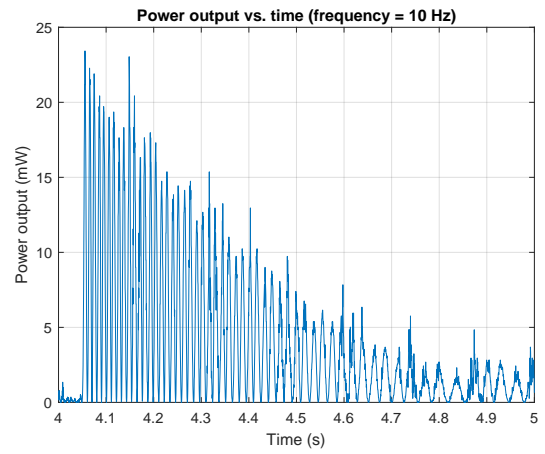
The behavior of the final prototype when excited is depicted in (Figure 20). This result is shown for an amplitude of 12 mm. This is due to the fact that at 12 mm (max amplitude) the design performs best and generates the most voltage. This can be seen in Figure 19, where the output voltage and power increases as the amplitude increases. Figures 20(c) and 20(d) show the voltage and power output for a time span of 10 sec. What can be seen is that as the compliant spring keeps on spinning there is still energy being harvested. Only slowly decreasing from initial excitation, until excited again. Figures 20(a) and 20(b) emphasize on this and zoom in on this behavior for a 1 second time interval.

5.2.1 Clutch dynamics

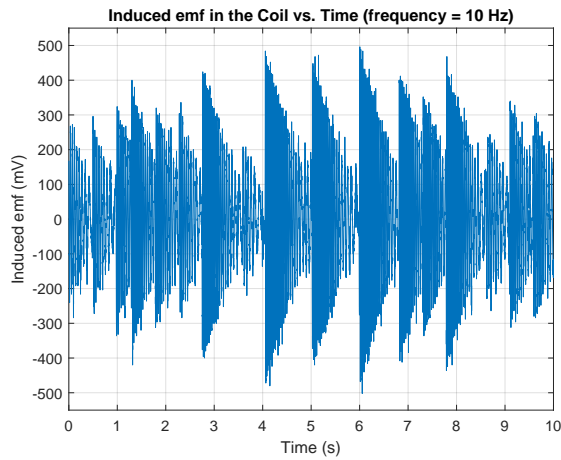
Figures 21(a) and 21(b) show the induced voltage for a time interval of 10 seconds. This is depicted for 3 Hz and 4 Hz. For 3 Hz it can be seen that for every input stroke, the same amount of energy is converted. This due to the repetitive characteristic the plot shows. When increasing the frequency, this phenomenon is not seen anymore. This is due to the engagement of the clutch mechanism, where rotation is not transmitted properly. The plot does not show the repetitive characteristic anymore. This keeps on occurring for the remainder of the frequency sweep (4 - 10 Hz).



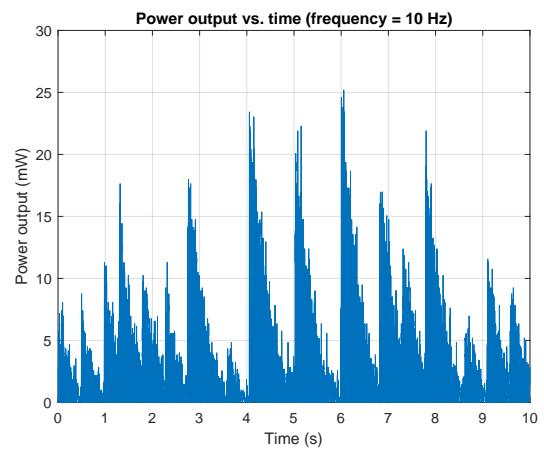
(a) Induced emf at 12mm amplitude and 10Hz frequency (1 sec interval)



(b) Power output at 12mm amplitude and 10Hz frequency (1 sec interval)

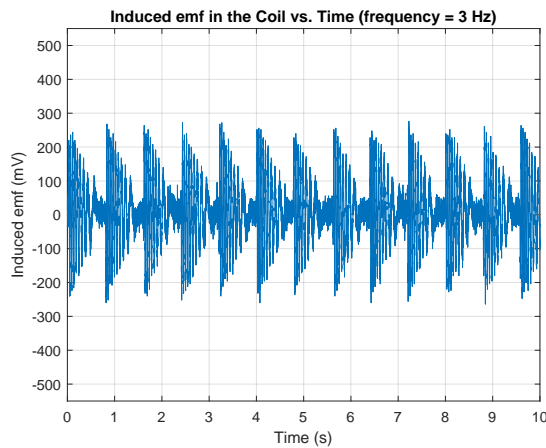


(c) Induced emf at 12mm amplitude and 10Hz frequency (10 sec interval)

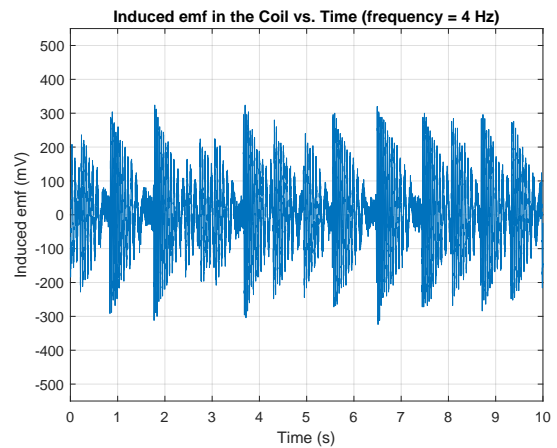


(d) Power output at 12mm amplitude and 10Hz frequency (10 sec interval)

Fig. 20: Voltage (a) and power output (b) for 1 second time interval. This interval is taken for 12 mm amplitude at 10 Hz frequency. Image (c) and (d) show the same results, only now for a time span of 10 sec. As can be seen the results are a bit more crowded due to the high frequency. The highlighted interval plots (a) and (b) do not show the highest output voltage and power peaks, but rather give an indication.

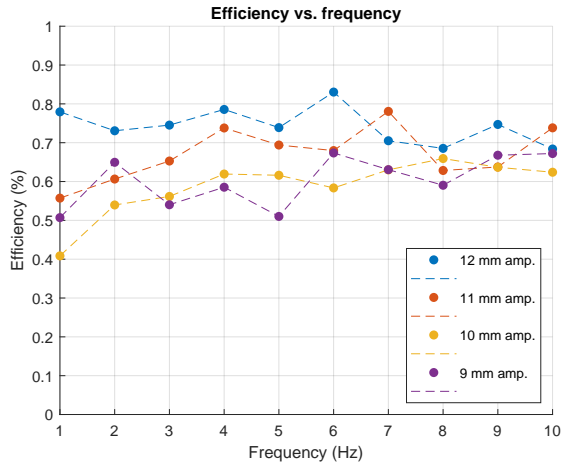


(a) Induced emf at 12mm amplitude and 3Hz (10sec interval)

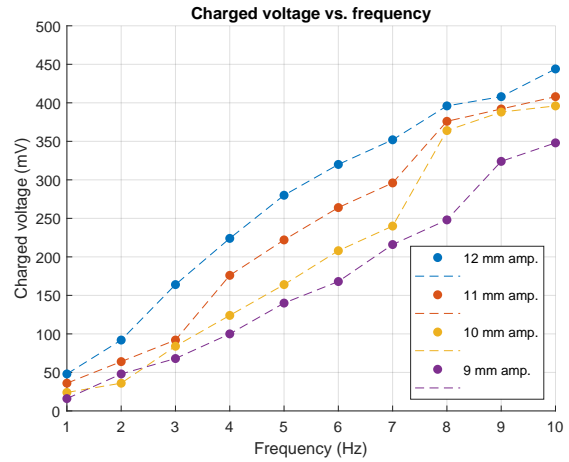


(b) Induced emf at 12mm amplitude and 4Hz(10sec interval)

Fig. 21: Induced emf voltages for 3 and 4 Hz frequency and 12 mm amplitude. Figure (a) shows repetitive behavior of the induced voltage, where every input stroke converts the same amount of energy. Figure (b) shows a change in this phenomenon where not every input stroke converts the same amount of energy. This can be seen in the 2 - 4 second time interval.



(a) Efficiency vs frequency plot

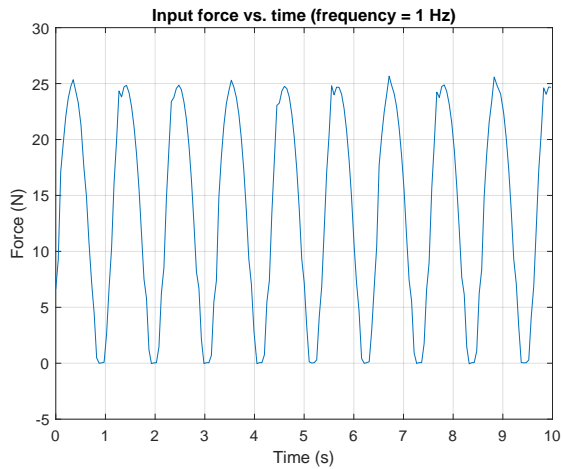


(b) Charged voltage in the capacitors

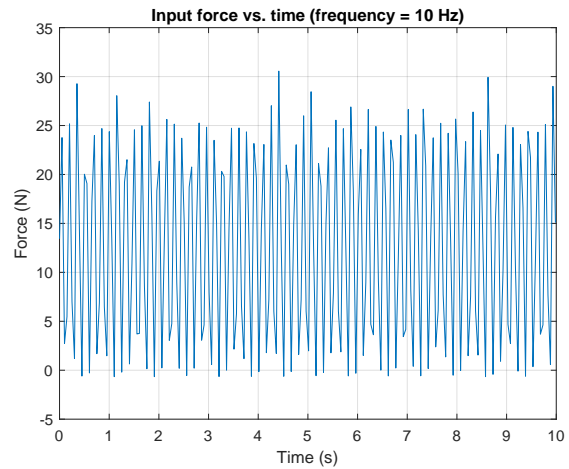
Fig. 22: The efficiency (a) and the charged voltage in the capacitors (b) are depicted for every amplitude.

5.3 Input results

In order to calculate the efficiency, the input energy is determined by recording the input force. From this the input power can be calculated. These results are shown in Figure 19 as well, together with the output results for a frequency sweep. The force sensor data is plotted for a frequency of 1 and 10 Hz and shown for a time span of 10 seconds. This is depicted below in Figure 23. What can be seen is that the peak input forces (10 Hz) differ from each other and in some cases do not return to zero. In reality however, the input force does return to 0 N.



(a) Input force for 12 mm amplitude at 1 Hz



(b) Input force for 12 mm amplitude at 10 Hz

Fig. 23: Input force vs time. (a) shows a plot of a 10 sec time interval for a frequency of 1 Hz. (b) shows the recorded input force over a time span of 10 seconds for a frequency of 10 Hz.

5.4 State of the art comparison

Table 7 shows this study together with other vibration energy harvester studies. The data has been presented such to make comparisons possible. The numbers 1 through 14 show studies on electromagnetic energy harvesting, 15 to 19 show piezoelectric energy harvesting studies and number 20 is a study on hydraulic vibration energy harvesting. As can be seen in the 'application' column, not all presented studies are based on human gait energy harvesting. They are however included to show the spectrum of energy harvesting based on vibrations (kinetic energy). The most important data is highlighted in grey. This data functions to draw a comparison between state of the art energy harvesters and this study.

TABLE 7: State of the art energy harvesters and this study [6]

No.	Reference	Energy harvesting technology	Frequency [Hz]	Amplitude [mm]	Power [mW]	Power/mass [W/kg]	Power density	Experiment	Application
1	This study	Electromagnetic harvester for lower limb prostheses	9	12	25,8	0,21	187 $\mu\text{W}/\text{cm}^3$	Vibration shaker	Lower limb prosthesis energy harvesting
2	Wei et al. [13]	Electromagnetic actuator for vibration suppression	5	3,045	95			Vibration shaker	Vibration suppression and energy regeneration
3	Mofidian et al. [14]	A dual-purpose vibration isolator energy harvester	12,5		0,115			Vibration shaker	Vibration suppression and energy regeneration
4	Halim et al. [15]	Human-limb driven electromagnetic energy harvester	5,17		2,15		333 $\mu\text{W}/\text{cm}^3$	Hand shaking	Hand shaking energy harvesting
5	Wang et al. [16]	Plane vibration-based electromagnetic energy harvester	4,5		0,27		5,68 $\mu\text{W}/\text{cm}^3$	Walking and jogging	Human gait energy harvesting
6	Chamanian et al. [17]	Wearable wireless sensor network with electromagnetic energy harvesting	2,65		0,127		4,30 $\mu\text{W}/\text{cm}^3$	Human waist motion	Human gait energy harvesting
7	Berdy et al. [18]	Magnetic levitation energy harvesting system	6,7		0,41	0,0532	263 $\mu\text{W}/\text{cm}^3$	Vibration shaker	Human gait energy harvesting
8	Abdelnaby et al. [19]	Energy harvesting system using flexensional compliant mechanism	1,4	4	0,012			Vibration shaker	Car suspension energy harvesting
9	Ali et al. [20]	Barrel cam based energy harvester	2	7,5	3850			Vibration shaker	Car suspension energy harvesting
10	Pan et al. [21]	Ball screw railroad based energy harvesting system	2	3	19900	1,326		Vibration shaker	Railroad energy harvesting. Weight = 15kg
11	Salman et al. [22]	Helical gears based energy harvester	1	2,5	270000			Vibration shaker	Car suspension energy harvesting
12	Gonzalez et al. [23]	Synchronous pulley and belt based harvester	2	10	2500			Vibration shaker	Motorbike suspension energy harvesting
13	Liu et al. [9]	Rack and pinion based energy harvesting backpack	1,1	25	2100			Vibration shaker	Human gait energy harvesting
14	Maravandi et al. [24]	Two-leg motion based energy harvester	1	5	540	0,135		Vibration shaker	Car suspension energy harvesting
15	Halim et al. [25]	Impact driven flexible side walls based vibration harvester	4,96		0,175		7,6 $\mu\text{W}/\text{cm}^3$	Hand shaking	Hand shaking energy harvesting
16	Zhong et al. [26]	Seesaw-type vibration energy harvester	7,34	2	0,09			Simulation	Vibration energy harvesting in general
17	Wang et al. [27]	Bistable nonlinearr vibration harvester	7	9	0,269			Vibration shaker	Vibration energy harvesting in general
18	Shukla et al. [28]	PENDEXE	2	15	0,29			Vibration shaker	Human gait energy harvesting
19	Zhou et al. [29]	Bio inspired bistable vibration harvester	4		0,1431			Vibration shaker	Vibration energy harvesting in general
20	Shi et al. [30]	Hydraulic vibration harvesting backpack		40	6200	0,413		Walking with load	Human gait energy harvesting

For every study, the available data is presented in the table. As can be seen, not every study publishes amplitude data, power/mass ratios or power density values. Still, all studies provided information regarding the experimental setup and the application. Where some studies just investigate energy harvesting based on vibrations in general, most studies are based on harvesting energy from human or vehicular induced vibrations.

These observations are also described by a study conducted by T. Blad and N. Tolou [31]. This paper describes the efficiency of miniaturized energy harvesters which operate under low-frequency excitation, as does this study. Numerous efficiencies of energy harvesters are examined. Energy harvesters in general have poor performance, leading to limited implementation in practice [31]. The efficiencies of 25 harvesters described in this paper range from 0.001% to 1%, with only 6 outliers that go into the range of 1% to 27.5%. All these harvesters are designed for low frequency applications.

This study also concluded that state of the art studies do not report all the relevant properties to draw a comparison. This includes parameters such as amplitude, frequency, mass and volume. These parameters are necessary to perform a proper analysis of the performance of energy harvesters and calculate relevant ratios.

6 DISCUSSION

6.1 Design advantages and limitations

6.1.1 Design characteristics and integration

The energy harvester shows potential in harvesting energy from vibrations, where excitations from 9 mm (up to 12 mm) are harvested. The design is very lightweight (122 g) and compact (138 cm³). Therefore it does not hinder normal gait with a lower limb prosthesis. Adding this to a lower limb prosthesis it is important to consider where in the human gait cycle the energy harvesting occurs. The energy harvester requires to be pressed upon. Therefore the integration into the prosthetic device is around the knee and harvests negative biomechanical power just before the swing phase of a normal gait pattern (pre-swing). This is also where knee flexion occurs. As discussed in section 1.1, the available energy for regeneration in the knee during walking is around 0.1 W/kg [8]. This is the negative biomechanical power generated by the knee. The maximum input power recorded during the experiment is 3.68 W. This means that people weighing more than 37 kg can theoretically provide enough input power during a normal swing phase. In such cases the biomechanical energy available is enough to introduce energy harvesting with the compliant spring.

6.1.2 Clutch dynamics and energy impulses

The harvesting is done through conversion of linear movement to rotary movement. The rotation velocity depends on a smooth conversion from linear to rotary movement and the impulse of the linear input. Lower frequencies harvest less energy than higher frequencies. This is due to the fact that higher frequencies give higher impulses of energy to the energy harvester. The clutch dynamics also influence the energy conversion (also consider appendix section A.5.2 for a more elaborate explanation). For frequencies above 3 Hz, not every input stroke is fully converted into rotation and eventually electricity (figures 21(a) and 21(b)). This is due to the continuous spinning of the energy harvester and proper timing and engagement of the clutch mechanism. Not all input energy is converted into output energy. As the harvester spins an AC voltage is generated, which oscillates as long as the inside case keeps spinning. The faster the device spins, the higher the peaks. As the spinning velocity decreases, the peaks decrease until another impulse of energy is converted to rotation. This behavior is also explained by the large peaks in figures 20(c) and 20(d), where an abrupt increase indicates an increase in spinning velocity and therefore harvested energy.

The continuous spinning effect however, makes it difficult for the clutch mechanism to engage. As the harvester's inside case is already spinning, it needs to slow down in order for the clutch mechanism's teeth to hook into each other and transmit another impulse of energy. If the device is still spinning fast, an input stroke which causes rotation of the nut to be transmitted to the case has very little to no effect. Since the spinning velocity of the nut and the case are close to each other if not the same, the nut won't be able to impose an increase of rotation towards the case. This means that at improper timing of the input all the input energy is lost. This occurs from 4 Hz up to 10 Hz. So timing the input is essential, and should be executed when the spinning velocity is relatively low. When the spinning velocity of the case decreases, the nut is able to impose an increase of rotation towards the case. As this occurs the peak power output values are reached.

Concluding, the power output is determined by the impulse of energy it is given. Which, in the conducted experiment in this study, is frequency dependent. Therefore the power output results increase as the frequency increases. In addition, proper and smooth transmission is required as well for the most efficient energy conversion. Therefore the power output is dependent on the impulse of energy and the clutch dynamics.

6.1.3 Power supply and demand

Considering the power requirements for lower limb prostheses' control systems (Table 1) and the power output characteristics of the energy harvester (Table 6), it can be concluded that the generated power (peak and average) is enough to power microprocessing units and sensors. This does not include wireless systems or any active actuators as they require more power. The peak power output is 25.8 mW, which is achieved at an amplitude of 12 mm and 9 Hz frequency input. The highest average power of 9.54 mW is achieved with the same input conditions. These parameters are both of value. Depending on the characteristic of the control system different values can be assessed. If the control system experiences occasional peaks in power demand, for instance during startup phases, the peak power output value is more relevant. However, if the control system experiences more consistent power demand, the average power output value is more relevant.

When the capacitors are fully charged (0.44 V reached in the experiment), the harvester can sustain power supply for the microprocessing unit and sensors. However, when the harvester is not generating any electrical energy the supply runs out. From the numerical analysis conducted by Jia et al. [3], a power budget is established for running microprocessors and sensors. Jia et al. [3] establishes this power level at 8.4 mW (including energy losses, see appendix Figure 35). This power budget includes 4 MPU units, 4 9DOF MEMS sensors, 4 MEMS pressure sensors, and 4 memory units [3]. Comparing this to the average power level of the energy harvester (9.54 mW), it is sufficient to continuously run microcontrollers

and sensors as long as energy is being harvested. Therefore the originally used battery power is still required. The energy harvesting system can be incorporated in a lower limb prosthesis, turning the prosthesis into a hybrid system.

Powering bionic prosthetic devices solely with energy harvesting is impossible, since the recovered power level is not enough to sustain the required power demands. The power level required for this is 62.15 mW (appendix Figure 35). This is also based on the fact that not all components are in active operation all the time. This power level sustains a hypothetical smart bionic leg, with wireless sensing functionality and intermittent motor controlled ankle and knee adjustments [3]. Considering the recovered power level from the compliant spring, the recovered power supplements the integrated battery. The control system can be designed to charge the prosthesis battery, with the flexibility to prioritize harvested energy to power the microprocessors and sensors when available and switch to battery power otherwise. The energy harvester can therefore help to minimise size and weight of the integrated battery.

6.1.4 Rectifying circuit

The voltage level across the capacitors increases as the frequency increases (figure 22(b)). This is due to the charging time and the size of the input voltage. Normally the capacitors can be charged up to the voltage level of the input and this takes a certain amount of time (depending on the input voltage). Higher input voltages charge the capacitors quickly. In the designed circuit however, the voltage is doubled (as discussed in section 4.2). So the maximum voltage that can be reached is double the input voltage. There are however some losses. The diodes experience a voltage drop of about 200 - 300 mV. This number is a characteristic of the diode's inherent properties and its operating principles. Different diodes have different voltage drops (V_f - forward voltage). This energy is lost in the form of heat [32]. Doubling the maximum input voltage and subtracting this loss determines the potential maximum of the charged voltage between 0.4 and 0.6 V. The highest achieved voltage in the capacitor is 444 mV, which means that the predicted losses are accounted for. The charged level of voltage is also dependent on the charging time as the capacitors are not charged fully at the first instance (dependent on the input voltage level). In reality it takes somewhere in between 5 - 10 seconds before the maximum voltage level is reached. The voltage in the capacitor is never higher than 2 times the input voltage minus the losses. The energy losses vary with frequency and amplitude. The energy loss is depicted in Figure 24. This is calculated by doubling the induced voltage (due to the multiplier circuit) and subtracting the actual stored voltage in the capacitors. This is done for every frequency.

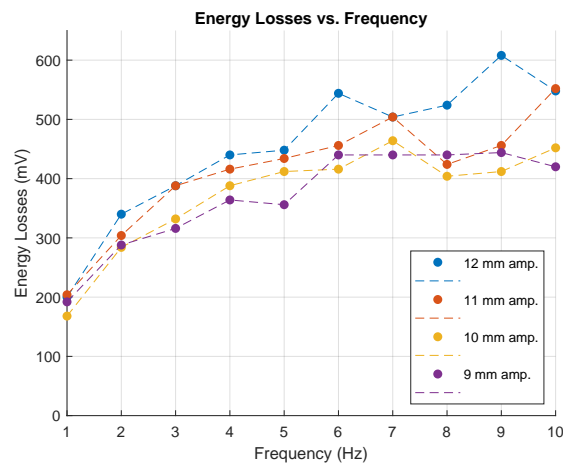


Fig. 24: Energy losses vs frequency, for every amplitude

The energy losses increase with the frequency and input voltage due to the exponential relation between forward voltage and the current across the diode [32]. As the current across the diode increases, the forward voltage increases. This particular behavior is as stated in appendix figure 36(b). For a more elaborate explanation concerning this phenomenon consider Appendix E. Additional losses can be found in the equivalent series resistance of the capacitors (ESR), where the current flowing through the capacitors experiences a small resistance [33]. This leads to energy losses in the form of heat [33]. This resistance however is very small and does not contribute as much as the V_f . Additional information concerning this phenomenon can be found in Appendix E as well.

6.1.5 Durability

During the conducted experiment, the amount of cycles the energy harvester experiences is tracked to assess the durability. A total of 59 400 cycles are executed before the compliant component started showing signs of material degradation.

These are mainly cracks in the side walls of the compliant component due to repetitive bending. The inside parts did not show any degradation during this course. The cracks of the compliant component are mainly caused by the 3D printing quality, which is not perfect. Depending on the performance of the 3D printer, most of the time the compliant component already showed cracks when extracted from the 3D printer. Still, the energy harvester is able to perform up to 59 400 cycles.

6.1.6 Efficiency

The efficiency of the energy harvester is very low. An efficiency of 0,83% is reached. Although the efficiency is relatively low, findings from a study conducted by T. Blad and N. Tolou indicate that it still falls on the higher end when compared to results reported in other studies [31]. There are multiple reasons for the relatively low efficiency results. The compliant component is crucial in influencing the input energy. The spring force must first be overcome in order for the device to be pushed down upon. The spring force of the compliant component can be decreased by making it less thick, or reducing the material infill for 3D printing. The required input energy can then be decreased. It is important to still maintain stability, so balancing the trade-off between these 2 characteristics is essential. In addition, there is energy lost in the transmission of linear movement to rotary movement. Namely friction between the nut and case, improper engagement of the clutch mechanism (slipping), misalignment of the whole harvester, bearing friction, and overcoming inertial resistance (weight of the magnets). Improper engagement can be improved by increasing the amount of teeth in the clutch mechanism. Increasing the number of teeth in a clutch mechanism enhances dynamics, facilitates more effective engagement, and mitigates slipping. Misalignment in the design occurs due to variations in 3D printing quality and slight deviations in part alignment. This also introduces more friction between the nut and case. Enhancing the 3D printing quality and smoothing part surfaces contributes in resolving this issue.

6.2 Prosthesis battery comparison

Placing the power supply of the energy harvester into perspective, it is important to remain a critical point of view. Knowledge on the batteries used in state of the art lower limb prostheses is required. Ottobock [4] only publishes information on battery packs used in an arm prosthesis. A 900mAh battery pack is used. This corresponds to an energy density of 13 846 mAh/g, compared to 245mAh/g of the energy harvester. This is based on the assumption that the harvester runs for one hour and sustains a current of 30mA. Batteries are significantly more energy dense than the supercapacitors used in the energy harvester [12]. Considering the numerically computed average power level requirements published by Jia et al. [3], it can be concluded that with a battery of 900mAh the runtime can be extended with 15.7%. This is when incorporating a battery of 900mAh and determining the lifetime based on the compensated power budget (appendix Figure 35). The prosthesis still requires sufficient battery power in order to buffer the high instantaneous power demand from actuators, servo's and wireless systems as well as supplying the remainder of the required energy that the harvester cannot provide.

It is still important to investigate the power requirement of state of the art lower limb prostheses, such as the C-leg and Rheo knee [4] [5]. Investigating the power requirements of the microprocessors and sensors used in these devices determines if energy harvesting actually extends battery lifetime. In addition, integrating energy harvesting technology demonstrates innovation in prosthesis designs. This shows the advancements in utilizing alternative power sources for energy harvesting. This opens possibilities for future improvements in energy harvesting not only in this application but in other branches as well.

6.3 3D-printer materials

6.3.1 Form flexible 80A

As for the material of the compliant component, multiple materials are tested with different thicknesses. The criteria for the compliant component is that it generates enough springback for the helix screw to move back to its original position, while remaining stable. TPU performs best considering these factors. The form flexible 80A resin provides the stability the design needs, only due to the more viscous properties the springback is not quick enough to be able to perform at above 1 Hz frequency. As the part is pressed upon, it loses contact with the edge of the vibrational force press as it moves back up again. Therefore, when the vibrational force press starts to push down again, the full amplitude is not achieved.

6.3.2 Form elastic 50A

As for the form elastic 50A resin, it does provide enough springback. Only this material does not provide the stability the design needs. The part remains in contact with the vibrational force press when pushed upon, even at higher frequencies. Only it is easily influenced by any sideward force or perturbation. As the inside mechanism starts spinning (as it is pushed upon) it can occur that the whole prototype deviates to the side due to the centrifugal forces. Friction is generated as the top and bottom are not vertically aligned and therefore the spinning quickly comes to a halt.

6.3.3 TPU

The TPU material provides enough stability and generates more than enough springback to make the prototype function properly. 3D printing this however should be done carefully, with at least 75% infill and slower speeds (20 - 25 mm/s) to achieve the best results.

6.4 Recommendations

6.4.1 Gait test

The next step for evaluation of the design is executing a gait test. What is concluded from the experiment in this study is that the energy harvester performs best as it receives high impulses of energy with proper clutch engagement. Clutch dynamics are best at lower frequencies (1 - 3 Hz). Higher frequencies as input show higher voltage output results, due to the higher impulse. Due to the clutch dynamics, it can be concluded that lower frequencies are the best operating conditions for this device. This frequency is in line with normal walking frequency (1 - 2 Hz). To validate this a gait test must be setup and executed, which should be included in future studies. This poses as the next step in evaluating the working of this energy harvester for lower limb prostheses.

6.4.2 Efficiency

In addition to the findings stated in the preceding section regarding the efficiency (section 6.1.6), future studies should also further investigate how to improve the efficiency of the design. The energy harvester already shows potential in power output at very low efficiency. When improving this there can be significant increases in power output. Achieving a higher efficiency and comparing it to state of the art energy harvesters gives more insight in the improvements made and the harvester's performance.

6.5 Limitations

6.5.1 State of the art data

There is a lack of relevant information published in state of the art studies, concluding from a prior conducted literature review [6] and a study conducted by T. Blad and N. Tolou [31]. Durability, efficiency, power/mass ratios and power density values are not well described in these studies. This makes it hard to draw a comparison. This study however shows all possible data to be able to be compared to future studies as well as prior studies that do include the lack of information stated earlier.

6.5.2 Force sensor sampling

Considering the peak force sensor values, these are plotted for all frequencies and amplitudes (figure 19(a)). Figure 23(b) however, shows the force value not returning to zero at some instances. This is due to the sampling time of the force sensor data. This can be altered and has initially been set to 50 ms. However, when increasing the frequency the sampling time does not fully keep up with the pushing of the vibrational force press and therefore it seems that the force does not return to zero. In reality it does however return to zero. Figure 23(a) shows a plot of a lower frequency (1 Hz), where it can be seen that the force value returns to zero before spiking back up. This accurately shows the behavior. In future experiments, avoiding the repetition of previous errors is crucial. After the conducted experiment the correct behavior is verified with the sampling time set to 10 ms. To enhance accuracy in force sensor values, it is advisable to reduce the sampling time for recording force values to its lowest value (10 ms).

6.6 Other applications

Energy harvesting has gained lots of interest over the past few decades [34]. This study focuses on the application of energy harvesting on lower limb prostheses. The principle of energy harvesting can also be applied elsewhere. Two other promising applications can be exploited in exoskeletons and electric bikes. Most (active) exoskeletons also require a battery to power control system and can therefore benefit from energy harvesting in the same manner that lower limb prostheses can benefit.

In addition, electric bikes are on the uprising. Especially in the Netherlands. During cycling, vibrations are introduced inevitably due to road irregularities and can therefore be harvested. By integrating energy harvesters in the suspension of these electric bikes they could benefit from the harvested electricity and for instance power the control system or charge the integrated battery. For both applications the power requirements must be investigated before embarking on this challenge.

7 CONCLUSION

The aim of this study was to design and experimentally evaluate an energy harvesting system to power the control system of a lower limb prosthesis. A working prototype for generating electricity from vibrational energy was developed and evaluated with a newly designed vibration shaker table. What can be concluded from the results is that the designed prototype suffices to power microprocessors and sensors of the control system of lower limb prostheses. A peak power output of 25.8 mW with a power/mass ratio of 0.21 W/kg is achieved at a frequency of 9 Hz and 12 mm amplitude. The design performs best as it receives higher impulses of energy at lower frequencies (1 - 3 Hz). These frequencies are in line with normal walking frequencies (1 - 2 Hz). Having investigated the dynamics of the energy harvester, it is recommended to exploit methods to improve overall efficiency, to validate the working of the design with a gait test, and compare results to state of the art energy harvesters based on vibrations. This design may also find use in other applications such as energy harvesting in exoskeletons or electric bikes, where vibrations are inherent.

Concluding this study, it is important to remain a critical point of view. The final prototype of the compliant spring design does not generate enough power to fully power a lower limb prosthesis' control system, only microprocessors and sensors. Battery power is still required. Battery life can be extended with 15%. Therefore, integrating the energy harvester into a prosthesis turns the system into a hybrid system. Still, this study presents all possible data for the energy harvester to be compared to state of the art miniature harvesting systems. The absence of data from previous studies limits the ability to draw comparable results. The results from this study demonstrate comparable data and present the innovations possible in prosthesis design and the advancements in utilizing ambient power sources for energy harvesting. Enhancing the overall efficiency of this design, and promoting comparable results to other designs in the existing literature, could emphasize upon the potential of energy harvesting applications.

REFERENCES

- [1] K. R. Rakeshsharma, K. Hemanth, and V. Shamanth, "Materials Today : Proceedings A review on design of lower appendage prosthesis," *Materials Today: Proceedings*, vol. 45, pp. 82–86, 2021. [Online]. Available: <https://doi.org/10.1016/j.matpr.2020.10.096>
- [2] M. Goldfarb, B. E. Lawson, and A. H. Shultz, "Realizing the promise of robotic leg prostheses," *Science Translational Medicine*, vol. 5, no. 210, 2013.
- [3] Y. Jia, X. Wei, J. Pu, P. Xie, T. Wen, C. Wang, and P. Lian, "A Numerical Feasibility Study of Kinetic Energy Harvesting from Lower Limb Prosthetics," pp. 1–17, 2019.
- [4] Wayne Williams, "Ottobock C-Leg Bionic Knee," *Bionics for Everyone*, pp. 1–10, 2023. [Online]. Available: <https://bionicsforeveryone.com/ottobock-c-leg-bionic-knee/>
- [5] —, "OSSUR: RHEO KNEE. <http://www.ossur.com/pages/12702>," pp. 1–11, 2023. [Online]. Available: <http://www.ossur.com/pages/12702>
- [6] J. Smits, "A review on energy harvesting systems from human and vehicular induced vibrations," vol. 1, no. 4583590, 2023.
- [7] H. Shi, Z. Y. Liu, and X. S. Mei, "Overview of Human Walking Induced Energy Harvesting Technologies and Its Possibility for Walking Robotics," *Energies*, vol. 13, no. 1, 2020. [Online]. Available: <https://www.scopus.com/inward/record.uri?eid=2-s2.0-85077319763&doi=10.3390%2Fen13010086&partnerID=40&md5=9b1f57afee79f3bf9e4d8183964894aa>
- [8] B. Laschowski and J. Mcphee, "Biomechanical Modelling of Sitting Movements for Designing Robotic Lower-Limb Prostheses and Exoskeletons with Energy Regeneration," no. 519.
- [9] M. Y. Liu, W. C. Tai, and L. Zuo, "Enhancing the performance of backpack energy harvester using nonlinear inerter-based two degrees of freedom design," *SMART MATERIALS AND STRUCTURES*, vol. 29, no. 2, 2020.
- [10] R. a. Serway and J. W. Jewett, "Physics for Scientists and Engineers with Modern Physic, 7 ed," *Brooks/cole*, vol. Cengage Le, p. 739(1215), 2008. [Online]. Available: <http://books.google.com/books?id=XgweHqlvtiUC&pgis=1>
- [11] T. Element, "Will stacking magnets together make them stronger? — totalElement," pp. 1–5, 2024. [Online]. Available: <https://totalelement.com/blogs/working-with-neodymium-magnets/will-stacking-magnets-together-make-them-stronger>
- [12] J. Sleppy, "Batteries vs . Supercapacitors ? The Answer is Both ." *Capacitech Energy inc*, pp. 1–5.
- [13] W. Wei, Q. Li, F. Xu, X. Zhang, J. Jin, J. Jin, and F. Sun, "Research on an electromagnetic actuator for vibration suppression and energy regeneration," *Actuators*, vol. 9, no. 2, 2020. [Online]. Available: <https://www.scopus.com/inward/record.uri?eid=2-s2.0-85086643386&doi=10.3390%2FACT9020042&partnerID=40&md5=b79c2d056d6dbe987e70325d4776a80f>
- [14] S. M. M. Mofidian and H. Bardaweel, "A dual-purpose vibration isolator energy harvester: Experiment and model," *Mechanical Systems and Signal Processing*, vol. 118, pp. 360–376, 2019. [Online]. Available: <https://www.scopus.com/inward/record.uri?eid=2-s2.0-85053069265&doi=10.1016%2Fj.ymssp.2018.08.054&partnerID=40&md5=da89d790052fe7c5eb1aa5acac3355ac>
- [15] M. A. Halim, J. Y. Park, and IOP, "A miniaturized human-motion energy harvester using flux-guided magnet stacks," Kwangwoon Univ, Dept Elect Engn, 447-1 Wolgye Dong, Seoul 139701, South Korea, 2016.
- [16] S. Wang and D. C. Li, "Design and analysis of a plane vibration-based electromagnetic generator using a magnetic spring and ferrofluid," *JOURNAL OF THE KOREAN PHYSICAL SOCIETY*, vol. 67, no. 5, pp. 818–822, 2015.
- [17] S. Chamanian, H. Ulsan, O. Zorlu, S. Baghaee, E. Uysal-Biyikoglu, and H. Kulah, "Wearable battery-less wireless sensor network with electromagnetic energy harvesting system," *SENSORS AND ACTUATORS A-PHYSICAL*, vol. 249, pp. 77–84, 2016.
- [18] D. F. Berdy, D. J. Valentino, and D. Peroulis, "Kinetic energy harvesting from human walking and running using a magnetic levitation energy harvester," *SENSORS AND ACTUATORS A-PHYSICAL*, vol. 222, pp. 262–271, 2015.
- [19] M. A. Abdelnaby and M. Arafa, "Energy harvesting using a flextensional compliant mechanism," *JOURNAL OF INTELLIGENT MATERIAL SYSTEMS AND STRUCTURES*, vol. 27, no. 19, pp. 2707–2718, 2016.
- [20] A. Ali, L. F. Qi, T. S. Zhang, H. Li, A. Azam, and Z. T. Zhang, "Design of novel energy-harvesting regenerative shock absorber using barrel cam follower mechanism to power the auxiliaries of a driverless electric bus," *SUSTAINABLE ENERGY TECHNOLOGIES AND ASSESSMENTS*, vol. 48, 2021.
- [21] Y. Pan, T. Lin, C. Liu, J. Yu, J. Y. Zuo, and L. Zuo, "A Compact Ball Screw Based Electromagnetic Energy Harvester for Railroad Application," Virginia Tech, Dept Mech Engn, Blacksburg, VA 24060 USA, 2018.
- [22] W. Salman, L. F. Qi, X. Zhu, H. Y. Pan, X. T. Zhang, S. Bano, Z. T. Zhang, and Y. P. Yuan, "A high-efficiency energy regenerative shock absorber using helical gears for powering low-wattage electrical device of electric vehicles," *ENERGY*, vol. 159, pp. 361–372, 2018.
- [23] A. Gonzalez, J. L. Olazagoitia, J. Vinolas, I. Ulacia, and M. Izquierdo, "An Innovative Energy Harvesting Shock Absorber System for Motorbikes," *IEEE-ASME TRANSACTIONS ON MECHATRONICS*.
- [24] A. Maravandi and M. Moallem, "Regenerative Shock Absorber Using a Two-Leg Motion Conversion Mechanism," *IEEE-ASME TRANSACTIONS ON MECHATRONICS*, vol. 20, no. 6, pp. 2853–2861, 2015.
- [25] M. A. Halim and J. Y. Park, "Piezoelectric energy harvester using impact-driven flexible side-walls for human-limb motion," *MICROSYSTEM TECHNOLOGIES-MICRO-AND NANOSYSTEMS-INFORMATION STORAGE AND PROCESSING SYSTEMS*, vol. 24, no. 5, pp. 2099–2107, 2018.
- [26] X. Zhong, B. Wang, R. Li, Y. Wu, M. Ma, and H. Deng, "Energy conversion mechanisms of a seesaw-type energy harvester," *Journal of Physics D: Applied Physics J. Phys. D: Appl. Phys.*, vol. 55, p. 11, 2022. [Online]. Available: <https://doi.org/10.1088/1361-6463/ac5941>
- [27] Z. Wang, T. Li, Y. Du, Z. Yan, and T. Tan, "Nonlinear broadband piezoelectric vibration energy harvesting enhanced by inter-well modulation," *Energy Conversion and Management*, vol. 246, p. 114661, oct 2021.
- [28] R. Shukla and A. J. Bell, "PENDEXE: A novel energy harvesting concept for low frequency human waistline," *SENSORS AND ACTUATORS A-PHYSICAL*, vol. 222, pp. 39–47, 2015.
- [29] J. X. Zhou, X. H. Zhao, K. Wang, Y. P. Chang, D. L. Xu, and G. L. Wen, "Bio-inspired bistable piezoelectric vibration energy harvester: Design and experimental investigation," *ENERGY*, vol. 228, 2021.
- [30] H. Shi, S. Luo, J. Xu, and X. S. Mei, "Hydraulic system based energy harvesting method from human walking induced backpack load motion," *ENERGY CONVERSION AND MANAGEMENT*, vol. 229, 2021.
- [31] T. W. A. Blad and N. Tolou, "On the efficiency of energy harvesters : A classification of dynamics in miniaturized generators under low-frequency excitation," *Journal of Intelligent Material Systems and Structures*, 2019.
- [32] "Diode Dynamic Resistance," *Electronics, Physics and radio*, vol. 10, no. September, pp. 1–6. [Online]. Available: <https://www.physics-and-radio-electronics.com/electronic-devices-and-circuits/semiconductor-diodes/dioderesistance-staticresistance-dynamicresistance.html#:~:text=Thedynamicresistanceisthe,currentflowthroughthediode>
- [33] J. Pikkarainen, "What Is ESR and Why Does It Matter ? Part 2," no. August 23, pp. 1–6, 2016. [Online]. Available: [https://www.skeletontech.com/skeleton-blog/what-is-esr#:~:text=Equivalentseriesresistance\(ESR\){%}2C,usuallydissipatedasundesirableheat](https://www.skeletontech.com/skeleton-blog/what-is-esr#:~:text=Equivalentseriesresistance(ESR){%}2C,usuallydissipatedasundesirableheat)
- [34] M. A. A. Abdelkareem, L. Xu, M. K. A. Ali, A. Elagouz, J. Mi, S. J. Guo, Y. L. Liu, and L. Zuo, "Vibration energy harvesting in automotive suspension system: A detailed review," *APPLIED ENERGY*, vol. 229, pp. 672–699, 2018.
- [35] Y. Zou, L. Bo, and Z. Li, "Recent progress in human body energy harvesting for smart bioelectronic system," *Fundamental Research*, vol. 1, no. 3, pp. 364–382, 2021. [Online]. Available: <https://doi.org/10.1016/j.fmre.2021.05.002>
- [36] Y. Zou, V. Raveendran, and J. Chen, "Wearable triboelectric nanogenerators for biomechanical energy harvesting," *Nano Energy*, vol. 77, no. June, p. 105303, 2020. [Online]. Available: <https://doi.org/10.1016/j.nanoen.2020.105303>

[37] Umicore, "Fuel cells vs . batteries : what ' s the difference ?" pp. 1-7, 2022.

[38] K. magnetics, "Magnetic Dipole Moment," pp. 1-5, 2023. [Online]. Available: <https://www.kjmagnetics.com/blog.asp?p=dipole>

APPENDIX A DESIGN STRATEGY

A.1 Concept generation

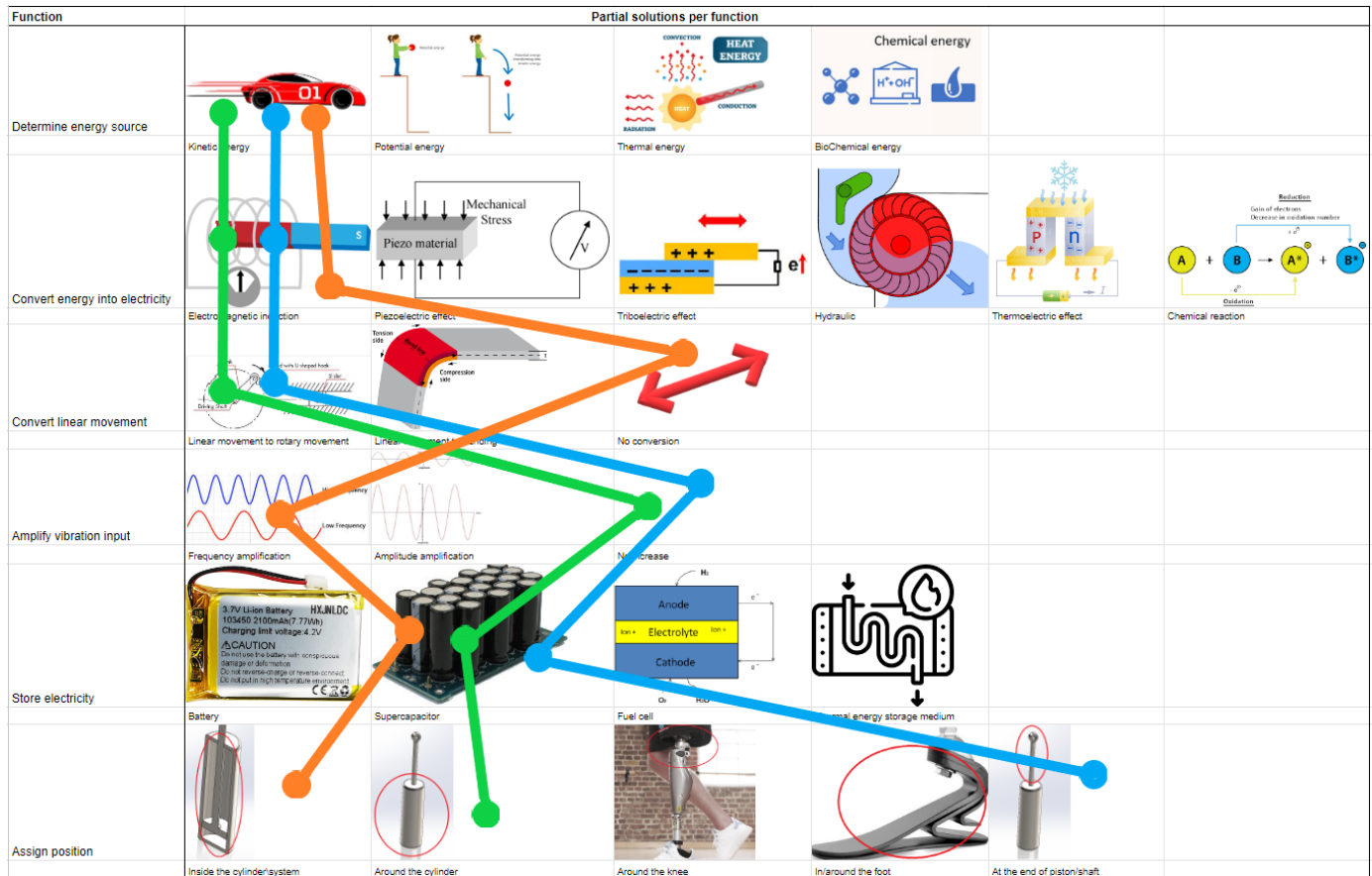


Fig. 25: Morphological chart. Concept 1 is depicted in orange, concept 2 in blue and concept 3 in green.

From the morphological chart a few paths are taken. For each concept the path taken is depicted in Figure 25. All three concepts use the electromagnetic induction principle to convert kinetic energy into electricity. The morphological chart has 6 rows which each pose as a step towards a concept. These are explained as follows:

A.1.1 Determine energy source

Mainly, biomechanical energy harvesting has three main sources. Limb movement, heat, and biochemical potential. From these three, body motions produce the most. Harvesting biochemical energy from bio-fluid is relatively difficult and the output signal is weak. Examples of this is harvesting electricity from human sweat, lactate, or water vapor from human breath [35]. Energy is harvested through a chemical reaction, for instance oxidation of organic compounds in sweat which generates protons and electrons [35]. This can be used to generate electrical energy.

Considering thermal energy, the thermoelectric effect is the direct conversion of temperature differences to electric voltage and vice versa via a thermocouple and can therefore be used to convert thermal energy into electricity [35].

Thermoelectric devices create a voltage when there is a different temperature on each side. Thermoelectric generators work and are promising, only the output is in micro watts which is very low [36]. An example of this is harvesting the heat energy from the human body (thermal energy). Thermoelectric generators are taped on your skin which generate electricity [36]. But for a larger power output you would need a larger surface area of thermoelectric generators on your skin which get uncomfortable [36].

Therefore kinetic energy and potential energy pose as the better energy sources. Human walking induced energy is much easier to harvest and convert into electricity in relatively greater quantities because it contains the kinetic and potential energy of the body. You have foot strike, body inertia and vibrations.

A.1.2 Convert energy into electricity

Hydraulics show potential only they require a pipeline system to work, which could leak and take up space which is already limited for the required application in this study. Also, hydraulics have very low efficiencies since lots of energy is lost in the hydraulic loop [6].

Piezoelectric structures have the advantage of simple architecture, flexible design, and easy fabrication. Therefore it is easier to produce task specific designs with this material. Effective deformation however is relatively small, which limits the generated electricity (μW). Therefore, most piezoelectric designs contain some sort of amplification mechanism to increase the effective strain or frequency [6]. Otherwise power output is even lower.

Considering the triboelectric effect, electricity is generated as two surfaces come in contact with each other or slide against each other. Triboelectric nanogenerators are proposed as biomechanical energy harvesters [36]. Due to the contact and sliding of the materials, the materials wear (friction, abrasion) and since it already uses expensive materials and complex fabrication, this method is not widely adopted [36]. Since it is placed on the skin, you also need anti sweat packaging to ensure chemical stability, and breathable material (like textiles for instance) [36]. To conclude, durability is low. For a larger power output you need a larger surface area of triboelectric nanogenerators which could become uncomfortable for the user. Also this material is embedded in for example shoes or textile which limits design freedom.

Electromagnetic induction shows great potential in power output (mW) and does not require that much space as it is also easily integrated into systems. It is a robust method with a long lifetime. Prior to this study a literature review was conducted in order to review the state of the art energy harvesting systems. This study concluded that electromagnetic, piezoelectric and hydraulic energy harvesting are the most intensely studied methods. With electromagnetic energy harvesting providing the highest power output. Higher than with the use of smart materials (triboelectric) or piezoelectric materials.

A.1.3 Convert linear movement

This discusses methods for converting the linear movement to rotary or bending to transmit the motion to the energy conversion medium. For instance the rack and pinion system or the use of bevel gears (differential). When linear movement is transferred to bending, it means that piezoelectric structures are in place since deformation/strain harvests electrical energy. No conversion means that the linear movement is used to generate electrical energy.

A.1.4 Amplify vibrational input

Amplitude amplification is realised by adding a proof mass or with magnetic repulsion for instance. Frequency amplification is realised by for instance using sets of gears or springs (elastic energy). This amplifies the vibrational input.

A.1.5 Store electricity

Fuel cells require electrolysis and then the hydrogen is stored for use. When you need electricity hydrogen is fed in the fuel cell and you have electricity [37]. During electrolysis an electric current passes through an electrolyte solution or molten compound to initiate chemical reactions that result in the decomposition of the electrolyte into its constituent elements [37]. However this requires hydrogen storage and an electrolysis system which is somewhat cumbersome. Electrolysis is not an energy-efficient process [37]. It requires a significant amount of energy input to drive the electrochemical reactions involved. Hydrogen is significantly more energy dense than batteries, which means a fuel-cell pushed powertrain weighs less [37].

Thermal energy storage media are materials or substances specifically designed to store thermal energy. Examples include phase change materials (PCMs), molten salt, concrete or rock beds, water and thermochemical storage materials. These all have the capability to absorb and release thermal energy. Heat exchangers facilitate the transfer of thermal energy, while thermal energy storage media are materials or substances to store and release thermal energy.

Considering batteries and supercapacitors, the supercapacitor is used for energy storage undergoing frequent charge and discharge cycles at high current and short duration [12]. While batteries can provide more energy over much longer periods of time than a supercapacitor, supercapacitors can deliver energy quicker than a battery. Delivering energy quickly, which is needed to level a load or provide the burst of current needed to turn on a motor, can waste the battery's capacity and put stress on the battery that shortens its operating life. For this reason, batteries are said to have a low power density or a low specific power [12]. Put another way, using a battery in applications where there is a short burst or pulse of power may be problematic. Supercapacitors have a much higher life cycle and can withstand a large number of charge and discharge cycles compared to batteries. They also have high efficiency, with minimal energy losses during charging and discharging. Batteries, while having a lower cycle life, can still provide long-term energy storage but may experience degradation over time due to chemical reactions and aging. Batteries are well suited for applications requiring high energy density and long term storage, while supercapacitors excel in applications requiring high power density, rapid discharge capabilities and a high number of cycles.

A.1.6 Assign position

This concerns the location of the harvesting system. This can be inside the hydraulic cylinder, around the hydraulic cylinder, around the knee, in or around the foot/ankle, or at the end of the hydraulic piston shaft.

A.2 Performance criteria

The criteria used to assess the concepts are the performance criteria described in Table 2. These criteria are first ranked based on their independent relevance to the project. This process is presented in Table 8.

Weight is the most important criteria. This is because if the final design is too heavy it hinders the gait pattern. The harvesting system should be an addition and not hinder or restrict the movement in any way. That is also why size comes in second. It is less important than weight since walking with a heavier system hinders the user more than walking with a larger system. Walking with a volume of 1 m³ feathers is always easier than walking with, for instance, 1m³ of bricks. Lighter systems burden the user less.

After this comes the potential power output. This is more important than feasibility and interoperability and less important than weight and size. Since the system is not an addition anymore, no matter how much power it generates if it is too heavy or too large. It is more important than feasibility and interoperability since this is the main goal the project. If the system does not generate power then there is no use.

Feasibility comes next and is more important than interoperability. This criteria assesses if the design can be built and operated using available technologies, materials and engineering principles. Design complexity is a part of this criteria. The complexity deals with the number of moving parts, interconnections, and hierarchy of subsystems. The interoperability deals with the integration of the concept into the prosthetic leg system. This considers the phase after the assembly of the concept. So can the designed concept be smoothly integrated in the prosthetic leg? And how well does it interact with with the prosthetic leg? It can be concluded that based on this analysis it is more important to first have a working concept and then making sure there is a smooth interaction between prosthetic device and harvesting system. A more complex system is harder to build and make function properly. If this is the case then interoperability is not necessary to assess if the prototype does not even function. A step by step approach is taken to from a firm basis. The 'Cost of materials' scores zero points and therefore the concepts are not assessed considering this criteria.

TABLE 8: Weighted criteria

	Weight	Size	Potential power output	Feasibility	Interoperability	Cost of materials	Score	Total factor
Weight	1	1	1	1	1	1	5	5
Size	0	1	1	1	1	1	4	4
Potential power output	0	0	1	1	1	1	3	3
Feasibility	0	0	0	1	1	1	2	2
Interoperability	0	0	0	0	1	1	1	1
Cost of materials	0	0	0	0	0	0	0	0

A.3 Concept selection - detailed explanation

The evaluation of the concepts is done with the use of a Harris profile. A Harris profile is a graphic representation to visualise the comparison of the concepts. The points regarding the criteria are given in a matrix and the different concepts are scored between +2 and -2 respectively (the score of zero is not possible). The outcome of this matrix shows specifically how well certain criteria are met and exposes each concept its strengths and weaknesses. From this procedure it can easily be seen which concept has the most potential to succeed. The concept with the most amount of points is worked out further.

A.3.1 Weight

The weight assessment of the concepts is done in Solidworks. For each concept material properties are assigned. If a material can not be found in Solidworks, a material with similar properties is assigned. The second concept contains a small generator. The weight for this is searched online. From this analysis the levitated magnet concept performed best and the rack and pinion concept performed the worst.

A.3.2 *Size*

The sizes of the concepts are determined in Solidworks as well. The volumes are evaluated for the whole system (incl. an hydraulic cylinder and piston) and for the harvesting system itself. From this analysis, concept 1 (the levitated magnet) performed best (+2) and concept 2 (the rack and pinion) performed worst (-1).

A.3.3 *Potential power output*

For this criteria a more in depth analysis is made, since it is very situation specific. For each concept a model is setup in MATLAB to calculate the potential power output in milliwatts. For the levitated magnet concept and the compliant spring formulas for determining the change in magnetic flux are setup to determine the induced voltage in the coils. For the rack and pinion concept the power output is determined by calculating the force and torque at the input which leads to a torque output at the generator through the gerset. The rack and pinion is predicted to have the largest power output (+2). The levitated magnet and the compliant spring have power output values that are very close to each other and therefore scored the same (+1).

A.3.4 *Feasibility*

This criteria assesses if the design can be built and operated using available technologies, materials and engineering principles. Design complexity is also a part of this criteria. The complexity is assessed based on the number of moving parts, interconnections and hierarchy (which is defined as the amount of subsystems interacting with each other to achieve overall system functionality). The levitated magnet concept has the least amount of moving parts, interconnections and hierarchy in subsystems. There are 3 moving magnets, 2 of which are placed on springs. Furthermore the whole system moves on the piston as well. There are three interconnects, the magnets on the springs and the system as a whole connected to the piston. For the system to function properly the middle magnet must impact the top and bottom magnet, therefore the hierarchy levels add up to two. Furthermore this design can be built using 3D printing technology, making manufacturing easier. Other parts such as springs, magnets and copper wire is also easy to get by. The levitated magnet scored a +2.

The second concept has 9 moving parts which are all interconnected to each other, via a shaft and one-way gears. For the whole system to function properly the rack and pinion must transfer the linear movement to rotary movement in the shaft to engage the bevel gears which rotate the generator shaft. Therefore hierarchy adds up to two. Manufacturing is a little bit more difficult since gears, rack and pinion must be precisely produced to realize smooth operation. Not all parts can be 3D printed since they need to be strong and durable. Also the generator must be carefully selected to ensure a good fit, this however should not be that hard to get by. During operation the rack is exposed to buckling and therefore strong material must be chosen. This concept scores a -1.

The compliant spring concept has 4 moving parts, the compliant component with helix screw, the helix nut, the case and the ball bearing. The clutch case is mounted on the ball bearing. The whole system is connected to the piston shaft. This is to make sure that there is a linear up and down movement pushing on top of the compliant component. The complexity lies in the clutch mechanism which must work well together with the helix screw and introduce rotation. Hierarchy adds up to two. Manufacturing can be done via 3D printing. Only the ball bearing, magnets and copper wire must be ordered. Material fatigue also plays a role as it must be durable. Therefore this concept scores second best (+1).

A.3.5 *Interoperability*

This criteria assesses the operational feasibility. So if the system can be smoothly integrated and how well it interacts with the leg prosthesis. The functioning of the levitated magnet concept is the easiest of the three concepts, since it can be placed inside or even outside the cylinder. It harvests any vibration due to the levitating magnet being easily influenced by perturbations. Also it is not dependent on some contact from other parts of the leg prosthesis, as it can function on its own.

The rack and pinion concept functioning is dependent on the overall smooth function of the gears rack and pinion. The rack must be firmly connected to the leg prosthesis. When everything is in place, the strong materials ensure smooth operation between prosthesis and harvesting system. It is however dependent on knee flexion and extension. So compared to the levitated magnet concept, the second concept is dependent on interaction with the leg prosthesis. When there is no knee flexion and extension, no energy is harvested.

The compliant spring concept functioning is dependent on the pressing down of the compliant component. Furthermore this design can be placed around a shaft. Interaction with the leg prosthesis is based on the pushing down of the compliant component which does not require any complex integration. It is however dependent on knee flexion and extension of the leg prosthesis, as this introduces reciprocating movement from the piston shaft. The overall assessment can be seen in Table 9.

TABLE 9: Harris profile

Criteria	Total factor	The Levitated magnet			The Rack and pinion			The compliant spring					
		-2	Score	+2	Total	-2	Score	+2	Total	-2	Score	+2	Total
Weight	5				5				-5				10
Size	4				8				-4				4
Potential power output	3				3			6					3
Feasibility	2				4				-2				2
Interoperability	1				2				-1				1
					22				-6				20

The levitated magnet concept and the compliant spring concept both score very well. Assessing each performance criteria it can be concluded that the designs are very similar in performance. To mainly validate the potential power output calculations (as well as the other performance criteria), both concepts are built into prototypes. This helps in choosing which concept to develop further into a final design.

A.4 Prototyping - detailed explanation

As stated in section 2.3.3, two proof of concept models are assembled in order to validate the power output predictions. All parts but the ball bearing, magnets and copper wire are 3D printed. During prototyping multiple design iterations are made. These iterations are explained in this section as well. For both the levitated magnet and the compliant spring the prototypes are not built around a hydraulic cylinder. This keeps assembly quick and simple. So in this stage, design alterations are made for the concepts to function without a hydraulic cylinder.

A.4.1 The levitated magnet prototype

The levitated magnet needs a shaft in order for the magnets not to flip inside the housing due to polar attraction. In the initial concept design the magnets remain in the same orientation due to the piston shaft. So in the prototype design an axis is added to the housing to replace the piston shaft. Also the steel springs are replaced by 3D printed conical springs. First the normal steel springs are tested. Only the windings of the steel springs are attracted to the magnet and therefore the springs do not function properly. So the springs are 3D printed. First in normal shape and then in conic shape. Conical springs have the advantage of very low solid height when compressed. Therefore the amplitude of the induced vibrations is not restrained by the solid height of a normal parallel spring, since this is experienced during testing. The design and prototype are depicted in Figure 26.

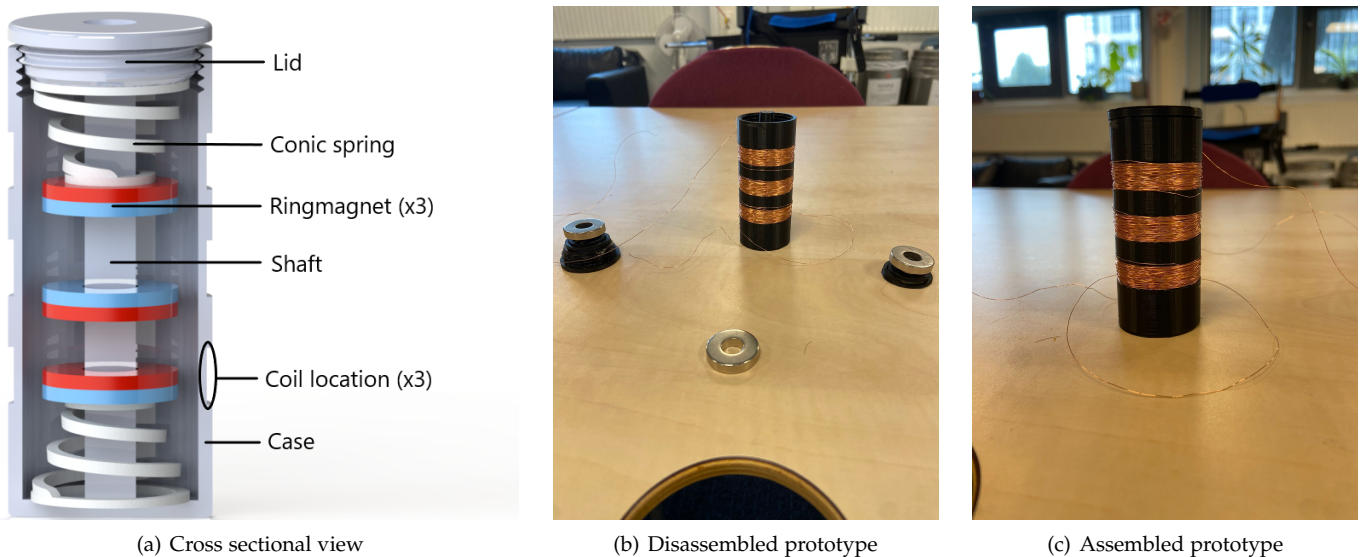


Fig. 26: The levitated magnet - prototype design. The hydraulic piston shaft is replaced by a 3D printed axis. This prevents the magnets to flip inside the housing. The springs are replaced by 3D printed conic springs. Copper wire is wound around the housing to form 3 coils. Each coil contains 100 windings. The images from left to right show a cross sectional view of the design (a), a disassembled view (b) and an assembled view (c).

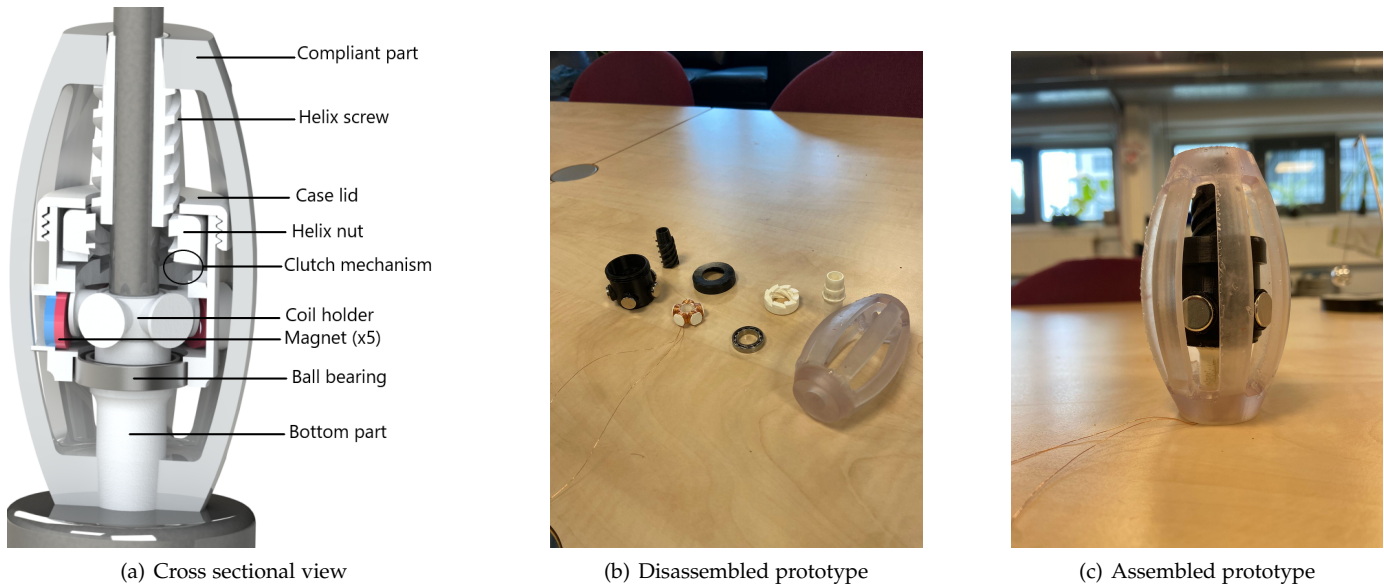


Fig. 27: The compliant spring - prototype design. The prototype is built and does not need the piston shaft or an additional axis. Each coil has 100 windings. The images from left to right show a cross sectional view of the design (a), a disassembled view (b) and an assembled view (c).

A.4.2 The compliant spring prototype

As for the compliant spring there are no design changes for the prototype to be built. There are however multiple iterations in dimensions in order to make all parts fit with the right tolerances. These iterations consider the helix crew and nut for smooth rotation and the holes in the walls of the clutch case to ensure a tight fit between case and magnets. In addition, the configuration of the magnets is also determined such that the magnetic field lines point through the coils. This is done by simulating the magnetic field lines and changing the orientation of a magnet or multiple magnets. For a magnet there are only two configurations possible, which is pointing the north pole towards the center in radial direction or the south pole (Figure 28). The prototype is depicted in Figure 27.

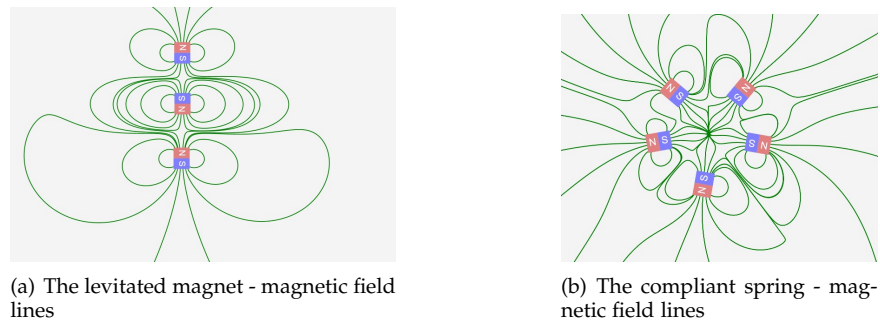


Fig. 28: Magnetic field lines simulation of the levitated magnet (a) and the compliant spring (b). For the compliant spring, this is the chosen configuration. When changing this to for instance North and South pole alternately, the magnetic field lines of one magnet approaches the other instead of pointing towards the coils. Therefore this configuration is chosen.

A.5 The compliant spring - final design

A.5.1 Compliant component material

One aspect which requires more elaboration is the material choice of the compliant component for the final design. Multiple materials are tested, with different thicknesses. These are:

- Resin form flexible 80A
- Resin form elastic 50A
- Black TPU

These are all printed with different thicknesses and assembled to assess the functioning. What can be concluded from this is that TPU with a thickness of 2 mm performs best and is incorporated in the final design (Figure 29).



Fig. 29: Different compliant base materials and different thicknesses of the side walls

A.5.2 Clutch mechanism

Figure 30 shows a zoomed in depiction of the clutch mechanism. The green parts (helix screw and nut) impose a rotation towards the yellow parts (case with top and bottom lid). In figure 30(a) there is no rotation transmitted, since the teeth of the nut and the case are not hooked into each other. As the helix screw moves further down, the nut's teeth are pushed into the case's teeth (figure 30(b)). When the engagement is strong enough to impose rotation towards the case it starts rotating. The helix screw moves further down to keep imposing rotational movement. As the helix screw moves up, it lifts the nut. This causes the teeth of the nut and case to be unhooked and no rotation is imposed towards the case. This whole process can be reversed and initiated again.

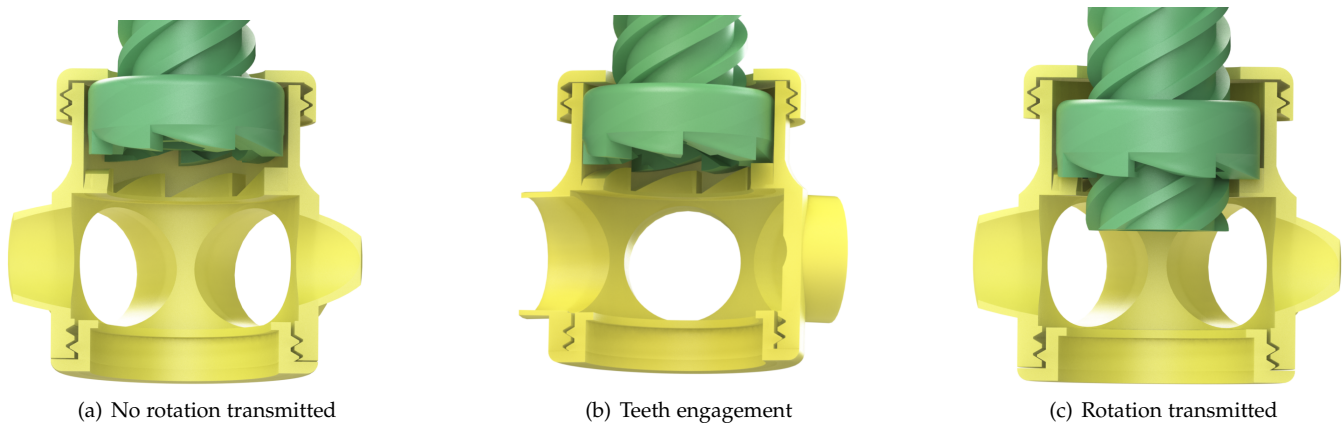


Fig. 30: Elaboration of the clutch mechanism. The first image (a) shows a depiction when no rotation is transmitted towards the case. The second image (b) shows that as the helix screw and nut move down, the teeth of the nut and case hook into each other and introduce rotation. Image (c) depicts the helix screw moving further down into the nut, and therefore introducing more rotations towards the case. This whole process can be reversed and initiated again.

A.6 Circuit design - detailed explanation

The voltage multiplier circuit is built, with the schematic depicted in Figure 31. This circuit functions to rectify the AC input to a DC output. In addition the voltage is doubled. Which is explained by the two half cycles depicted in Figure 32. When the current flows clockwise capacitor C1 is charged to voltage V_{in} . When the current flows anticlockwise capacitor C2 is charged to $2V_{in}$. During this anticlockwise flow C1 is discharged and therefore the voltages of V_{in} and VC1 add up. This is due the polarity of the capacitors. In this situation there are no losses assumed. There is however a voltage drop (V_f , forward voltage) across the diodes. Selecting a diode is done carefully, since different diodes have different V_f . Diodes with a low voltage drop of about 0.2 - 0.3 V are selected (Schottky BAT43).

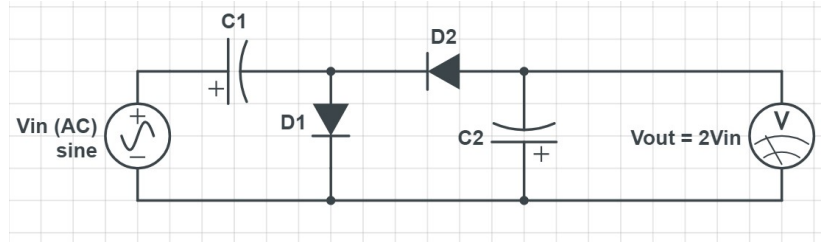


Fig. 31: Energy harvesting circuit design. The circuit contains 2 diodes and 2 capacitors in a ladder like design. The AC input is rectified to be a DC output where the voltage is doubled.

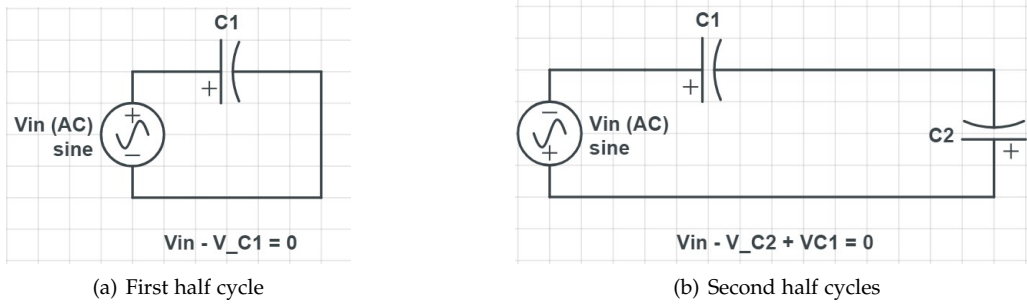


Fig. 32: Electrical circuit first (a) and second half cycle (b). This illustrates the flow of the current when an AC voltage is applied.

APPENDIX B

CALCULATION DESCRIPTION

B.1 EMF and power calculations

In this section the step by step descriptions of the calculations are presented:

Step 1: Calculate the magnetic field strength (B).

This is determined with the formula $B = \frac{\mu_0 m}{2\pi(z^2 + r^2)^{3/2}}$

Where:

B = the magnetic field strength [T]

$\mu_0 = 4\pi * 10^{-7}$. The permeability of free space [N/A^2].

m = Magnetic moment [Am^2].

z = Distance from the magnet to the coil [m].

r = Magnet radius [m].

For both concepts a more simple approach is taken for the calculations. For the first concept (the levitated magnet) the power calculation is done for a magnet moving through a coil. For the third concept (the compliant spring) the power is calculated for a magnet rotating around a coil. For the levitated magnet the distance z is varying linearly as the central axis of the magnets and the central axis of the coils are aligned. Since the input is a vibration, a harmonic motion is assumed as the input. For the third concept (the compliant spring) the distance x and y both vary as well as the angle between the normal of the magnet and the normal of the coils surface. The magnetic moment is determined based on the size and strength of the magnets. The magnetic moment for concept 1 has been set on $m = 1.8$ and for concept 3 $m = 0.89$. This is based on their volume. The magnetic moment of a Neodymium Iron Boron (strongest grade) disc the same size as a US Penny has a magnetic moment of $m = 0.422$ [38]. The other magnetic moment values are then calculated to ratio. Since the magnets used in both concepts are composed of the same material, their magnetization value is the same. The magnetization M is defined as the magnetic moment divided by the volume. So this effectively gives the formula $\frac{m_2}{m_1} = \frac{v_2}{v_1}$.

Step 2: Calculate the magnetic flux (Φ)

The magnetic flux through the coil is determined with the formula $\Phi = BA \cos(\theta)$

Where:

Φ = the magnetic flux at the coil [Wb]

B = The magnetic field strength [T].

A = The area of the coil [m^2].

θ = The angle between the normal of the coil and the normal of the magnet [deg].

For the levitated magnet concept this formula is simplified to $\phi = BA$, since $\cos(0)$ is 1 and remains such. For the compliant spring concept the angle changes with respect to time.

Step 3: Calculate the rate of change of change of the magnetic flux ($\frac{d\Phi}{dt}$)

This is determined by taking the derivative of Φ with respect to time. The magnetic flux is a function of time due to the varying of z for both concepts and θ for concept 3. For the first concept the linear movement is a function of time. The distance from magnet to coil varies and is implemented in the magnetic field strength B . As stated earlier a harmonic input is assumed: $z(t) = A \sin(\omega t)$. Where A is the amplitude and ω is $2\pi f$.

For the third concept the x and y positions as well as the angle changes with respect to time. The magnet moves around the coil with an angular speed ω . So Φ becomes $\Phi(t) = BA \cos(\omega t)$. The distance between the magnet and coil is determined based on the circular path of the magnet. The magnet rotates around the coil (stationary) on a circle of radius 14.5 mm. Since the magnet rotates around the coil, the distance between magnet and coil is determined with a harmonic motion in the xy -plane. So z becomes a distance vector of x and y , where x and y are harmonic motions with the amplitude being the radius of the circular path.

The change of magnetic flux with respect to time for both designs is calculated with a simple loop. Where for every time step from 0 to 1000 the difference between the magnetic flux at that instance and the previous instance is calculated.

Step 4: Calculate the induced emf (ϵ)

This is determined with the formula $\epsilon = N \frac{d\Phi}{dt}$.

Where:

ϵ = the induced voltage [V].

N = the amount of coil windings.

$\frac{d\Phi}{dt}$ = the magnetic flux change with respect to time.

To assess concepts fairly, the same amount of coil windings for both concepts is used. For both concepts $N = 100$.

For both concepts the emf is plotted versus time (Figure 9 and Figure 10). The graph of the first concept should have two positive and two negative peaks (for 1 period). As the magnet approaches the coil from the top (south pole pointing down), the magnet's magnetic field causes a change in magnetic flux through the coil. This induces a current. For the direction Lenz's law states: "Direction of the induced emf is such as to oppose the change that caused it." This means that as the magnets enters and exits the coil, a change of direction of the current is experienced. First the current flows clockwise (south pole) and after anticlockwise (north pole). Therefore having a positive and negative peak, going through zero in between. The voltage is zero as the magnet is in the middle of the coil. This is due to the fact that at that instance, the magnetic field lines from the magnet's north and south pole both induce a current but in opposite directions. The voltages therefore cancel each other out and the emf becomes zero. The same happens as the magnet approaches the coil from the bottom.

For concept 3 the graph (for 1 period) is explained as follows with Lenz's law: As the magnet approaches the coil (with the north pole pointing in radial direction), it is such that the coil rejects the approach. So a north pole establishes at the top of the coil. When the magnet starts to move away, it wants to attract the magnet creating a south pole. First the current in the coil flows anticlockwise and after it flows clockwise.

When the magnet approaches the bottom of the coil, there is a north pole created at the bottom and a south pole at the top. The same as when it left the coil from the top part. Therefore the current flows clockwise again. When the magnet leaves the bottom part it wants to attract the magnet and have a south pole at the bottom and north pole at the top. The current flows anticlockwise again. That is why in the emf you first have a negative peak, then two positive peaks and end with a negative peak again. When the magnetic field lines are aligned with the windings of the coil, the emf is zero since the magnetic field lines are not cutting the coil windings.

Step 5: Calculate the power output (P)

This is determined with the formula $P = \frac{\epsilon^2}{R}$

Where:

P = the output power [W].

ϵ = the induced emf voltage [V].

R = the resistance [Ω].

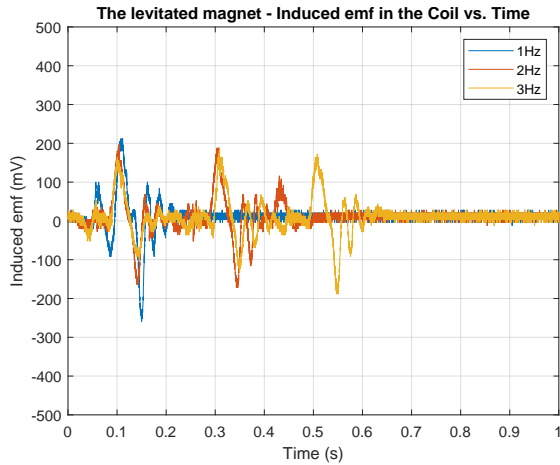
For a fair comparison both designs have the same resistance in their energy harvesting circuit. For now the resistance of both concepts has been set to $R = 100 \Omega$.

APPENDIX C

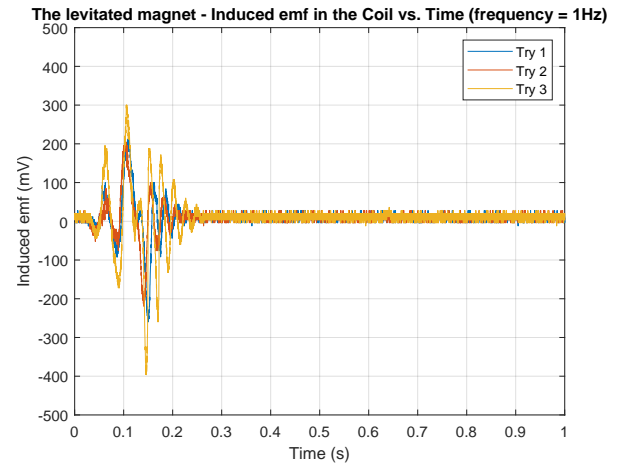
ADDITIONAL PROTOTYPE RESULTS

C.1 Prototype oscilloscope recordings - full results

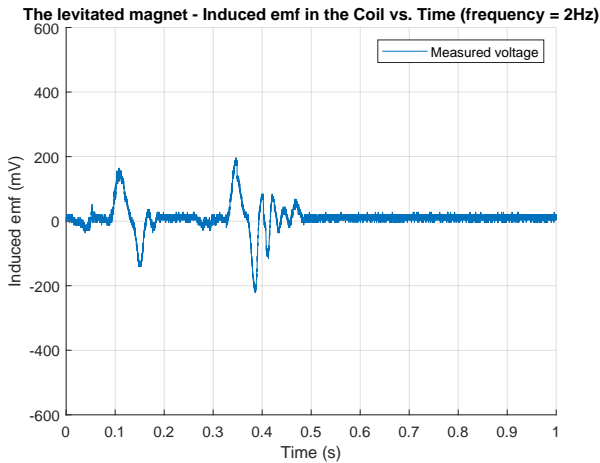
During the prototyping stage for both prototypes the induced emf is measured with an oscilloscope and the results are compared with each other for 2 Hz (normal walking frequency). The tests however are done for 1 - 3 Hz, these results are depicted in Figure 33 and Figure 34. It shows that for each tested frequency the compliant spring performs better in terms of induced voltage. Therefore this prototype is chosen to be developed into a final design.



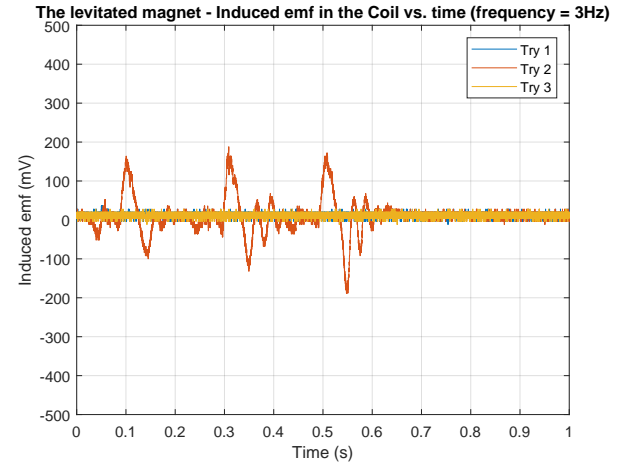
(a) Induced voltage (1 - 3 Hz)



(b) Induced voltage (1 Hz)

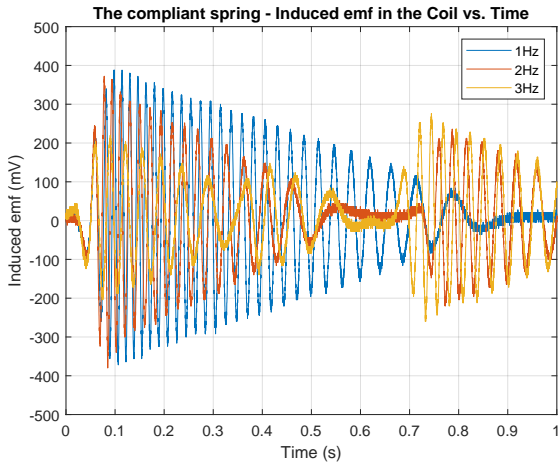


(c) Induced voltage (2 Hz)

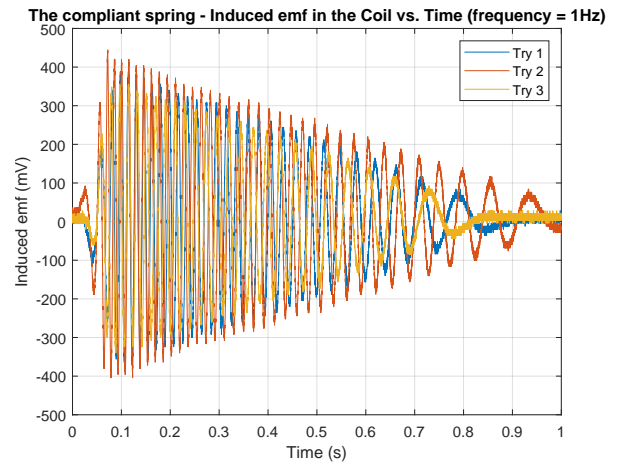


(d) Induced voltage (3 Hz)

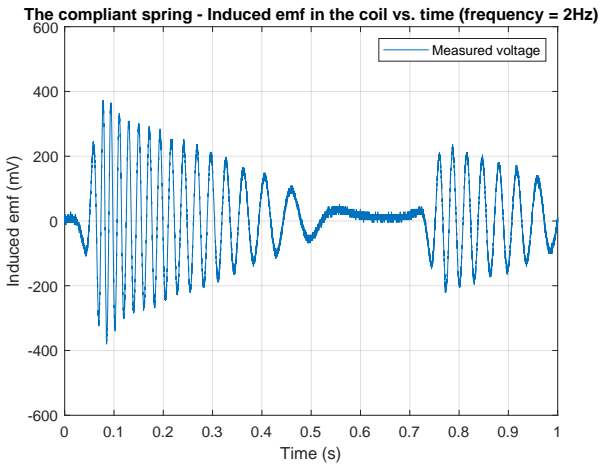
Fig. 33: Oscilloscope measurements for the levitated magnet. Input has been done by hand for 1 - 3 Hz.



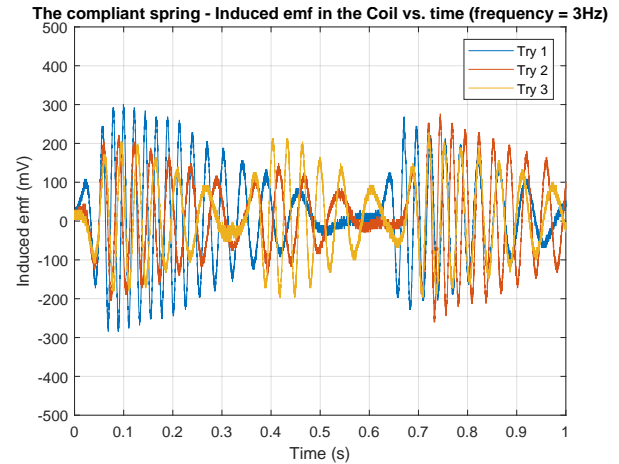
(a) Induced voltage (1 - 3 Hz)



(b) Induced voltage (1 Hz)



(c) Induced voltage (2 Hz)



(d) Induced voltage (3 Hz)

Fig. 34: Oscilloscope measurements for the compliant spring. Input has been done by hand for 1 - 3 Hz.

APPENDIX D
ADDITIONAL EVALUATION RESULTS
D.1 Experiment results overview

Table 10 shows the results for every amplitude and frequency input that is tested during the experiment. The figures depicted in section 5 are based on this data.

TABLE 10: Result highlights for 9mm, 10mm, 11mm and 12mm amplitude

Amplitude [mm]	Frequency [Hz]	Peak Voltage [mV]	Peak input force [N]	Peak input power [mW]	Peak output power [mW]	Power mass [mW/g]	Charged voltage [mV]	Efficiency (peak) [%]
9	1	104	23,665	213,0	1,08	0,009	16	0,507
9	2	168	24,12	434,2	2,82	0,023	48	0,65
9	3	192	25,23	681,2	3,68	0,030	68	0,54
9	4	232	25,53	919,1	5,38	0,044	100	0,59
9	5	248	26,79	1205,6	6,15	0,050	140	0,51
9	6	304	26,75	1444,5	9,73	0,080	168	0,67
9	7	328	27,06	1704,8	10,75	0,088	216	0,63
9	8	344	27,83	2003,8	11,83	0,097	248	0,59
9	9	384	27,27	2208,9	14,75	0,121	324	0,67
9	10	384	28,6	2574,0	17,3	0,142	348	0,67
10	1	96	22,52	225,2	0,92	0,008	24	0,409
10	2	160	23,72	474,4	2,56	0,021	36	0,54
10	3	208	25,7	771,0	4,33	0,035	84	0,56
10	4	256	26,44	1057,6	6,55	0,054	124	0,62
10	5	288	26,91	1345,5	8,29	0,068	164	0,62
10	6	312	27,79	1667,4	9,73	0,080	208	0,58
10	7	352	28,09	1966,3	12,39	0,102	240	0,63
10	8	384	27,95	2236,0	14,74	0,121	364	0,66
10	9	400	27,92	2512,8	16	0,131	388	0,64
10	10	424	28,8	2880,0	17,97	0,147	396	0,62
11	1	120	23,49	258,4	1,44	0,012	36	0,557
11	2	184	25,41	559,0	3,39	0,028	64	0,61
11	3	240	26,32	868,6	5,67	0,046	92	0,65
11	4	296	26,98	1187,1	8,76	0,072	176	0,74
11	5	328	28,19	1550,5	10,76	0,088	222	0,69
11	6	360	28,89	1906,7	12,96	0,106	264	0,68
11	7	400	28,78	2216,1	17,3	0,142	296	0,78
11	8	400	28,93	2545,8	16	0,131	376	0,63
11	9	424	28,49	2820,5	17,98	0,147	392	0,64
11	10	480	28,37	3120,7	23,04	0,189	408	0,74
12	1	124	25,66	307,9	2,4	0,020	48	0,779
12	2	216	26,6	638,4	4,665	0,038	92	0,73
12	3	276	28,4	1022,4	7,62	0,062	164	0,75
12	4	332	29,7	1425,6	11,2	0,092	224	0,79
12	5	364	30	1800,0	13,3	0,109	280	0,74
12	6	432	31,11	2239,9	18,6	0,152	320	0,83
12	7	428	30,9	2595,6	18,3	0,150	352	0,71
12	8	460	32,22	3093,1	21,2	0,174	396	0,69
12	9	508	31,98	3453,8	25,8	0,211	408	0,75
12	10	496	30,711	3685,3	25,2	0,207	444	0,68

APPENDIX E

EXTENDED DISCUSSION

E.1 Power demand

Figure 35 shows the power budget for sustaining a smart bionic leg with wireless sensing and motor controlled ankle and knee adjustments. Fully sustaining all electrical components requires an average power of 62.15 mW. Sustaining microprocessors and sensors requires an average power of 8.4 mW.

Power Budget Item	Active Power (W)	Period (s)	Active in Period (%)	Active Time in 1 min. (s)	Average Power in 1 min. (W)
MPU, ×4 units	2.00×10^{-3}	1.0	100	60	2.000×10^{-3}
Bluetooth 5.0 + RF chip Tx, ×4 units	1.08×10^{-1}	5.0	20	12	2.160×10^{-2}
Bluetooth 5.0 + RF chip sleep, ×4 units	1.80×10^{-4}	5.0	80	48	1.440×10^{-4}
MEMS 9 DOF, ×4 units	2.00×10^{-3}	1.0	100	60	2.000×10^{-3}
MEMS pressure sensor, ×4 units	2.00×10^{-3}	1.0	100	60	2.000×10^{-3}
Memory + misc. electric, ×4 units	2.00×10^{-3}	1.0	100	60	2.000×10^{-3}
Power conditioning circuit, ×4 units	4.00×10^{-4}	1.0	100	60	4.000×10^{-4}
Misc. elec. and leakage, ×4 units	2.00×10^{-3}	1.0	100	60	2.000×10^{-3}
DC motor, ×3 units, right ankle	$1.50 \times 10^{+0}$	6.0	0.17	0.1	2.501×10^{-3}
DC motor, ×3 units, left ankle	$1.50 \times 10^{+0}$	6.0	0.17	0.1	2.501×10^{-3}
DC motor, ×3 units, right knee	$1.50 \times 10^{+0}$	6.0	0.17	0.1	2.501×10^{-3}
DC motor, ×3 units, left knee	$1.50 \times 10^{+0}$	6.0	0.17	0.1	2.501×10^{-3}
Servo actuator, ×3 units, right ankle	$3.00 \times 10^{+0}$	6.0	0.17	0.1	5.001×10^{-3}
Servo actuator, ×3 units, left ankle	$3.00 \times 10^{+0}$	6.0	0.17	0.1	5.001×10^{-3}
Servo actuator, ×3 units, right knee	$3.00 \times 10^{+0}$	6.0	0.17	0.1	5.001×10^{-3}
Servo actuator, ×3 units, left knee	$3.00 \times 10^{+0}$	6.0	0.17	0.1	5.001×10^{-3}
Sum					6.215×10^{-2}

(a) Power budget of smart bionic leg

Fig. 35: Estimated power budget of a hypothetical smart prosthetic bionic leg with wireless sensing functionality and intermittent motor controlled ankle and knee adjustments.

E.2 Rectifying circuit - extended discussion

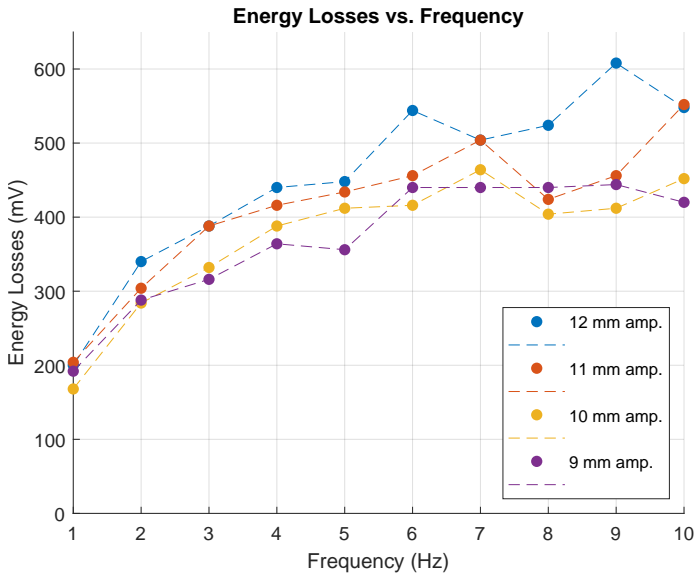
Discussing the energy loss in the rectifying circuit, there are some parts that need more explaining. As can be seen in Figure 36 the voltage loss increases with the frequency. An increase in input AC voltage is coupled to an increase in input frequency. The increase in loss is explained by the characteristics of the diode. The forward voltage drop is influenced by the exponential relation between the voltage and the current [32]. This is depicted in figure 36(b). It shows the forward voltage behavior in relation to the diode current. The diode has two conditions: the forward bias condition and the reverse bias condition. The forward bias condition is where current passes through the diode and the reverse bias condition is where the current is blocked.

In the forward bias condition, the forward voltage is influenced by the current through the diode. As the AC voltage (amplitude) increases there is more diode current during the forward bias stage. Looking at figure 2 in the worksheet, an increase in diode current means that the forward voltage increases. This is up to a certain point, where an increase in current does not increase the forward voltage and the voltage drop in the circuit remains relatively constant.

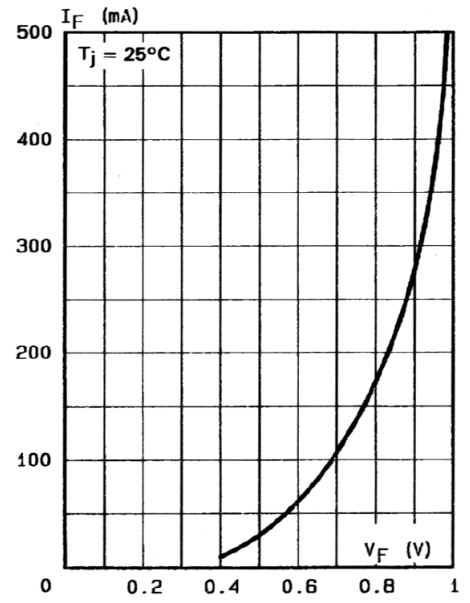
Additionally in the initial stages of the forward bias condition, as the input voltage increases the increase in voltage has to overcome a 'barrier'. This is known as the dynamic resistance of the diode. Due to the exponential relation, the resistance decreases as the current increases and therefore the losses decrease ($R_d = \frac{\Delta V}{\Delta I}$ [32]). Since an increase in diode current does not give the same increase in forward voltage. Theoretically, the voltage drop remains the same for a DC voltage or an AC voltage with a constant amplitude. Only in this case, due to the alternating current and the variations in amplitude, the voltage drop experiences non-idealities and affects the behavior of the diode.

Due to the switching characteristic from positive and negative of the AC voltage, the barrier must be overcome every time a voltage peak is experienced. These losses accumulate over time and add to the total energy losses as well.

Another factor which contributes to the energy loss is the resistance experienced in the supercapacitors. Equivalent series resistance (ESR) is a very low resistance that results in dissipated energy in the form of heat. This resistance is very low (0.08 Ω).



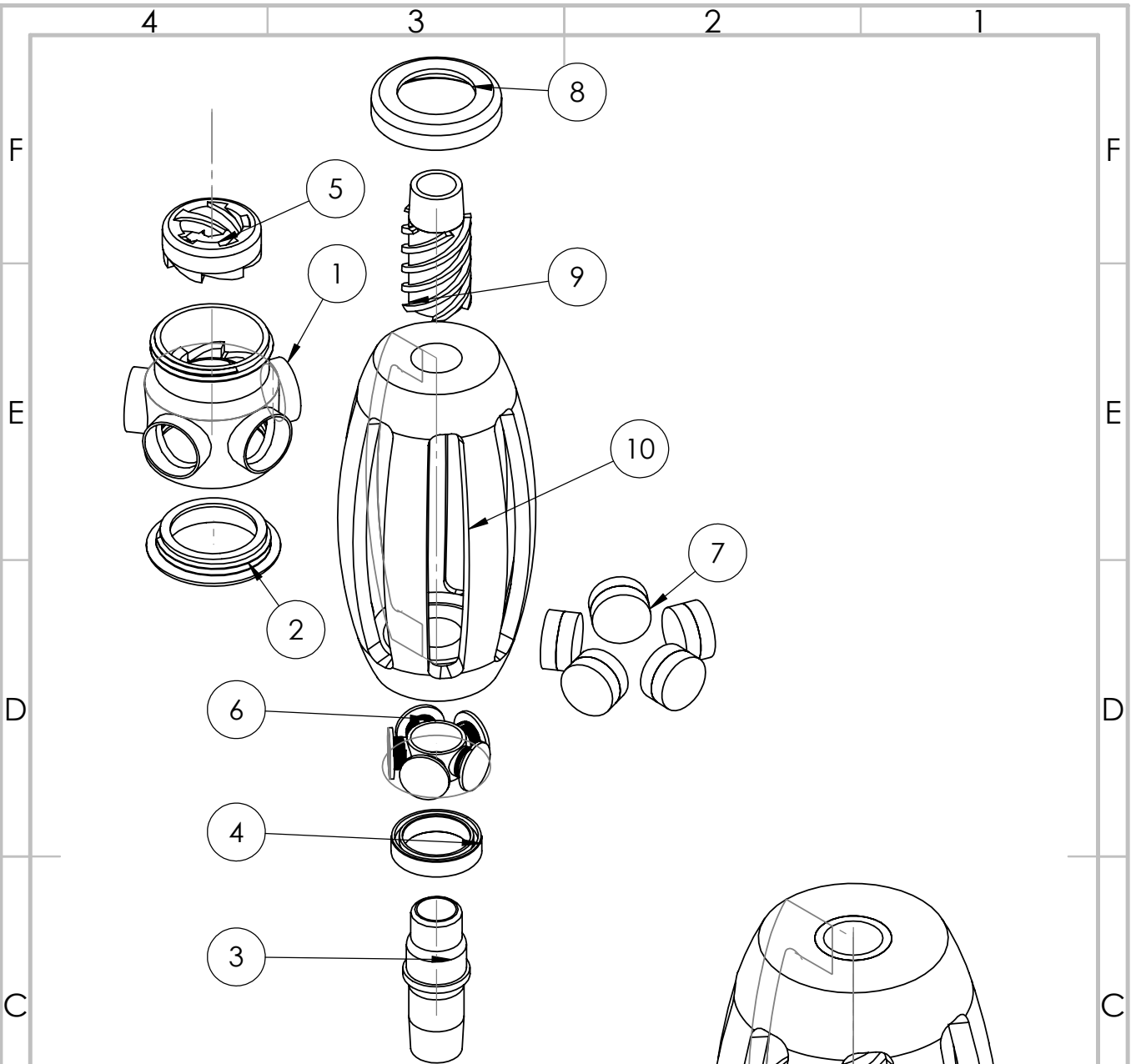
(a) Energy losses vs frequency



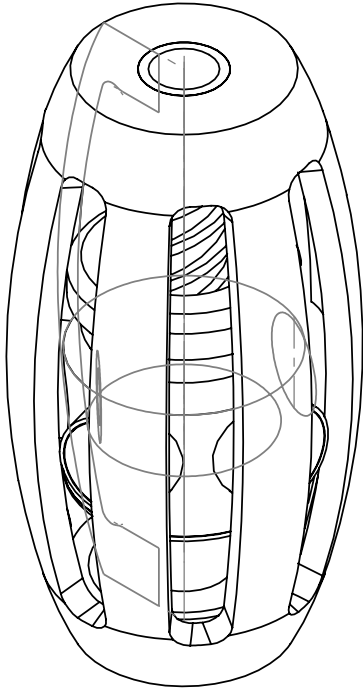
(b) Forward voltage vs current

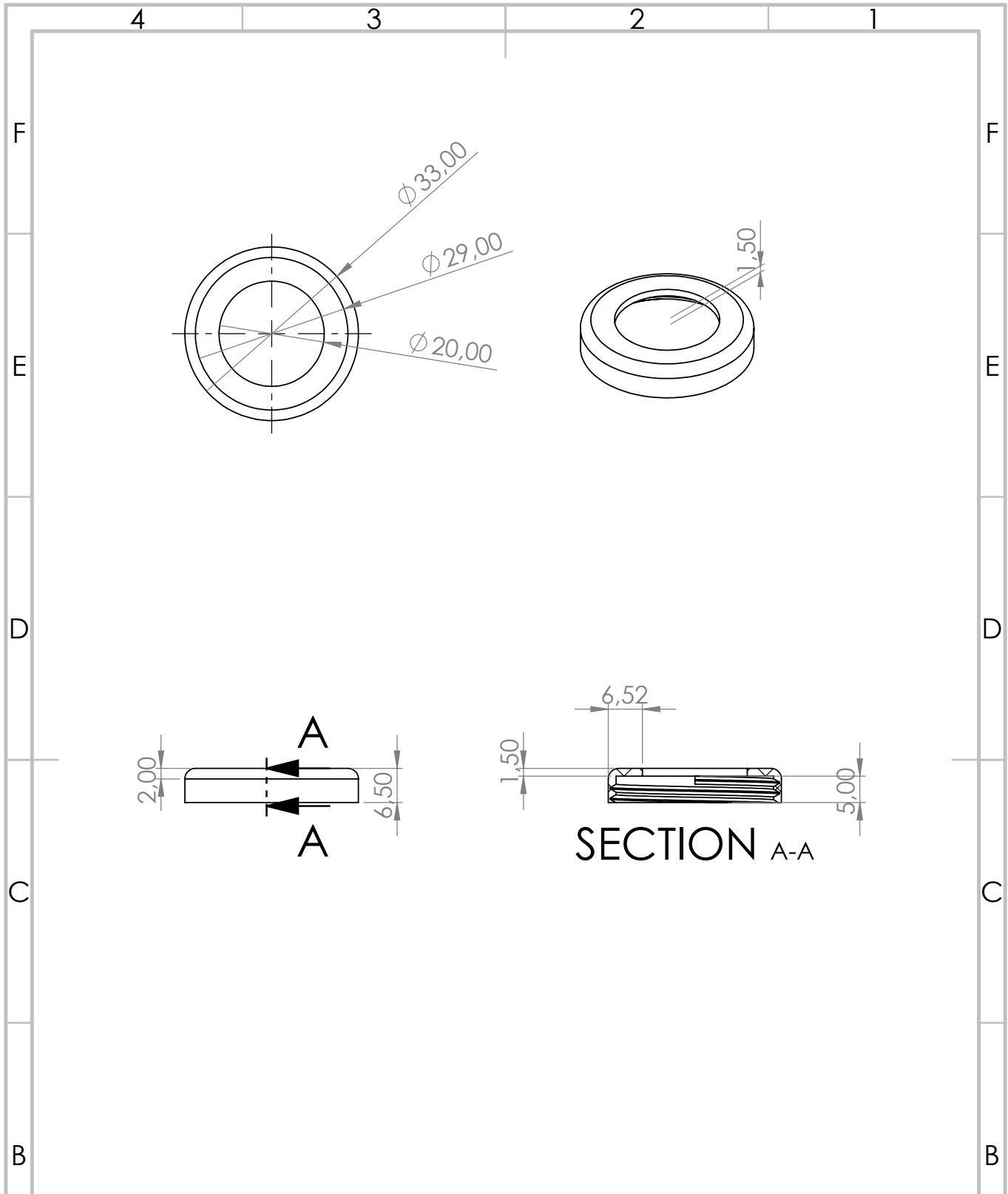
Fig. 36: Energy losses vs frequency, for every amplitude. The image on the right (b) shows the behavior of the diode, as characterized in the diode's worksheet.

APPENDIX F
COMPONENT WORKSHEETS



ITEM NO.	PART NUMBER	DESCRIPTION	QTY.
1	Clutch case	PLA	1
2	Bottom lid	PLA	1
3	Lantern	PLA	1
4	Ball bearing	SS	1
5	Helix nut	PLA	1
6	Coil ring	PLA	1
7	Magnet	Neodymium	5
8	Clutch case lid	PLA	1
9	Helix screw	PLA	1
10	Compliant base	TPU	1





UNLESS OTHERWISE SPECIFIED:
 DIMENSIONS ARE IN MILLIMETERS
 SURFACE FINISH:
 TOLERANCES:
 LINEAR:
 ANGULAR:

FINISH:

DEBURR AND
 BREAK SHARP
 EDGES

DO NOT SCALE DRAWING

REVISION

	NAME	SIGNATURE	DATE		
DRAWN					
CHK'D					
APP'VD					
MFG					
Q.A					
				MATERIAL:	
				WEIGHT:	

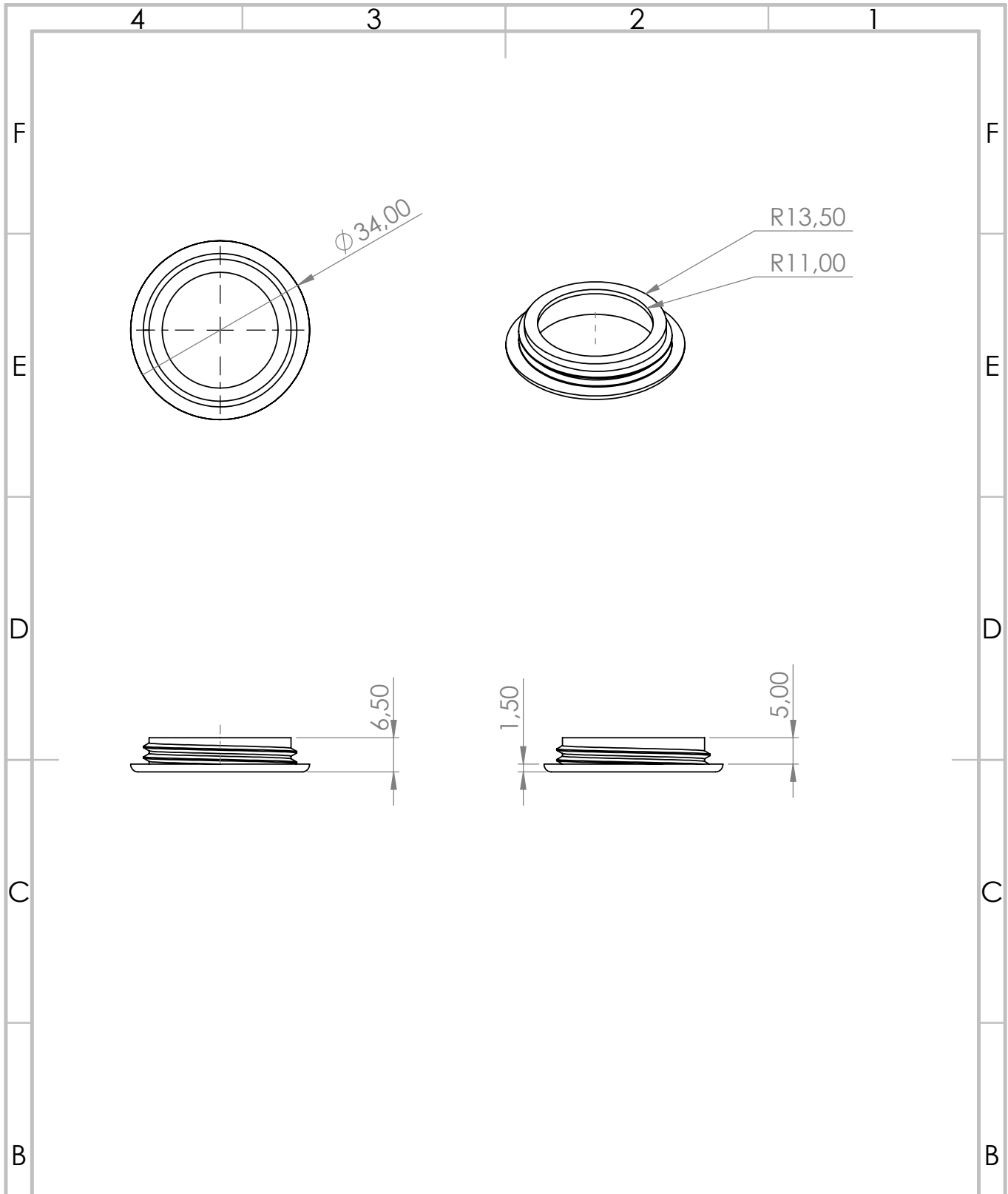
TITLE:

DWG NO.

Clutch case lid sheet

SCALE:1:1

SHEET 1 OF 1



UNLESS OTHERWISE SPECIFIED:
 DIMENSIONS ARE IN MILLIMETERS
 SURFACE FINISH:
 TOLERANCES:
 LINEAR:
 ANGULAR:

FINISH:

DEBURR AND
 BREAK SHARP
 EDGES

DO NOT SCALE DRAWING

REVISION

	NAME	SIGNATURE	DATE		
DRAWN					
CHK'D					
APP'VD					
MFG					
Q.A					
				MATERIAL:	
				WEIGHT:	

TITLE:

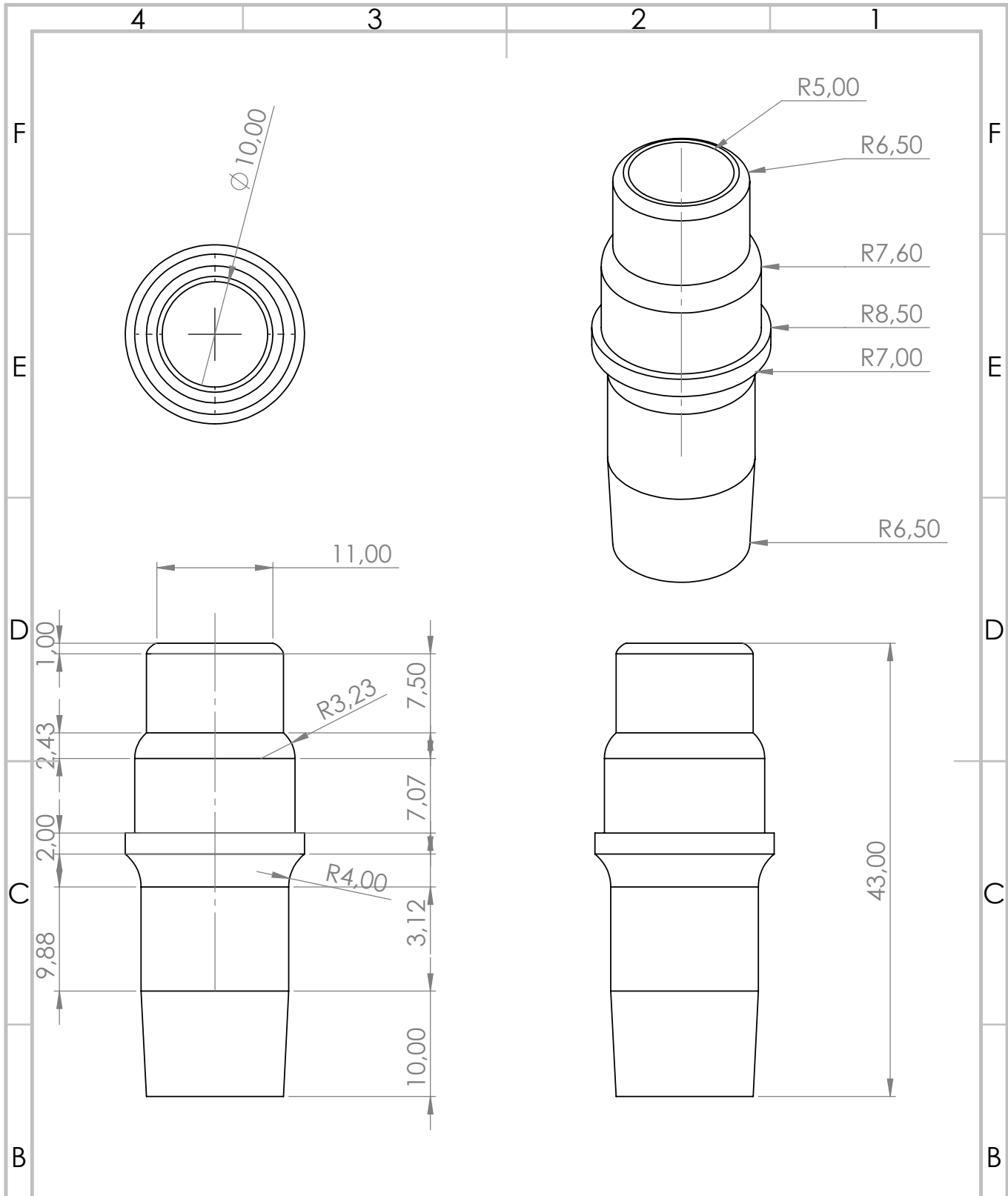
DWG NO.

Bottom lid sheet

A4

SCALE:1:1

SHEET 1 OF 1



UNLESS OTHERWISE SPECIFIED:
DIMENSIONS ARE IN MILLIMETERS
SURFACE FINISH:
TOLERANCES:
LINEAR:
ANGULAR:

FINISH:

DEBURR AND
BREAK SHARP
EDGES

DO NOT SCALE DRAWING

REVISION

	NAME	SIGNATURE	DATE		
DRAWN					
CHK'D					
APPVD					
MFG					
Q.A					
				MATERIAL:	
				WEIGHT:	

TITLE:

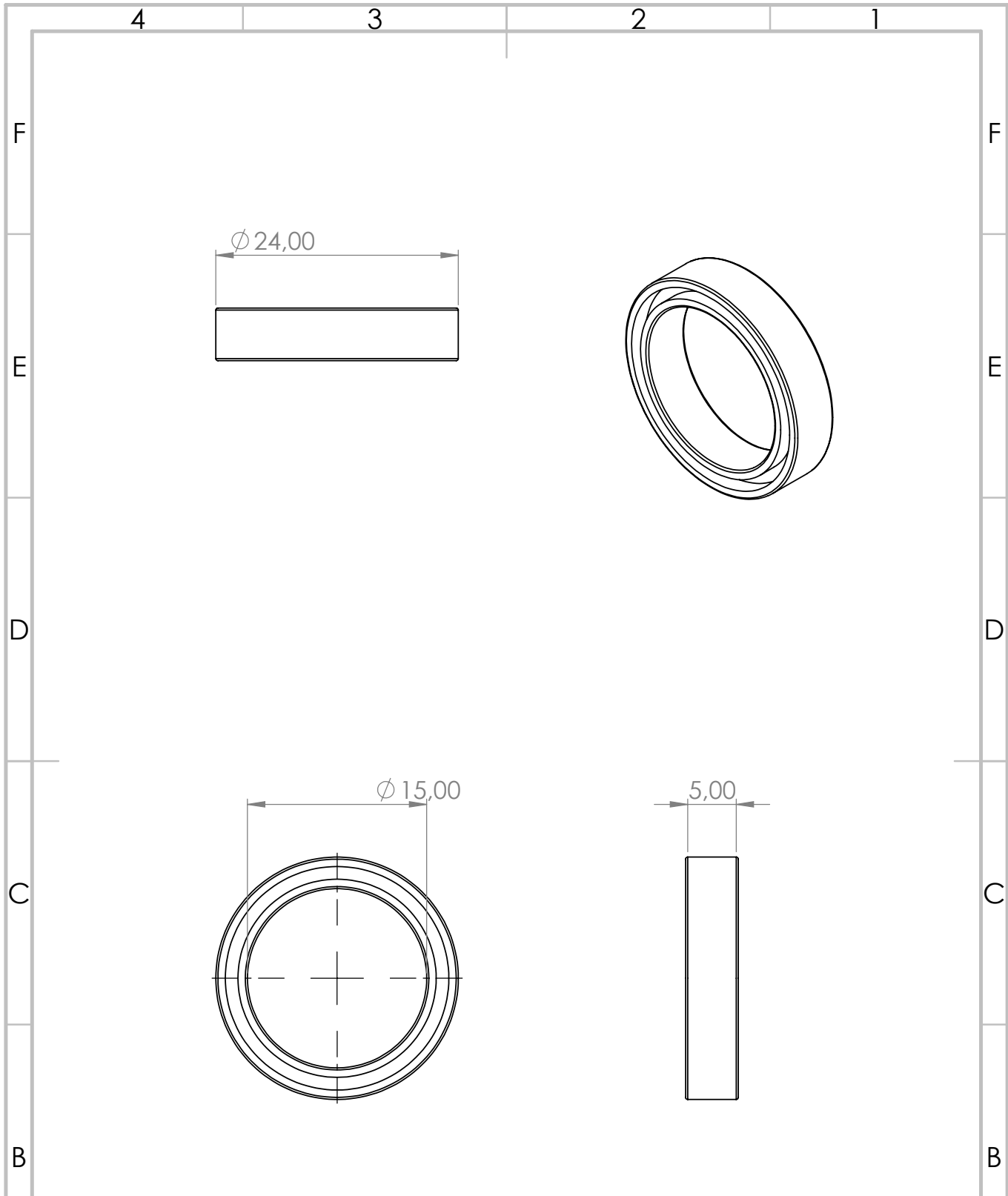
DWG NO.

Lantern sheet

A4

SCALE:2:1

SHEET 1 OF 1



UNLESS OTHERWISE SPECIFIED:
 DIMENSIONS ARE IN MILLIMETERS
 SURFACE FINISH:
 TOLERANCES:
 LINEAR:
 ANGULAR:

FINISH:

DEBURR AND
 BREAK SHARP
 EDGES

DO NOT SCALE DRAWING

REVISION

	NAME	SIGNATURE	DATE		
DRAWN					
CHK'D					
APP'VD					
MFG					
Q.A					
				MATERIAL:	
				WEIGHT:	

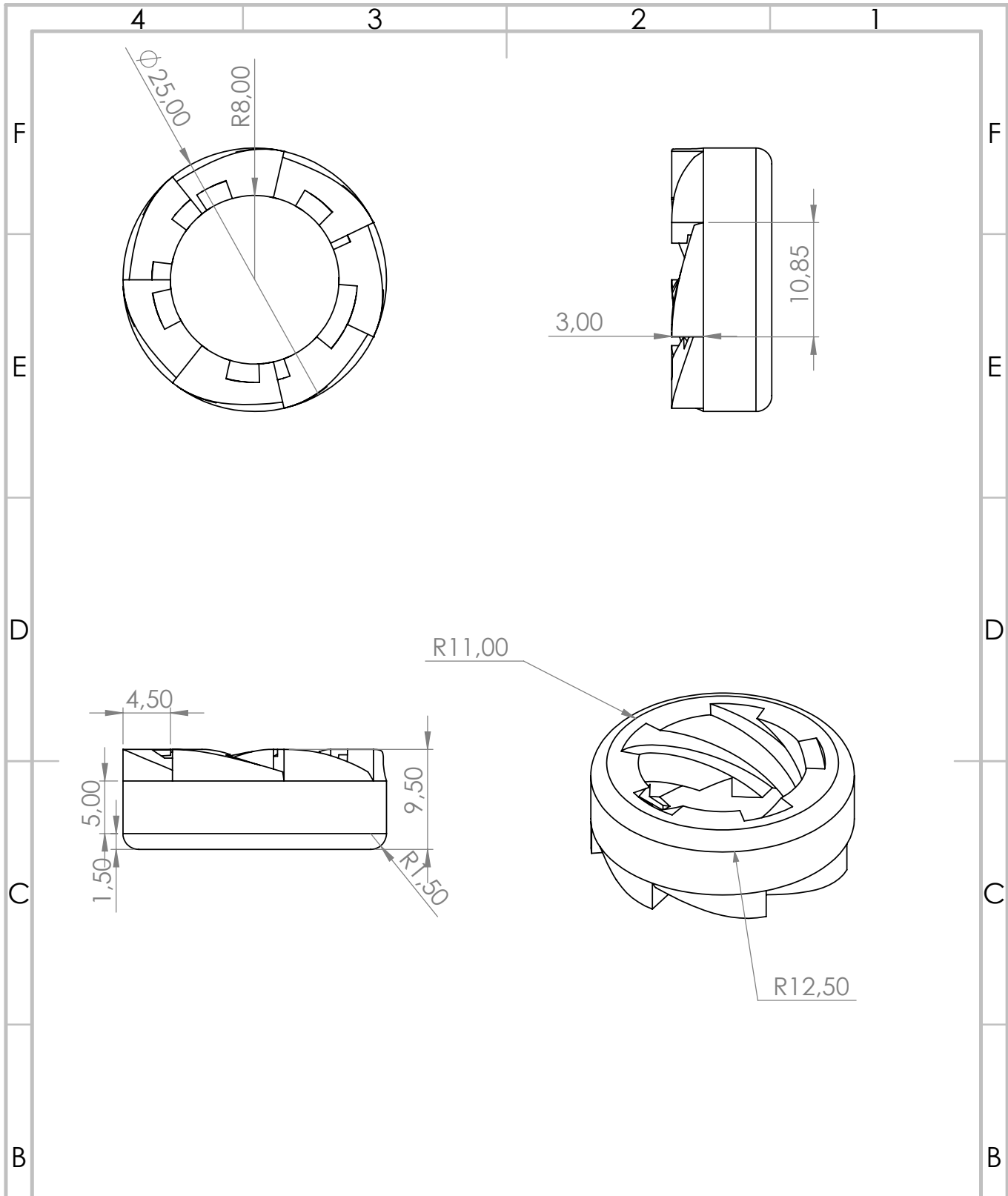
TITLE:

DWG NO.

Ball bearing sheet^{A4}

SCALE:2:1

SHEET 1 OF 1



UNLESS OTHERWISE SPECIFIED:
 DIMENSIONS ARE IN MILLIMETERS
 SURFACE FINISH:
 TOLERANCES:
 LINEAR:
 ANGULAR:

FINISH:

DEBURR AND
 BREAK SHARP
 EDGES

DO NOT SCALE DRAWING

REVISION

	NAME	SIGNATURE	DATE		
DRAWN					
CHK'D					
APP'VD					
MFG					
Q.A					
				MATERIAL:	
				WEIGHT:	

TITLE:

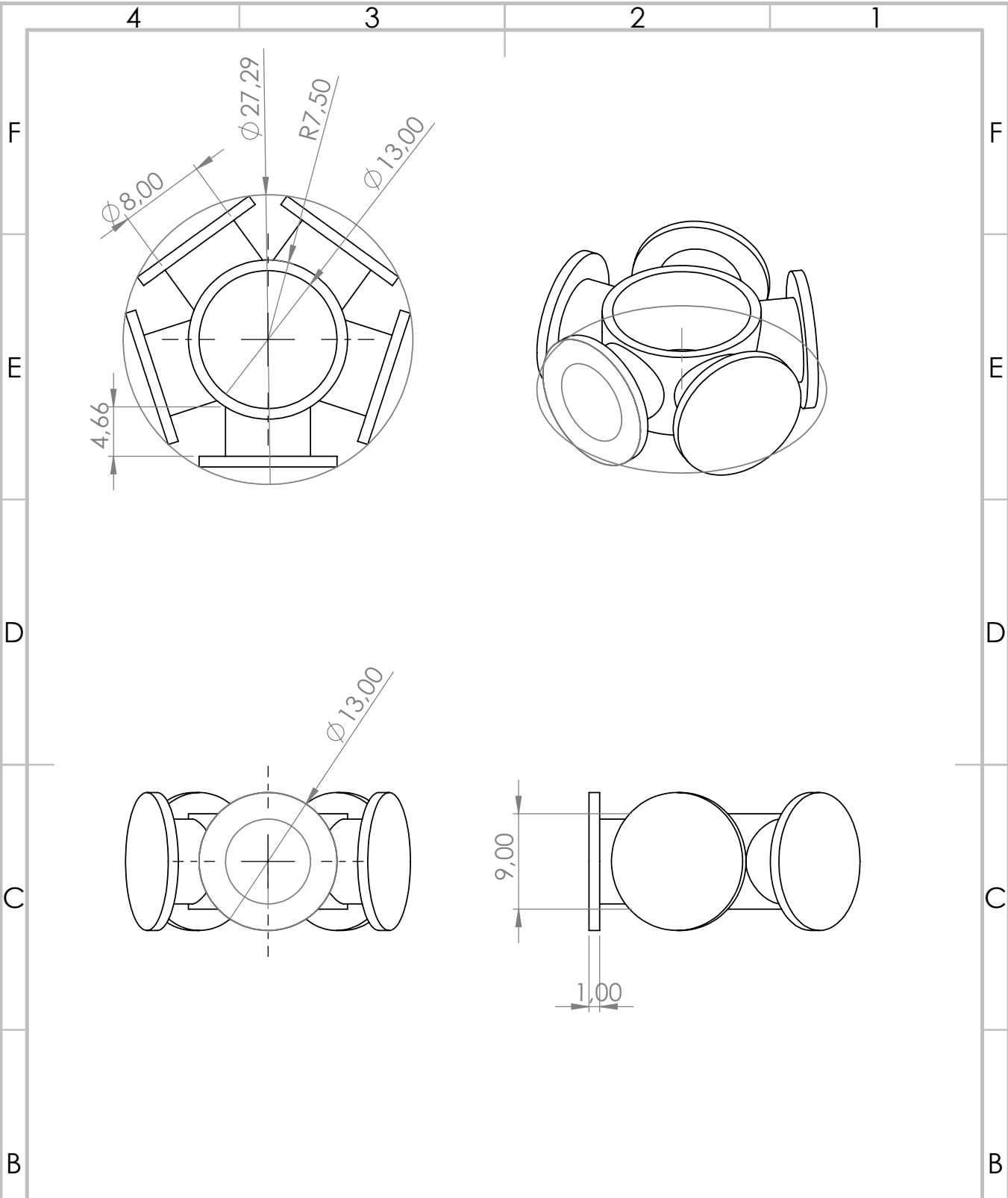
DWG NO.

Helix nut sheet

A4

SCALE:2:1

SHEET 1 OF 1



UNLESS OTHERWISE SPECIFIED:
 DIMENSIONS ARE IN MILLIMETERS
 SURFACE FINISH:
 TOLERANCES:
 LINEAR:
 ANGULAR:

FINISH:

DEBURR AND
 BREAK SHARP
 EDGES

DO NOT SCALE DRAWING

REVISION

	NAME	SIGNATURE	DATE		
DRAWN					
CHK'D					
APP'VD					
MFG					
Q.A					
				MATERIAL:	
				WEIGHT:	

TITLE:

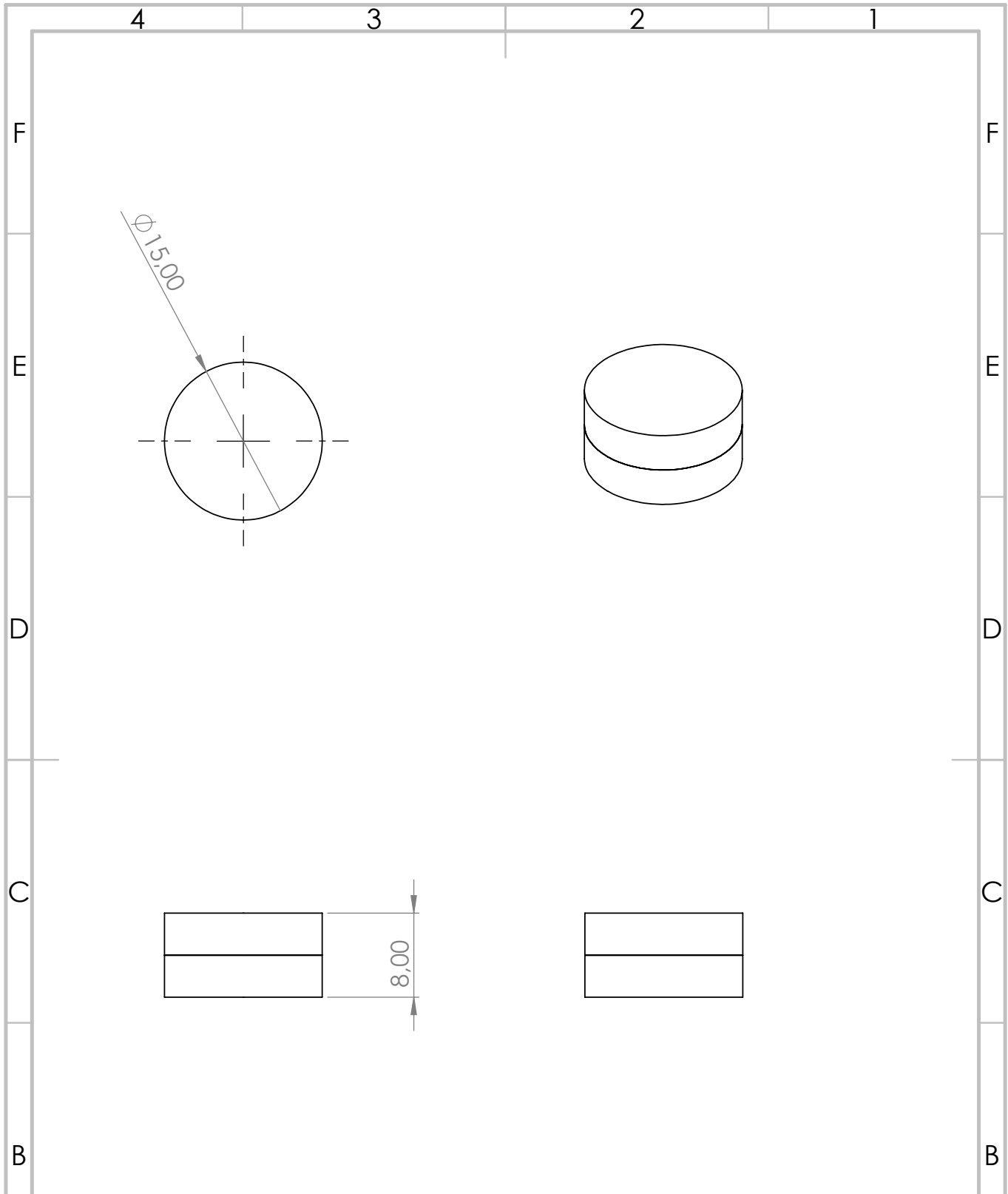
DWG NO.

Coil ring sheet

A4

SCALE:2:1

SHEET 1 OF 1



UNLESS OTHERWISE SPECIFIED:
 DIMENSIONS ARE IN MILLIMETERS
 SURFACE FINISH:
 TOLERANCES:
 LINEAR:
 ANGULAR:

FINISH:

DEBURR AND
 BREAK SHARP
 EDGES

DO NOT SCALE DRAWING

REVISION

	NAME	SIGNATURE	DATE		
DRAWN					
CHK'D					
APP'VD					
MFG					
Q.A					
				MATERIAL:	
				WEIGHT:	

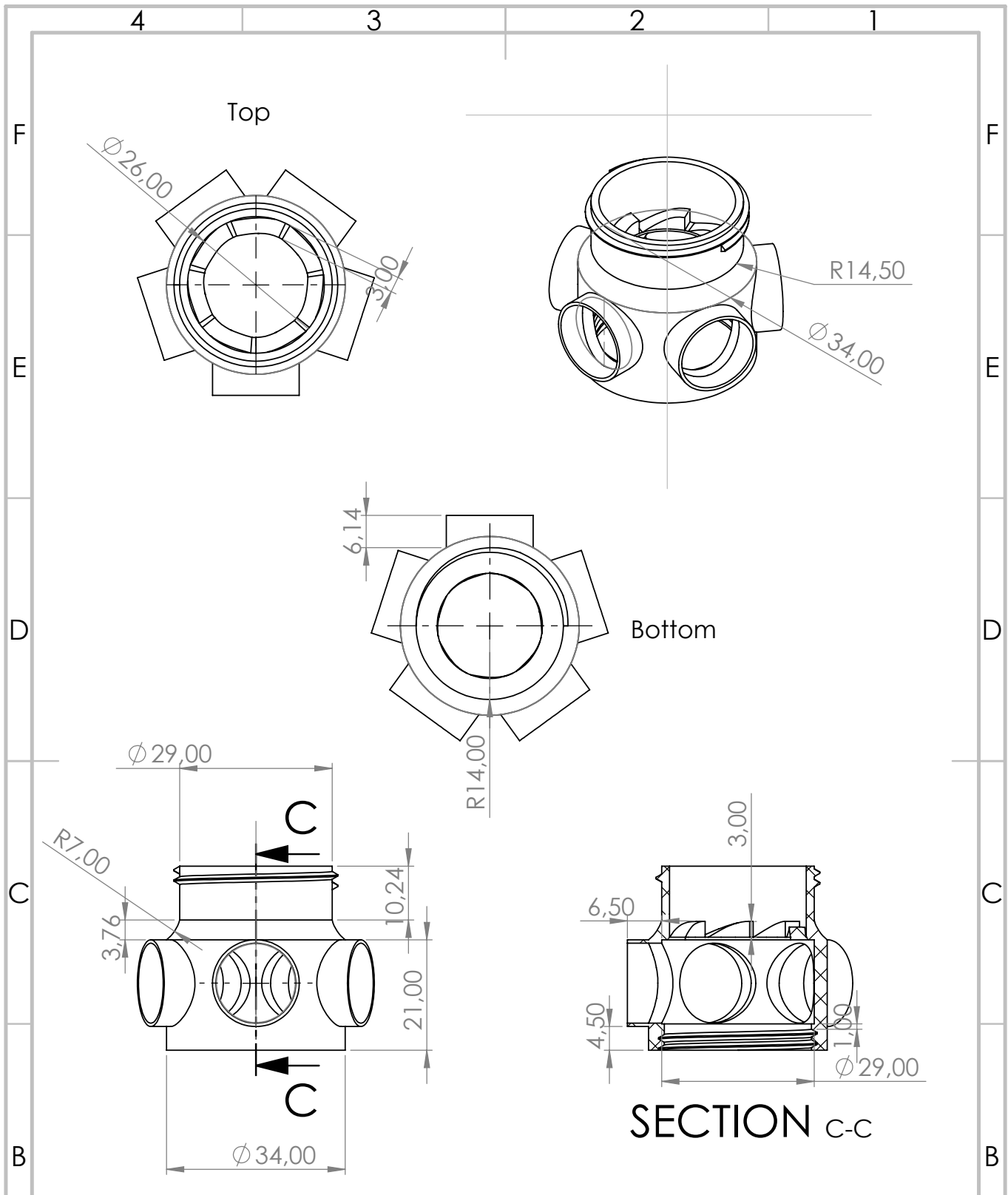
TITLE:

DWG NO.

magnet 15mm sheet

SCALE:2:1

SHEET 1 OF 1



UNLESS OTHERWISE SPECIFIED:
 DIMENSIONS ARE IN MILLIMETERS
 SURFACE FINISH:
 TOLERANCES:
 LINEAR:
 ANGULAR:

FINISH:

DEBURR AND
 BREAK SHARP
 EDGES

DO NOT SCALE DRAWING

REVISION

	NAME	SIGNATURE	DATE		
DRAWN					
CHK'D					
APP'VD					
MFG					
Q.A					
				MATERIAL:	
				WEIGHT:	

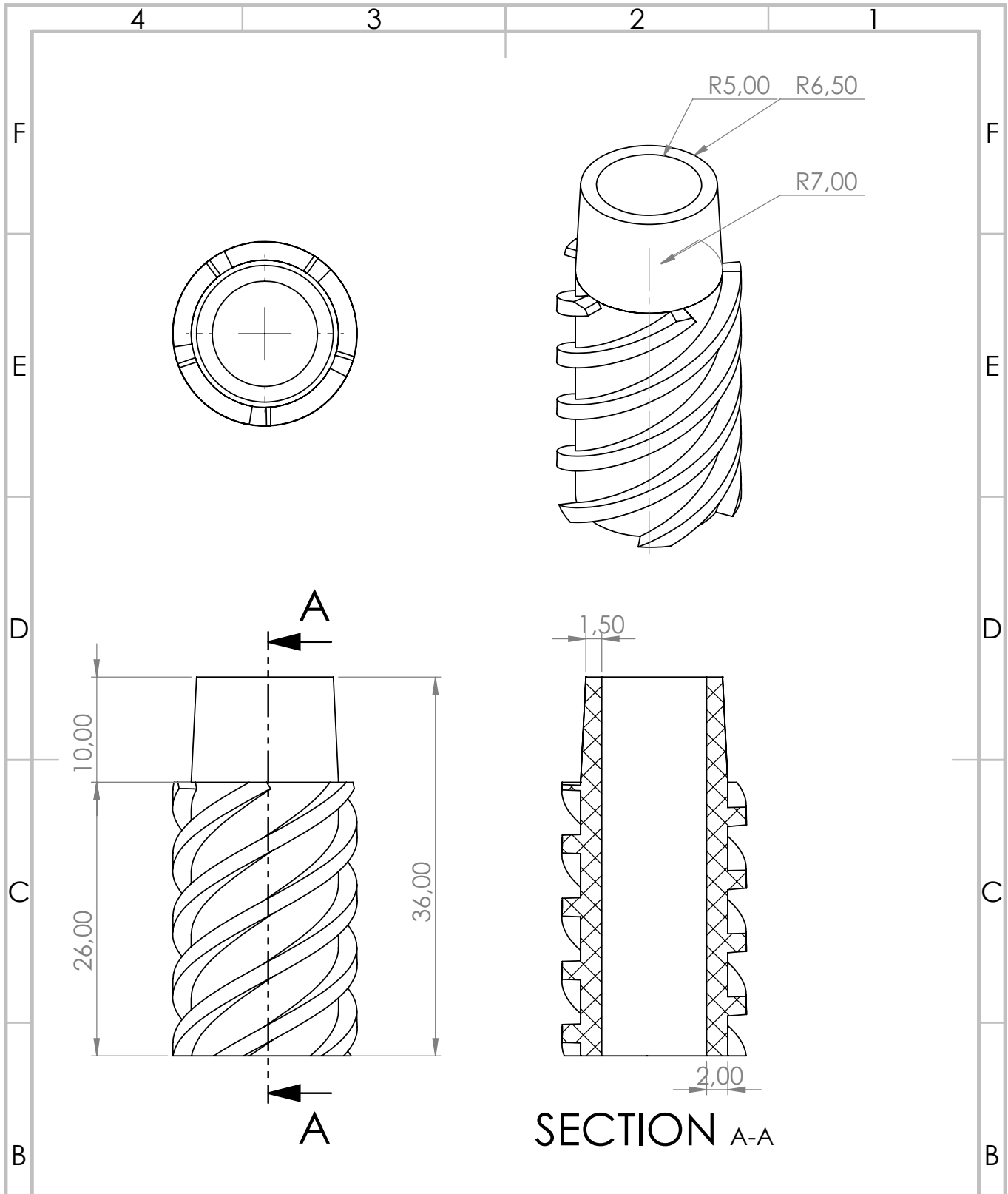
TITLE:

DWG NO.

Clutch case sheet^{A4}

SCALE:1:1

SHEET 1 OF 1



UNLESS OTHERWISE SPECIFIED:
 DIMENSIONS ARE IN MILLIMETERS
 SURFACE FINISH:
 TOLERANCES:
 LINEAR:
 ANGULAR:

FINISH:

DEBURR AND
 BREAK SHARP
 EDGES

DO NOT SCALE DRAWING

REVISION

	NAME	SIGNATURE	DATE		
DRAWN					
CHK'D					
APP'VD					
MFG					
Q.A					
				MATERIAL:	
				WEIGHT:	

TITLE:

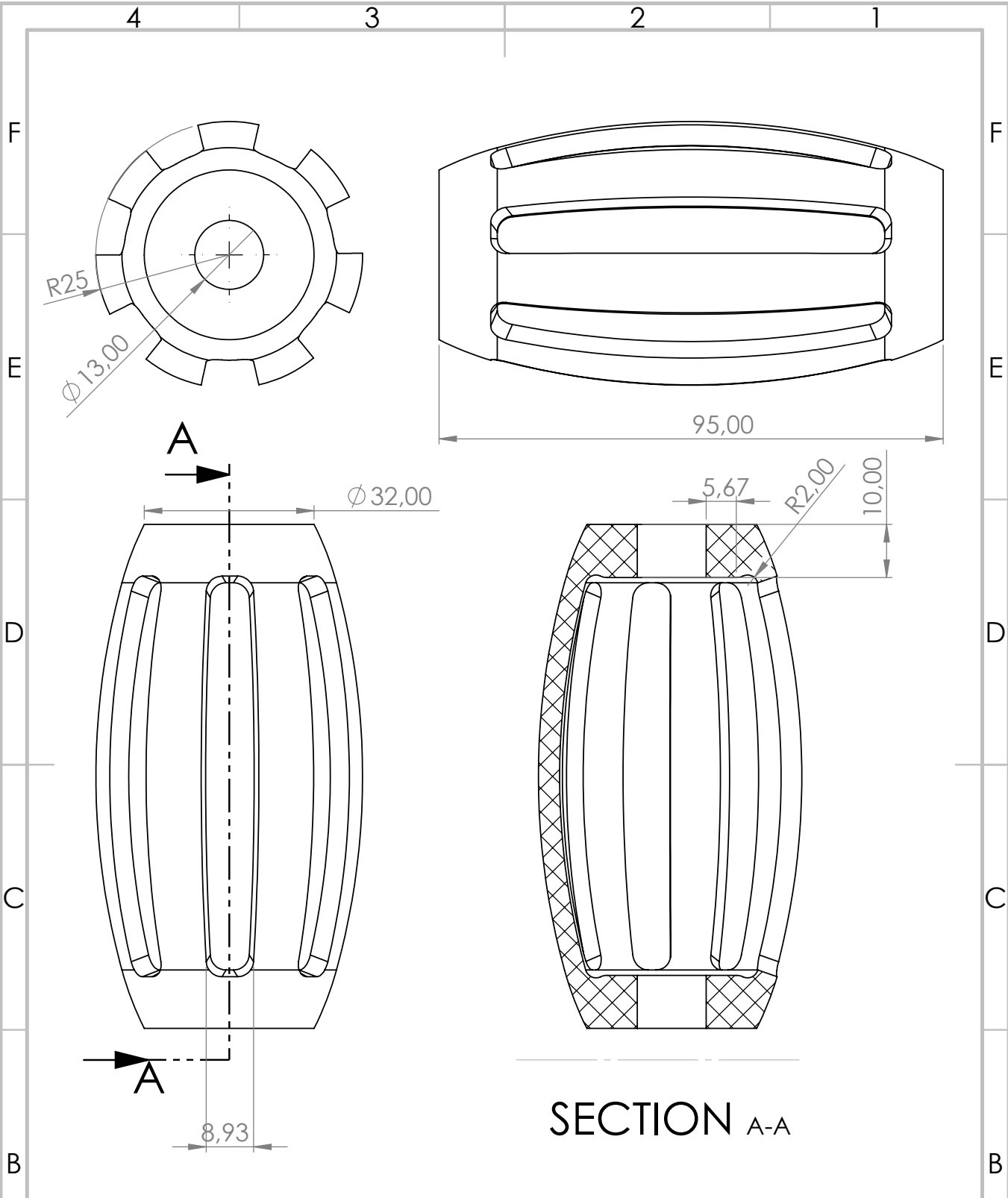
DWG NO.

Helix screw sheet

A4

SCALE:2:1

SHEET 1 OF 1



SECTION A-A

UNLESS OTHERWISE SPECIFIED: DIMENSIONS ARE IN MILLIMETERS SURFACE FINISH: TOLERANCES: LINEAR: ANGULAR:			FINISH:		DEBURR AND BREAK SHARP EDGES		DO NOT SCALE DRAWING		REVISION		
DRAWN						TITLE:					
CHK'D											
APPV'D											
MFG											
Q.A						MATERIAL:		DWG NO.			
						WEIGHT:		SCALE:1:1		SHEET 1 OF 1	

Compliant base sheet ^{A4}

APPENDIX G

MATLAB SCRIPTS

G.1 Concept 1 - the levitated magnet emf and power output calculations

```

1  %% Power output estimation
3  %Master thesis Jurrien Smits
4  %Concept 1 potential power output
5
6  % The levitated magnet concept
7  clear all;
8  clc;
9  close all;
10 %% Introduce variables
11 % Parameters
12 mu0 = 4*pi*1e-7; % Permeability of free space (N/A^2)
13 radius_of_coil = 0.0175; % Radius of the coil in meters
14 Amplitude = 0.01; % Amplitude of the magnet's motion in meters
15 frequency = 2; % Frequency of the magnet's motion in Hz
16 angular_frequency = 2 * pi * frequency; % Angular frequency in rad/s
17 N = 100; % Number of coil windings
18 M = 1.8; % Magnetic moment of the magnet in A*m
19 % Holding force 7,8kg 24x5mm
20 magnet_radius = 0.012; % Radius of the magnet in meters
21 Resistance = 100; % Assumption
22
23 %% Create a time vector
24 t = linspace(0, 1, 1000); % Time vector
25
26 %% Calculate the induced emf as a function of time
27
28 emf = zeros(size(t));
29 prev_flux = 0; % Initial flux value
30 Power_output = zeros(size(t));
31 mV = zeros(size(t));
32
33 % Calculate the induced EMF at each specific time point
34 for i = 1:length(t)
35     % Calculate the vertical position of the magnet (z) at time t(i)
36     z = Amplitude * sin(angular_frequency * t(i));
37
38     % Calculate the position vector (r) between the magnet and the coil at time t(i)
39     r = [0, 0, z];
40
41     % Calculate the magnitude of the position vector
42     magnitude_r = norm(r);
43
44     % Calculate the magnetic field strength (B_magnet) produced by the magnet at time t(i)
45     B_magnet = (mu0 * M) / (2 * pi * (magnitude_r^2 + magnet_radius^2)^(3/2));
46
47     % Calculate the magnetic flux ( ) through the coil at time t(i)
48     flux = B_magnet * pi * radius_of_coil^2;
49
50     % Calculate the induced emf at time t(i)
51     if i == 1
52         emf(i) = 0; % Initial emf is zero as there is no
53         previous_flux = flux;
54     else
55         % Calculate the change in magnetic flux with respect to time

```

```

55     dFlux_dt = (flux - prev_flux) / (t(i) - t(i - 1));
        % Calculate the induced emf
57     emf(i) = -N * dFlux_dt;
        end
59
        % Update flux value
61     prev_flux = flux;
63     Power_output(i) = (emf(i)^2/Resistance)*3000; % Power output in mW for three magnets
        mV(i) = emf(i)*3000; % Induced emf in mV for three magnets
65
        end
67
69 max(mV)
71 %% Plot the induced emf and power output as a function of time
        figure(1);
73 plot(t, mV);
        xlabel('Time (s)');
75 ylabel('Induced emf (mV)');
        xlim([0 1])
77 ylim([-800 800])
        title('The levitated magnet - Induced emf in the coil vs. time (frequency = 2Hz)');
79 grid on;
81 figure(2);
        plot(t, Power_output);
83 xlabel('Time (s)');
        ylabel('Power output (mW)');
85 xlim([0 1])
        ylim([0 1])
87 title('The levitated magnet - Induced power output vs. time (frequency = 2Hz)');
        grid on;

```

G.2 Concept 2 - the rack and pinion emf and power output calculations

```

1 % Power output estimation
  % Master thesis Jurri n Smits
3 % Concept 2 potential power output
5 % The rack and pinion
  clear all;
7 clc;
  close all;
9 %% Variables
  % Define various parameters and constants related to the system
11 mass = 0.639; % Mass in kg (Solidworks)
  Frequency = 2; % Frequency of harmonic motion (Hz)
13 Angular_frequency = 2 * pi * Frequency;
  Amplitude = 0.05; % Amplitude of harmonic motion (meters)
15 Gear_ratio = 1.64; % Gear ratio
  Efficiency = 0.4; % Generator efficiency (General assumption)
17 Radius_pinion = 0.00585; % Radius of the pinion (meters)
19 %% Time Calculation
  % Generate a time vector for simulation
21 t = linspace(0, 1, 1000); % One complete cycle

```

```

23 %% Calculate the Power Output over Time using a for loop
    % Initialize arrays to store power values
25 P_elec = zeros(size(t));

27 % Calculate power output for each time point using a for loop
    for i = 1:length(t)
29         displacement = Amplitude * sin(Angular_frequency * t(i));
           force = -mass * Angular_frequency^2 * displacement;
31         torque_input = force * Radius_pinion;
           torque_output = torque_input * Gear_ratio; % Apply the gear ratio
33         P_mech = torque_output * Angular_frequency;
           P_elec(i) = P_mech * Efficiency*1000;
35     end

37 Peak_power_output = max(P_elec);
    fprintf('Peak power output = %.8f mW\n', Peak_power_output);
39

41 %% Plot Power Output over Time
43 figure;
    plot(t, P_elec);
45 xlabel('Time (s)');
    ylabel('Power Output (mW)');
47 title('Power Output vs. Time for Harmonic Motion with Gear Ratio');
    grid on;

```

G.3 Concept 3 - the compliant spring emf and power output calculations

```

2 %% Power output estimation
    %Master thesis Jurrien Smits
4 %Concept 3 potential power output

6 % The compliant spring
    clear all;
8 clc;
    %% Constants
10 mu0 = 4*pi*1e-7; % Permeability of free space (N/A^2)
    M = 0.89; % Magnetic moment of the magnet (A/m ) (holding force
           6kg 12x8mm)
12 R_coilpath = 0.0045; %0.010 % Radius of the coil's circle (m)
    R_magnetpath = 0.0145; %0.013 % Radius of the magnet's circular path (m)
14 R_magnet = 0.006;
    N = 100; % Number of windings in the coil
16 frequency = 2;
    R_coil = 0.004;
18 Resistance = 100; % Assumption

20 % Angular velocity of the magnet (radians per second)
    omega = 2 * pi * frequency; % Complete rotation in one second
22

    t = linspace(0, 1, 1000);
24 % Distance from the magnet's central axis to the coil (constant in this setup)
    %Amplitude_y = ((R_magnetpath + R_coilpath) - (R_magnetpath - R_coilpath))/2; %Oscilating
           distance
26 Amplitude_y = R_magnetpath - R_coilpath;

```



```

Amplitude_x = R_magnetpath - R_coilpath;
28
30 % Area of the coil that the magnetic field passes through
A = pi * R_coil^2;
32
%% Calculate the induced emf as a function of time
34
emf = zeros(size(t));
36 Power_output = zeros(size(t));
mV = zeros(size(t));
38 prev_flux = 0; %initial flux value

40 % Calculate the induced EMF at each specific time point
for i = 1:length(t)
42
    % Calculate the position vector between magnet and coil at time t(i)
44    x = Amplitude_x * sin(omega*t(i));
    y = Amplitude_y * sin(omega*t(i));
46    r = [x, y, 0];
    z = norm(r);
48
    % Calculate the magnetic field at the coil location for each angle
50    B = (mu0 * M) / (2 * pi * (z^2 + R_magnet^2)^(3/2));

52    % Calculate the rate of change of the magnetic flux with respect to time
flux = B * A * cos(omega*t(i));
54

    % Calculate the induced emf at time t(i)
56    if i == 1
        emf(i) = 0; % Initial emf is zero as there is no
        previous flux value
58    else
        % Calculate the change in magnetic flux with respect to time
60        dFlux_dt = (flux - prev_flux) / (t(i) - t(i - 1));
        % Calculate the induced emf
62        emf(i) = N * dFlux_dt;
    end
64
    %Update flux value
66    prev_flux = flux;

68
    Power_output(i) = (emf(i)^2/Resistance)*5000; % Power output in mW for 5 magnets
70    mV(i) = emf(i)*5000; % Induced emf in mV for 5 magnets

72 end

74 max(mV)
%% Plot the induced EMF and Power output versus time
76 figure(1);
plot(t, mV);
78 xlabel('Time (s)');
ylabel('Induced emf (mV)');
80 xlim([0 1])
ylim([-800 800])
82 title('The compliant spring - Induced emf in the coil vs. time (frequency = 2Hz)');
grid on;
84
figure(2);
86 plot(t, Power_output);

```

```
xlabel('Time (s)');  
88 ylabel('Power output (mW)');  
xlim([0 1])  
90 ylim([0 1])  
title('The compliant spring - Induced power output vs. time (frequency = 2Hz)');  
92 grid on;
```

APPENDIX H

ARDUINO SKETCH

H.1 Nema 23 stepper motor control sketch

```

1 #include <AccelStepper.h>
3 const int stepPin = 5;
  const int dirPin = 2;
  const int enPin = 8;
7 float steps = 3200;
  float resolution = (float)360/steps;
  String RPM;
  float T;
11
13
15 void setup() {
17   Serial.begin(115200);
19   pinMode(stepPin,OUTPUT);
21   pinMode(dirPin,OUTPUT);
23   pinMode(enPin,OUTPUT);
25   digitalWrite(enPin,LOW);
27 }
29 void loop() {
31   if(Serial.available() > 0){
33     RPM = Serial.readString();
35     T = setRPM(RPM.toInt(), resolution); //calls a function to calculate the frequency at the same time the
      rpm its set, need two parameters RPM in an integer format and the resolution variable, finally it is
      assigned to variable T
37     Serial.print("RPM set to: ");
39     Serial.println(RPM); //Prints the RPM needed
41   }
43   digitalWrite(dirPin,HIGH); // Enables the motor to move in a particular direction
45   for(int x = 0; x < steps; x++) {
47     digitalWrite(stepPin,HIGH);
49     delayMicroseconds(T);
51     digitalWrite(stepPin,LOW);
53     delayMicroseconds(T);
55   }
57 }
59 float setRPM(int rpm, float res){
61   float freq = (float)rpm/((res/360)*60); //calculates the frequency to a related RPM
63   float period = 1/freq; //calculates the inverse of the frequency A.K.A the period
65   return (period*0.5)*1000000 ; // returns half of the period in microseconds
67 }

```

Listing 1: Arduino sketch used to control the Nema 23 stepper motor. Digital pins 2 5 and 8 are used. Microstepping is set to 3200 steps per revolution. To control the stepper motor speed an RPM input is required which can be provided in the serial monitor.

H.2 Durability test sketch

```

1 #include <AccelStepper.h>
3 const int stepPin = 5;
  const int dirPin = 2;
  const int enPin = 8;
7 float steps = 3200;

```

```

float resolution = (float)360 / steps;
9
int targetRPM = 60; // Default target RPM
11 int targetRotations = 10; // Set the desired number of rotations
int cycleCounter = 0;
13
void setup() {
15   Serial.begin(115200);

17   pinMode(stepPin, OUTPUT);
   pinMode(dirPin, OUTPUT);
19   pinMode(enPin, OUTPUT);
   digitalWrite(enPin, LOW);
21 }

23 void loop() {
   if (cycleCounter < targetRotations) {
25     // Continue the durability test
     float delayMicros = setRPM(targetRPM, resolution);
27

     Serial.print("Cycle: ");
29     Serial.print(cycleCounter + 1);
     Serial.print(", RPM set to: ");
31     Serial.println(targetRPM);

33     digitalWrite(dirPin, HIGH); // Set the direction (adjust as needed)

35     for (int x = 0; x < steps; x++) {
       digitalWrite(stepPin, HIGH);
37       delayMicroseconds(delayMicros);
       digitalWrite(stepPin, LOW);
39       delayMicroseconds(delayMicros);
     }

41     cycleCounter++;
43   } else {
     // Durability test completed
45     Serial.println("Durability test completed.");
     delay(10000);
47     exit(0);
     // You can add any additional actions or reset the test as needed
49   }
}

51 float setRPM(int rpm, float res) {
53   float freq = (float)rpm / ((res / 360) * 60);
   float period = 1 / freq;
55   return (period * 0.5) * 1000000;
}

```

Listing 2: Arduino sketch used to control the Nema 23 stepper motor to perform a durability test. Digital pins 2 5 and 8 are used. Microstepping is set to 3200 steps per revolution. To control the stepper motor speed an RPM input is required and a certain number of cycles.

APPENDIX I
LITERATURE REVIEW



DELFT UNIVERSITY OF TECHNOLOGY

BMD LITERATURE RESEARCH
BM51010

**A review on energy harvesting systems
from human and vehicular induced vibrations**

Jurriën Smits (4583590)

January 15, 2024

Supervisor:
Gerwin Smit (TU Delft)

Abstract—Energy harvesting from vibrations has gained lots of interest over the last two decades. By tapping into surrounding sources, the use of batteries can be decreased, aiding in reducing the carbon footprint in the world. Vibrations induced by humans and vehicles provide promising energy sources for vibration harvesting. Over the last two decades lots of different designs have been proposed. Therefore the goal of this review is to present an overview of the most novel vibration energy harvesting systems from human and vehicular induced vibrations. This overview is presented based on the characteristics of the harvesting mechanism. These are split up in the categories electromagnetic, piezoelectric and hydraulic energy harvesters. In a systematic search, a total of 655 papers was narrowed down to 44 relevant papers. The relevant findings are laid out in the results. A total of 33 energy harvesting systems are discussed. From these results, interpretations and implications on these systems are discussed further, concerning advantages and limitations of the energy harvesters. It can be concluded that vibration energy harvesters containing hydraulics generally have the highest power output. However, high power output does not necessarily mean high efficiency, for all described systems. This is influenced by multiple factors, for instance amplification mechanisms, motion rectification or piezoelectric material. These factors all influence the power output. In addition, the challenging issues that remain unresolved are mentioned and some recommendations regarding these challenges are stated for future research.

I. INTRODUCTION

A. Background

Energy harvesting can be defined as the ability to harness, store, and distribute energy from local surroundings [1]. This topic has gained lots of interest over the last two decades [2]. By tapping into surrounding energy sources, the use of batteries or fuels can be decreased. Therefore it helps in the reduction of the carbon footprint in the world. This paper focuses on surrounding energy from human movement and vehicular movement. In particular, periodic back-and-forth motion (oscillation) of a body or medium. Also known as vibrations.

Energy is a basic need in human life. The human body contains great amounts of energy produced by metabolism and provides a great energy source for harvesting. In general, the majority of energy provided by the human body comes from limb movement, heat and biochemical potentials [3]. The energy generated by these sources is estimated to be capable of powering small electronic devices [3]. Harvesting this energy therefore shows potential.

Harvesting biochemical energy is proven relatively difficult [3], in addition the output power is weak. Human body heat can be harvested using a thermoelectric generator. Experiments with a thin layer of polydimethylsiloxane spread on a body part have been conducted [3]. This method however requires more area of the human body to obtain more power, this may make people feel uncomfortable [3]. Interest in harvesting energy from human walking has received considerable attention. This energy is much easier to harvest and transform into electricity in greater quantities [3]. More in particular, kinetic energy from inertial body movement and vibrations. The center of mass of the human body moves continuously, as well as limbs. The human gait cycle is composed of periodic motions, where

mechanical vibrations exist inevitably [3]. When capturing this movement it can be used to drive a generator to produce power.

Vehicular motion presents itself as another promising source of kinetic energy. Traveling on roads, vehicles tend to be subjected to road irregularities, braking forces, acceleration forces, and centrifugal forces on a curved road [2]. This will induce vibrations and therefore discomfort to driver and passengers. Vibrations in vehicles are dissipated with conventional passive suspensions. This means that all the kinetic energy is lost. These suspensions are composed of hydraulic shock absorbers or springs to suppress vibrations. The vibrational energy dissipated by these shock absorbers provide a source for energy regeneration. Nowadays the concept of regenerative braking in hybrid vehicles is a common term. This proves to be a valid method for improving engine and powertrain efficiency [2]. Regenerative suspension systems with energy harvesting shock absorbers have also gained considerable interest over the past two decades. These systems would not only enhance vehicle dynamics but also convert the otherwise wasted vibration energy into electricity.

Learning from this, these two surrounding energy sources (human and vehicular vibrations) show great potential for energy harvesting and have already shown great potential in the past decades. It is however, still a challenge since these vibrations have extremely low-frequencies and amplitudes [4]. Numerous systems have been proposed and experiments have been conducted to provide evidence for these methods of energy harvesting.

B. Energy harvesting technology

As stated in the preceding subsection, there is potential for harvesting vibrational energy induced by human motion and vehicular motion. These two domains provide a broad spectrum of possibilities when it comes to harvesting technologies. In general, these systems all have four [5] components. An energy capture mechanism (input), a transmission mechanism, a generator module and an energy storage device. These systems can generally be classified based on how the vibrational movement is translated into electricity. The following harvesting technologies will be discussed:

- Electromagnetic
- Piezoelectric
- Hydraulic

1) **Electromagnetic energy harvesting:** This method is the most popular type of energy harvesting technology. This is due to the high-energy conversion efficiency, quick response, strong controllability and capability in energy recovery [2]. The technology is based on Faraday's law of electromagnetic induction [6]. With the introduction of a coil and a magnet, a small voltage can be produced. This is due to the relative movement between coil and magnet induced by every vibration that occurs [6]. Therefore the induced relative motion of the permanent magnet(s) and inductive coil is a key factor to improve the output electricity.

This harvesting technology can be split up into two types. Namely, linear electromagnetic harvesters and rotary electromagnetic harvesters [2]. Linear electromagnetic harvesters

use simple structures to directly convert the vibrations into electricity based on electromagnetic induction. Rotary electromagnetic harvesters translate the linear vibration into rotation to drive a generator. This generator will generate electricity.

The translation from linear to rotary motion is done with a transmission system. These systems are typically mechanical or hydraulic. Mechanical transmission systems are deemed more simple, have greater efficiency, and considerable average power [2]. Therefore these mechanical systems have developed rapidly. Examples of these systems are the ball screw mechanism and the rack-pinion mechanism [2].

Hydraulic based transmission harvests the vibration energy by capturing oscillatory motion and driving the generator with a hydraulic motor. The linear motion is converted to rotary motion with the use of hydraulics.

2) **Piezoelectric energy harvesting**: This method has the advantage of simple architecture and easy fabrication. Effective strain in the material, induced by vibrations, is converted into electrical energy by a piezo crystal [6]. A piezo crystal turns these vibrations into a low-level electrical energy [6].

3) **Hydraulic**: These types of energy harvesters use hydraulic cylinders and accumulators to regenerate energy. Kinetic energy from vibrations is absorbed and converted into potential hydraulic energy [7]. The accumulator is used to store energy.

C. Aim

To further elaborate on the need for scavenging power from vibrational energy, this paper presents a review on the current state of affair. The aim of this paper is to present an overview of the newest vibration energy harvesting systems from human and vehicular induced vibrations based on their energy harvesting mechanism. Each method will be elaborated on with designs found in literature, after which an overview of the power generation capabilities will be presented.

D. Report structure

section II discusses the methods on how this literature review was set up. After which, the results from the systematic search are presented in section III. All relevant interpretations, limitations and recommendations are given in section IV. This review will end with a conclusion (section V).

II. METHOD

For this review, a systematic search was set up. In order to get more in touch with the research topic at hand, familiarization was done with the use of Google Scholar. The aim of this review (stated in the preceding section) is inserted into Google Scholar to find relevant keywords. The databases of Scopus, Web of Science and Pubmed were utilised. From this a search query iteration followed.

The systematic search is initialized with the use of a boolean search query. To promote and maintain a structural overview, the query was set up using 6 different categories relating to the research topic. The first category is based on the type of energy. For instance, kinetic or vibration energy. The second

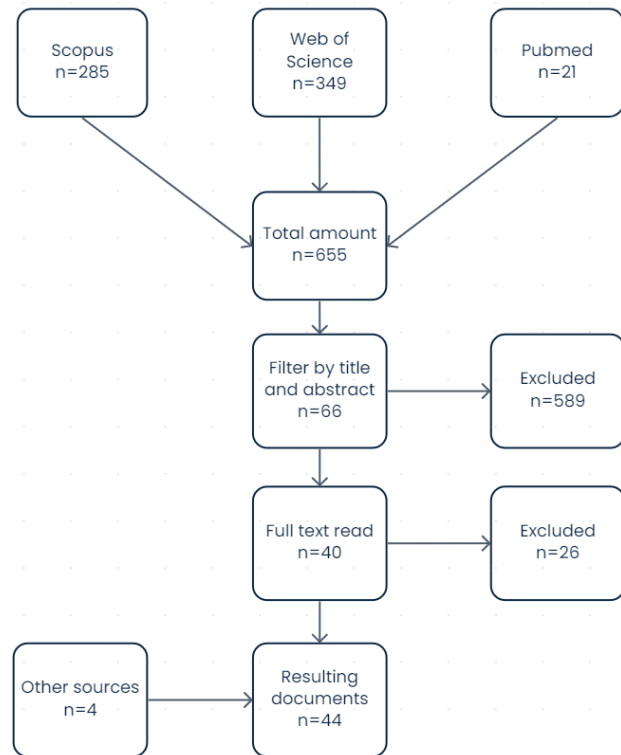


Fig. 1. Flowchart of obtained documents

category contains terms what to do with the energy. These are terms such as harvest or recover. The third category deals with the system where the original energy is lost, such as hydraulic systems. The fourth category includes solution systems, compliant mechanisms or piezoelectric structures for example. The fifth category relates the search to the human body or vehicles. The sixth and final category determines the outcome to be designs. Terms that are terminated with an asterisk (*) are terms that have a wildcard ending. Absorb* may give absorption for example. This resulted in the search query shown in Table I.

From this query, 655 documents were found across 3 databases. These documents are filtered on title, abstract and duplicates. From the 655 documents 589 were excluded, leaving 66 documents for a full text read. Papers were included if they are relevant to energy regeneration based on vibrations. The full text read resulted in 40 relevant papers for this review. Finally, 4 other papers were added from other sources, reaching a total of 44 papers. The process can be seen in Figure 1.

III. RESULTS

The technologies described in subsection I-B energy harvesting based on vibrations can be done in numerous ways. With the main categories electromagnetic, piezoelectric and hydraulic energy harvesting. This section will present all relevant methods found in literature, and are classified based on the type of technology.

TABLE I
SEARCH QUERY

AND						
OR	Vibrat*	Energy absorb*	Hydraulic system	Suspension	Lower limb	Design
	Shock	Energy regenerat*	Mechanical motion	Damp*	Leg	
	Kinetic	Energy harvest*	Biomechanic* energy	Rectif*	Joint	
	Negative work	Energy recover*	Exoskeleton	Compliant	Knee	
			Robot	Cam	Hip	
			Dynamic system	Braking	Ankle	
			Pendulum	Piezo	Vehicle	
				Bevel	Human	
				Accumulator		

A. Electromagnetic energy harvesting

As stated in section subsection I-B can be divided in linear and rotary electromagnetic harvesting. Both will be discussed in this subsection.

1) **Linear electromagnetic harvesting:** These systems have no need for a transmission system. Electricity is generated from linear movement and electromagnetic induction with simple structures. Wei et al. [8] discusses a novel electromagnetic actuator that produces energy, while suppressing said vibrations. This system can be installed in many mechanisms to reduce energy losses [8]. The electromagnetic actuator consists of a controlled object, four permanent magnet rings (PM rings), a soft iron outer shell, four soft iron rings, three springs, an acceleration sensor, and a displacement sensor (Figure 2). The energy regeneration function of the system collects energy from vibrations of the controlled object. Relative motion between the controlled object and the PM rings, coil 1 and coil 3 cut magnet flux in the air gap of the electromagnetic actuator. Coil 2 is used for suppressing vibrations. An electromotive force (EMF) is produced and can be stored in a battery by a series of circuits. These are a voltage boosting circuit, rectifier circuit, and a voltage stabilizing circuit.

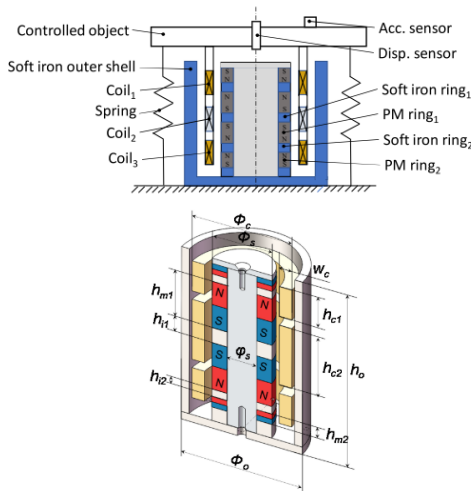


Fig. 2. Linear electromagnetic actuator [8]. Electricity is generated via the electromagnetic induction principle.

A similar structure is discussed by Abdelkareem et al. [2]. A linear generator is presented with 2 parts. A magnet assembly and a coil assembly. Together this damper converts the

vibrational kinetic energy of the body/vehicle into electricity. The magnet arrangement consists of ring-shaped permanent magnets and ring-shaped high magnetically permeable spacers. These are stacked on a rod of high reluctance material [2]. The system is depicted in Figure 3, together with a similar shock absorber discussed in a study conducted by Xiao et al. [9]. Namely, the cylindrical Halbach permanent magnet linear generator. This regenerative shock absorber is mainly composed of coil windings between the inner and outer cylinder of the stator. The mover is composed of a piston rod and permanent magnets. The rod is composed on non-magnetic, light material. The relative movement between mover and stator generates electrical energy.

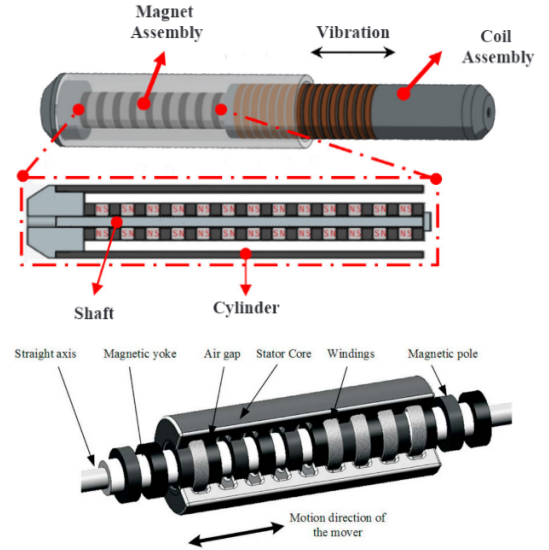


Fig. 3. Linear electromagnetic actuator [2] (top) and the cylindrical Halbach permanent magnet linear generator [9] (bottom). These two shock absorbers have similar working principles, both utilising multiple coil windings on the stator and multiple magnets on the mover.

The work presented by Mofidian et al. [10] focused on developing a dual-purpose vibration isolation recovery system. The dual functionality is achieved by the use of elastic and magnetic elements [10]. The main purpose is preventing vibrations from travelling through isolated mass with the use of magnetic and viscous dampers and elastic and magnetic springs [10]. The secondary task however, is converting the kinetic energy from vibration oscillations into electricity. Energy that would otherwise go to waste heat [10]. The levitated

magnet moves vertically when the device is subjected to external vibration. Subsequently, the air is forced through the holes and around the levitated magnet mass. As the magnet moves, voltage is induced in the coil by electromagnetic induction. As a result, vibrational kinetic energy is converted into electric energy. The function of the spiral spring is to guide and align the movement of the levitated magnet. A depiction of the system can be seen in Figure 4.

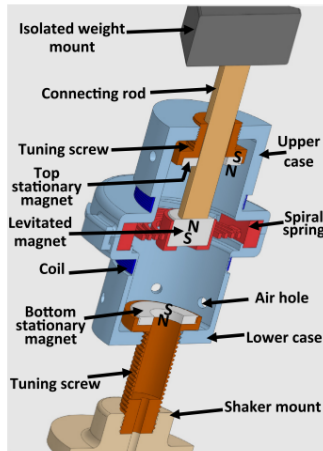


Fig. 4. Dual purpose vibration isolation harvester. Functions to prevent vibrations from travelling through isolated mass and to convert kinetic energy into electricity [10].

The four models described by Wei et al. [8], Abulkareem et al [2], Xiao et al [9], and Mofidian et al. [10] are posed as dampers in literature as well as having energy harvesting capabilities. These systems are mostly found in vehicle suspension systems, harvesting vehicular induced vibration energy. A model discussed by Halim et al. [11] however, harvests energy from human body induced vibrations. The system up-converts the vibration of human limb motion to high-frequency vibrations by mechanical impact of a freely movable ball on two optimized frequency up-converted generators [11]. The movable ball is non-magnetic. The generators are composed of a compact helical compression spring, a magnet, and a coil wound around the cylindrical housing [11]. The non-magnetic ball acts as an inertial mass. This ball couples the human induced low-frequency vibration into high-frequency oscillations when impact on the spring occurs. The power output of the system depends on multiple factors, namely the coil characteristics (number of turns, relative position to the magnet), relative motion between magnet and coil, and magnetic flux linkage with the coil [12]. The relative motion between the magnet and the coil generates electrical energy. A depiction of the model is presented in Figure 5.

A study conducted by Wang et al. [13] discussed a similar principle. Namely, a plane vibration-based electromagnetic generator using a magnetic spring and ferrofluid. This model could harvest energy from human body induced vibrations as well. The schematic model as well as the produced concept are depicted in Figure 6. The movable and fixed permanent magnets are placed above and below the bottom of the housing, which is non-magnetic. The magnets are placed such

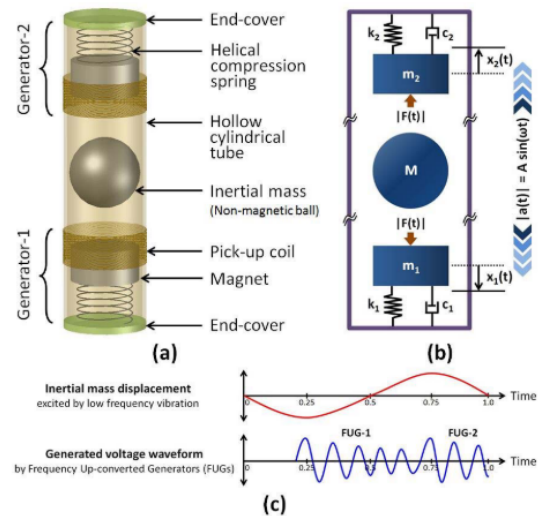


Fig. 5. Frequency up-converting linear electromagnetic harvester [11]. (a) Schematic structure, (b) mechanical model, and (c) operation principle. Up-conversion is achieved by mechanical impact of a metal ball on a helical compression spring. Converting low frequency vibrations into high frequency vibrations.

that they face each other with opposite poles. A copper coil is fixed below the top of the non-magnetic housing. A ferrofluid (kerosene-based) is deployed at the bottom of the movable magnet to suspend the movable magnet and reduce friction due to the magnetic attractive force [13]. This force acts as a balancing force to return the movable magnet to its original position. Electrical energy is generated when the movable permanent magnet oscillates due to external vibrations.

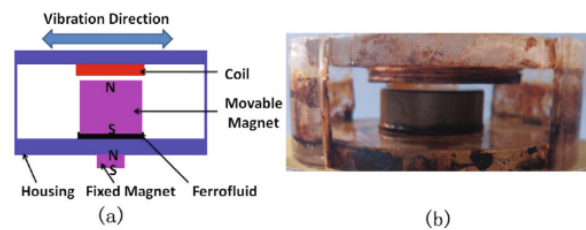


Fig. 6. Plane vibration-based electromagnetic generator. (a) Schematic model and (b) Produced concept. Electrical energy is generated when the movable permanent magnet oscillates due to external vibrations [13].

A study conducted by Chamanian et al. [14] presented a wearable battery-less wireless sensor network with an electromagnetic energy harvester. This electromagnetic energy harvester is developed and optimized to power a typical wireless sensor mote, scavenging electrical energy from human induced vibrations [14]. The harvester is composed of a cylindrical package, a fixed magnet at the bottom, a moving magnet suspended by a magnetic spring, and a coil wound around the cylindrical package. The top and bottom of the cylinder are closed with caps. Electrical energy is extracted when the magnet vibrates along the tube according to the electromagnetic induction principle. An image of the harvester

can be seen in Figure 7.

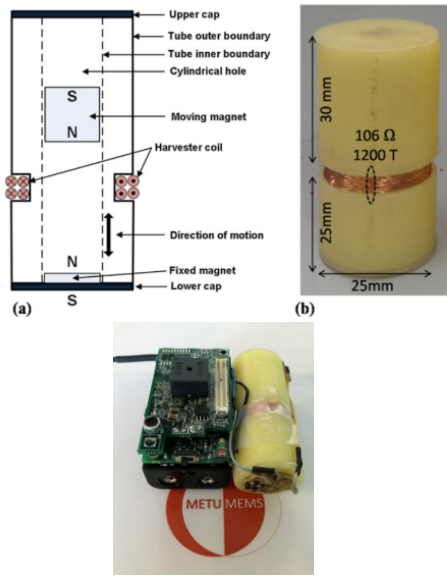


Fig. 7. Wearable electromagnetic energy harvester. Top image shows (a) Schematic, and (b) produced concept. Bottom shows harvester plus sensor mote. Electrical energy is extracted when the magnet vibrates along the tube according to the electromagnetic induction principle [14].

The models discussed in the studies by Halim et al., Wang et al., and Chamanian et al. all elaborate on cylindrical structured electromagnetic energy harvesters. A study conducted by Berdy et al. [15] however utilizes a rectangular box to harvest energy with the same principle of magnetic levitation as Chamanian et al. discussed. The harvester consists of a levitating magnet, fixed magnets, a coil, and a guide box [15]. When vibrations are experienced by the box, the magnet will oscillate. As the levitated magnet moves, a voltage is induced in the coil wrapped around the box. This produces a current that flows into an attached electrical load [15]. The device is shown in Figure 8.

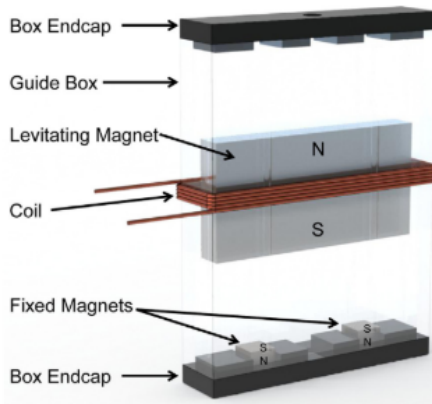


Fig. 8. Levitating magnet vibration energy harvester. When the levitated magnet moves, a voltage is induced in the coil wrapped around the box. This produces a current that flows into an attached electrical load [15].

Abdelnaby et al. [16] presents a vibration-based electromagnetic energy harvester that relies on a motion amplification mechanism. This mechanism, which aim is to

convert a small persistent base motion into larger oscillations to generate electric power, is composed of compliant material (acrylic plates). This will promote fewer mechanical parts and attains mobility from the elasticity of the material [16]. The mechanism contains two convex strips, both with radius of curvature R (see Figure 9) and are connected by two straight sides with length c . Input displacement (x) will result in a perpendicular output motion. The flexure joints are characterized by a fillet of radius r . The mechanism aims to amplify the input motion in perpendicular direction. Energy is extracted from the mechanism by placing a permanent magnet on the expanding side of the mechanism. This magnet moves past a stationary coil. The terminals of the stationary coil are connected across a load resistance to generate power.

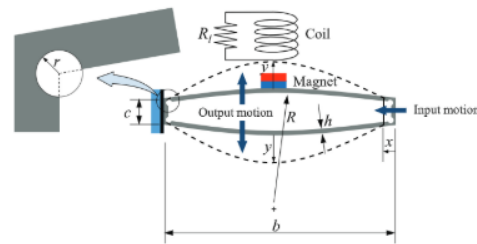


Fig. 9. Schematic of flexensional compliant mechanism. Energy is extracted from the mechanism by the permanent magnet on the expanding side of the mechanism. The magnet moves past a stationary coil. The terminals of the stationary coil are connected across a load resistance to generate power [16].

To conclude this section on linear electromagnetic energy harvesting, Table II shows the energy harvesting capabilities of the proposed designs. The proposed designs by Abdelkareem et al. [2] and Xiao et al. [9] are excluded since too little information was found on their energy harvesting capabilities.

TABLE II
ENERGY HARVESTING CAPABILITIES - LINEAR ELECTROMAGNETIC

No.	Reference	Energy harvesting technology	Frequency (Hz)	Amplitude (mm)	Acceleration (m/s^2)	Power (mW)	Experiment	Comment
1	Wei et al. [8]	Electromagnetic actuator for vibration suppression	5.0	3.045		95.0	Sinusoidal excitation	
2	Mofidian et al. [10]	A dual-purpose vibration isolator energy harvester	12.5		1 g	0.115	Vibration shaker	
3	Halim et al. [11]	Mechanical impact driven electromagnetic energy harvester	5.17		2 g	2.15	Hand shaking	
4	Wang et al. [13]	Plane vibration-based electromagnetic energy harvester	4.5			0.270	Walking and jogging	
5	Chamanian et al. [14]	Wearable wireless sensor network with electromagnetic energy harvesting	2.65		0.15 g	0.127	Human waist motion	
6	Berdy et al. [15]	Magnetic levitation based energy harvesting	6.7		0.1 g	0.410	Vibration shaker	Power output limited by levitating magnet displacement limit
7	Abdelnaby et al. [16]	Flexensional compliant based energy harvesting	1.4	4		0.0120	Sinusoidal excitation	

2) **Rotary electromagnetic harvesting:** These energy harvesters are characterized by their transmission mechanisms. These can be mechanical or hydraulic as mentioned earlier in [subsection I-B1](#). Mechanical transmission systems are the most common, since they are more simple with greater efficiency and considerable power generation. This review not only discusses the typical mechanisms such as ball-screw transmission and rack pinion transmission, but the more novel mechanisms as well. First the mechanical based transmission systems will be discussed, followed by hydraulic transmission based systems.

Li et al. [17] investigated the power generation capabilities of an energy harvesting shock absorber where a pair of rack and pinion, a shaft and three bevel gears are used. The system also includes two roller clutches. This system is fitted inside a traditional shock absorber cylinder. The transmission system rectifies the oscillatory vibrational motion into unidirectional rotary motion (mechanical motion rectification (MMR)). This movement is initialized when the rack moves up and down, the pinion and shaft will rotate clockwise and counterclockwise. Due to the engagement of one-way roller clutches, only one large bevel gear will be engaged and driven by the shaft. The other large bevel gear will remain stationary. As a result the shaft of the generator and planetary gear will always move in one direction, generating power. A depiction of the system can be seen in [Figure 10](#).

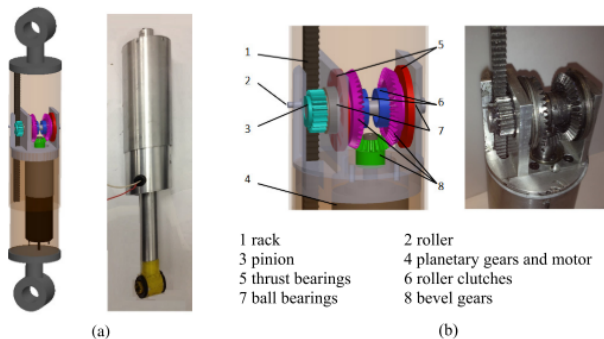


Fig. 10. Rack and pinion electromagnetic energy harvester. (a) overall view, (b) inner structure. The inner structure with rack and pinion converts linear motion into rotary motion to drive the generator unidirectionally and produce power [17].

Ali et al. [5] conducted a study which investigated the power generation capabilities of a novel barrel cam follower mechanism. This mechanism is fit into a shock absorber as well. The system typically consists of a vibration input module, energy conversion module, generator module, and power storage module. The barrel cam follower is designed to convert linear motion into rotary motion. The input shaft of the transmission mechanism is connected with the barrel cam. The transmission module includes bevel gears, input shaft, output shaft, and one-way bearings. When an input force is given, the follower moves in the helical groove (see [Figure 11](#)) to rotate the barrel cam and input shaft. A downward stroke will rotate the barrel cam counterclockwise. Conversely,

upward strokes will result in clockwise movement. Both times a one-way bearing is engaged, which will determine the unidirectional motion of the generator. This rotation will generate power. A depiction of the working principle is shown in [Figure 11](#).

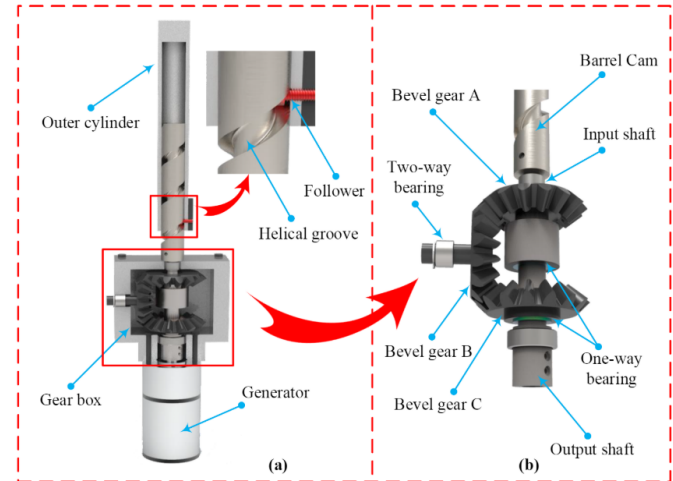


Fig. 11. (a) Barrel cam rotary regenerative shock absorber and (b) Transmission mechanism. The barrel cam converts linear motion into rotary motion to drive a generator [5].

Pan et al. [18] used a compact ball screw based electromagnetic harvester for railroad energy harvesting. The harvester is placed between two sleepers. The input nut plate ([Figure 12](#)) is clamped to the railway track. Ball screw are connected with the driven shaft. The working principle is as follows; when the track moves down due to a passing train, the ball screw will rotate counter-clockwise. At this moment the upper bevel gear is engaged and becomes the driving gear. The lower bevel gear disengages, resulting in counterclockwise movement of the generator. When the track moves upward again, the ball screw will rotate clockwise, engaging the lower bevel gear. This results in a counterclockwise movement of the generator. This means that it does not matter whether the track moves up or down. The reciprocal movement is converted to unidirectional movement of the generator.

Zhang et al. [19] discussed a renewable energy harvesting system for railroad application as well. Only this system uses another mechanical transmission system to rectify the vibrations induced by trains. This transmission system is composed of rack, and a set of gears and pinions that rectify the reciprocal motion. A generator and supercapacitor are used for power generation and storage. This system contains two one-way bearings inside the gears that transform the bidirectional vibration of the rack into unidirectional rotation of the generator. Passing trains affect the rack with small amplitude and frequency. The set of gears function to increase amplitude to generate more power. When in working, the two one-way bearings work alternately, meaning when one is engaged the other is disengaged. A depiction of the working principle is given in [Figure 13](#). When the rack moves upward, the one-way bearing on the right side is engaged and torque

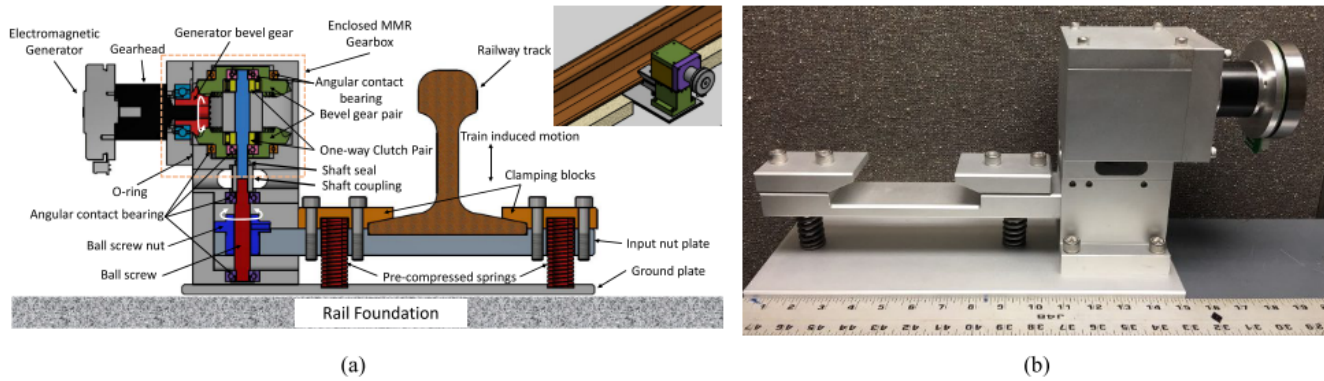


Fig. 12. (a) Detailed design of ball screw based energy harvester and (b) Prototype. The ball screw mechanism converts linear motion into rotary motion to drive the generator and produce power [18].

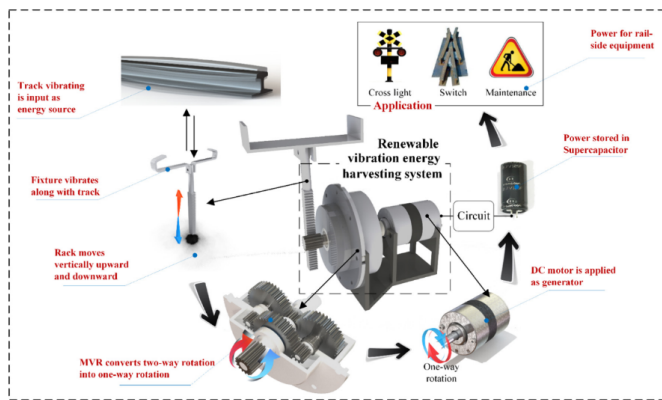


Fig. 13. Vibration energy harvesting system railroad application. The system uses rack and pinion to convert linear motion into rotary motion. The set of gears functions to increase the amplitude and to convert two-way rotation into one-way rotation [19].

is transmitted. The left side does not transmit any torque and simply rotates along. The generator rotates counterclockwise. In reverse, when the rack moves down, the left one-way bearing is engaged and therefore the left side transmits torque. The generator shaft rotates counterclockwise again.

A study conducted by Maravandi et al. [20] discusses a novel shock absorber for cars, which uses a two-leg motion conversion mechanism. In addition to the two-leg motion conversion mechanism, this system contains a planetary gearhead and a brushless permanent magnet rotary machine as well. The two-leg mechanism converts translational motion induced by road roughness into rotary motion. The planetary gearhead functions to increase the rotary motion amplitude, which results in a higher power output. Figure 14 depicts the design and built prototype.

Salman et al. [21] conducted an analysis on another novel regenerative shock absorber for cars. The discussed design contains helical gears to convert the linear vibrational motion into rotary motion. The system consists of a helical pinion shaft with two helix hands, two helical gears in the different

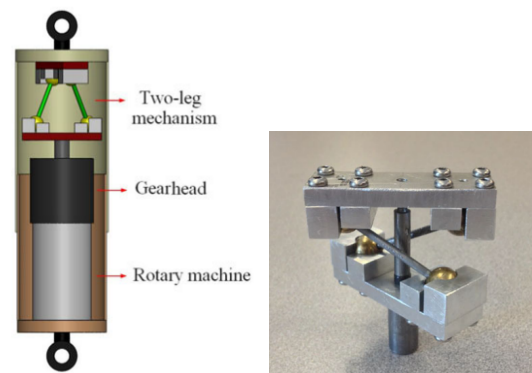


Fig. 14. Two leg motion conversion mechanical shock absorber system. Design and prototype. The two-leg mechanism converts translational motion into rotary motion. The planetary gearhead functions to increase the rotary motion amplitude, which results in a higher power output [20].

helix hands, two tapered roller clutches, two tapered roller bearings, two guide cylinders, an inner cylinder and outer cylinder, a joint cylinder, a planetary gearbox, a generator, and a supercapacitor. As this is a shock absorber, the mechanism functions to resist force from induced vibrations and harvest electrical energy at the same time. The vibrations induced by road roughness are transferred to the cylinders of the absorber. This results in a linear motion between inner and outer cylinder. This reciprocal linear motion is converted into a one-way rotary motion with the use of the helical gears and tapered roller clutches. As the helical pinion shaft moves up or down, the two helical gears will rotate oppositely. Due to the two tapered roller clutches the cylinders rotate unidirectionally, which is the input motion to the generator. The design and working principle are depicted in Figure 15.

Energy harvesting shock absorbers are not only studied for railroad or car application, Gonzalez et al. [22] designs and analyses a regenerative shock absorber for motorbikes. This system converts linear movement into rotational movement with the use of synchronous pulleys and belts. The linear movement is transmitted to a piston that is clamped to a belt with a crimp block (Figure 16). This block connected to

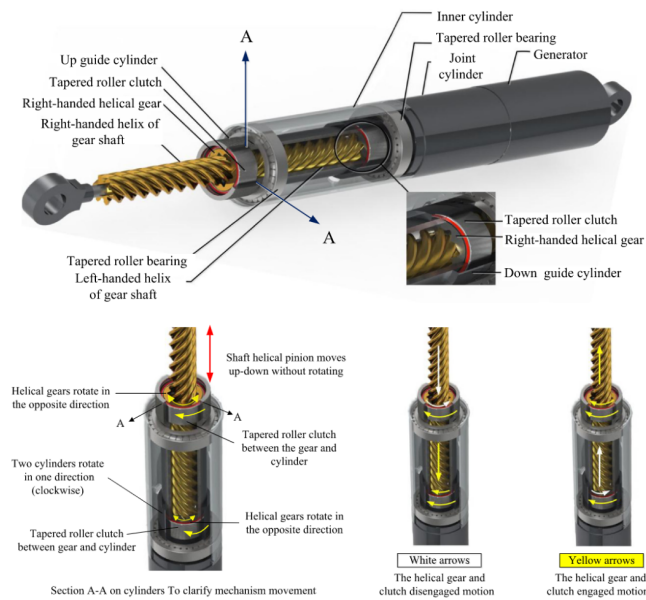


Fig. 15. Design of the shock absorber containing helical gears (top) and working principle (bottom). Reciprocal linear motion is converted into a one-way rotary motion with the use of the helical gears and tapered roller clutches. As the helical pinion shaft moves up or down, the two helical gears will rotate oppositely. Due to the two tapered roller clutches the cylinders rotate unidirectionally, which is the input motion to the generator [21].

a linear guide system, which is attached to the suspension cylinder. The belt is connected to the two synchronous pulleys. One of these pulleys rotates freely, while the other one transmits rotation via bevel gears to the planetary gearbox and generator. The pulleys are fixed to two shafts that rotate on a system of bearings. The power shaft transmits rotation to the bevel gears. The bevel gears correct the rotation axis towards the gearbox and generator with 90° .

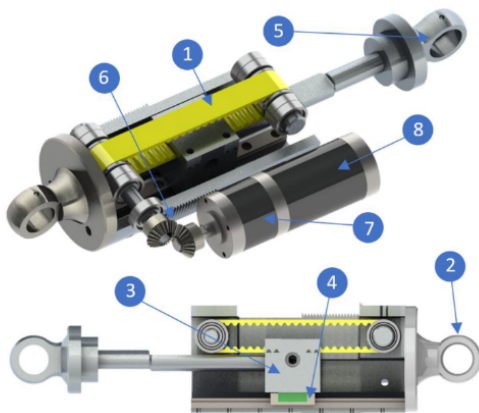


Fig. 16. Vibration energy harvester using synchronous pulleys. Linear movement is converted to rotary movement with the use of synchronous pulleys and belts. The pulleys are fixed to two shafts that rotate on a system of bearings. The power shaft transmits rotation to the bevel gears. The bevel gears correct the rotation axis towards the gearbox and generator with 90° [22].

A similar concept conducted in a study by Bowen et al. [23] uses a cable transmission system instead of a belt transmission system. Translational movement is transferred by means of a piston to a mobile skate. This mobile skate rests on linear guides. The skate has two tensioners that pull the cable according to the movement. There are 2 pulleys present, one driven pulley and one generator pulley. The generator pulley is coupled to a larger diameter pulley, which functions to double the rotational speed. The last pulley is coupled to a multiplier, which in turn is connected to a generator to generate power. The system is depicted in Figure 17.

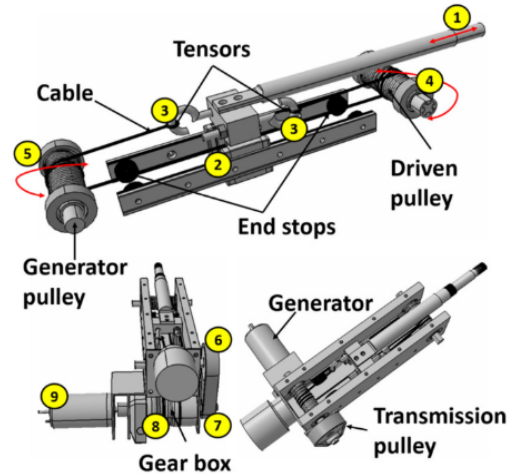


Fig. 17. Cable transmission vibration energy harvester. Translational movement is transferred by means of a piston to a mobile skate. The skate has two tensioners that pull the cable according to the movement. The generator pulley is coupled to a larger diameter pulley, which functions to double the rotational speed. The last pulley is coupled to a multiplier, which in turn is connected to a generator to generate power [23].

Another study conducted by Li et al. [24] discusses an energy harvester that uses a transmission system composed of helical racks. The total system consists of four modules, namely an energy capture module, a motion conversion module, a generator module, and an electric energy storage module. The energy capture module is composed of an upper, middle, and lower cylinder. Linear reciprocating motion occurs between upper and middle cylinder due to vibrations. The motion conversion module functions to convert the bidirectional motion into unidirectional motion. The system contains two helical racks with opposite threads. Added to this, an upper right-hand helical gear is mounted on the main shaft with a one-way clutch, and a left-hand helical gear is also mounted with a one-way clutch. When the upper cylinder moves down, the two helical gears rotate. With the disengagement of one one-way clutch when triggered by the racks, the generator will always be driven in one direction. The gearbox functions to increase the rotational speed. The generator generates electrical power which is stored in the supercapacitor. The system is depicted in figure Figure 18.

Fan et al. [25] proposed an innovative vibration energy harvesting backpack, which rectifies bidirectional motion into unidirectional motion to drive a generator as well. This proposed system is composed of a flexible mechanical motion

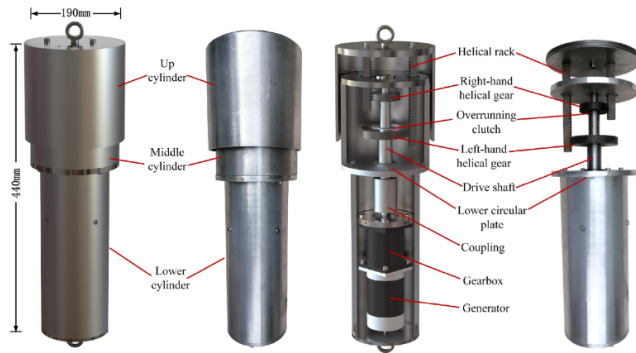


Fig. 18. Vibration energy harvester with helical gears. Linear reciprocating motion occurs between upper and middle cylinder due to vibrations. The motion conversion module functions to convert the bidirectional motion into unidirectional motion. When the upper cylinder moves down, the two helical gears rotate. With the disengagement of one one-way clutch when triggered by the racks, the generator will always be driven in one direction to generate power [24].

rectifier (MMR), consisting of an inelastic strap, an elastic strap, a shaft with a double layered plectrum, and a ratchet (rotor). The flexible MMR converts the reciprocating motion into an alternating spin of the shaft. When a downward force is applied to the inelastic strap (vibration induces reciprocating motion of the backpack load), the inelastic strap is unwrapped. This forces the shaft to rotate counterclockwise. The ratchet is actuated by the double-layered plectrum to rotate counterclockwise. The double layered plectrum is composed of a rigid layer and a flexible layer. With reversed excitation, the strap restores to its original length (induced by the elastic strap), rotating the shaft clockwise. The flexible layer of the plectrum slides across the ratchet, inducing no rotation. This means that the stiffness of the double-layered plectrum is determined such that it drives the ratchet in one direction while disengaging in the other. Six permanent magnets are arranged in the rotor and six sets of coils are attached to the ring shaped stator to generate power. The system is packed in a cylindrical chamber that consists of a cover, left shell, and right shell. A depiction of the system is shown in Figure 19.

Liu et al. [26] conducted a study on a similar concept as Fan et al. [25]. Only this vibration energy harvesting backpack rectifies motion with 2 sets of rack and pinion. Each pinion contains a one-way bearing. The one-way bearing has free rotation in one direction and is locked in the other direction. Both one-way bearings determine the rotation of the shaft in clockwise direction. When the rack moves towards the right, pinion A rotates in clockwise direction and pinion B in counterclockwise direction. Pinion A is engaged and pinion B is not, resulting in clockwise rotation of the shaft. When the rack moves towards the left, pinion B is engaged and drives the shaft. This movement is induced by vibrations that result in the reciprocating motion of the backpack. The shaft is connected to a gearbox and generator to produce electrical energy. The system is depicted in Figure 20.

Satpute et al. [27] designed and analysed an energy regulating vibration harvester with a different mechanism to

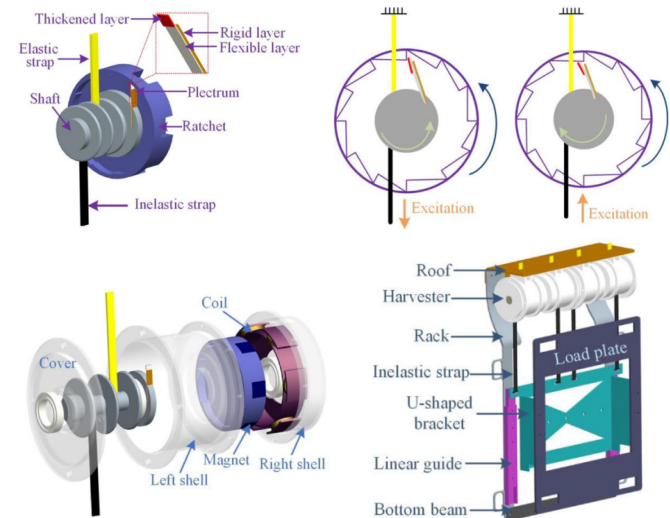


Fig. 19. Vibration energy harvesting backpack. The flexible mechanical rectifier is composed of an elastic strap, a shaft with a double layered plectrum, and a ratchet (rotor). The working principle is depicted above, where excitation introduces rotation of the shaft. With counterclockwise rotation the ratchet is actuated. With clockwise rotation the flexible layer of the double layered plectrum slides across the ratchet. This results in no rotation from the ratchet [25].

rectify bidirectional movement into unidirectional movement. This system is depicted in Figure 21, which comprises of the mechanical motion rectifier, an energy storage element (torsional spring), gear train, and a rotary electric generator. The mechanical motion rectifier is mainly composed of mechanical levers, a spherical joint, two sliding joints, and one-way bearings. When oscillating force occurs due to vibrations, the reciprocating movement is captured and transmitted to a shaft. The energy is stored in the torsional spring, receiving angular deflection. The energy is stored up to a certain threshold, after which the energy is released to the electric generator through the gear train to generate electric power. The system with collar, sliding bush, tapered support and engagement pins (Figure 21) make it such that when the energy threshold from the energy storage element is reached, the MMR disengages to release the energy. Therefore power is generated with pulses. The MMR transmits torque to the torsional spring. At maximum threshold, the projecting pins are pressed against tapered support 2, which initiates the sliding bush to move in axial direction. As this occurs, the sliding bush disengages from the MMR. The counterclockwise rotation has charged the torsional spring, therefore energy is released in clockwise rotation. During counterclockwise rotation of the shaft, the sliding bush rotates from tapered support one to tapered support two. At the final instance of clockwise rotation, the sliding bush comes into contact with the engagement pins to again connect with the MMR. The working principle is depicted in Figure 21.

As for mechanical transmission systems to generate power, there are some hydraulic transmission based electromagnetic energy harvesters as well. These systems are mainly composed of an hydraulic cylinder, containing hydraulic fluid to transmit

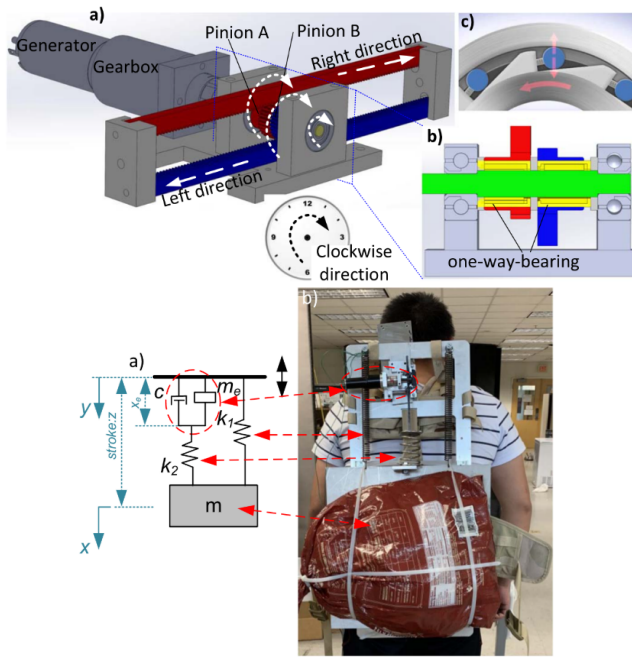


Fig. 20. Vibration energy harvesting backpack. Mechanical motion rectifier (top) and model and prototype (bottom). Motion is rectified with 2 sets of rack and pinion. Each pinion contains a one-way bearing. The one-way bearing has free rotation in one direction and is locked in the other direction. When the rack moves towards the right, pinion A rotates in clockwise direction and pinion B in counterclockwise direction. When the rack moves towards the left, pinion B is engaged and drives the shaft. This movement is induced by vibrations that result in the reciprocating motion of the backpack [26].

reciprocating motion, a hydraulic rectification system, and a hydraulic motor. For instance, Fang et al. [28] prototyped a hydraulic electromagnetic shock absorber, containing a hydraulic rectifier and integrated accumulator. These components are all packed in a cylinder. The piston of the shock absorber is driven under external reciprocating motion. High pressure oil flows into the hydraulic rectifier. After which, the oil goes through the accumulator which drives the hydraulic motor to generate electricity. Figure 22 depicts the shock absorber and schematics of the system.

Zhang et al. [29] conducted a study on a twin-tube pumping regenerative damper, depicted in Figure 23. The working principle is illustrated in Figure 23 as well. When the piston rod moves upward, check valve 1 closes and check valve 2 opens. High pressure oil in the upper cavity flows into the motor outlet through the middle cavity and pipe and drives the motor. After which the low pressure oil flows out of the motor outlet to the reserve cavity and flows back into the lower cavity through check valve 2. When the piston moves down, check valve 1 opens and check valve 2 closes, therefore the high pressure oil flows from the lower cavity into the upper cavity. The oil continues to flow into the motor inlet through middle cavity and pipe, driving the motor. So upward or downward movement both drive the motor in the same direction (unidirectional rotation) to generate power.

Li et al. [30] based a shock absorber system on a hydraulic rectifier to turn bidirectional motion into unidirectional motion. The core of the system is a hydraulic cylinder with a pis-

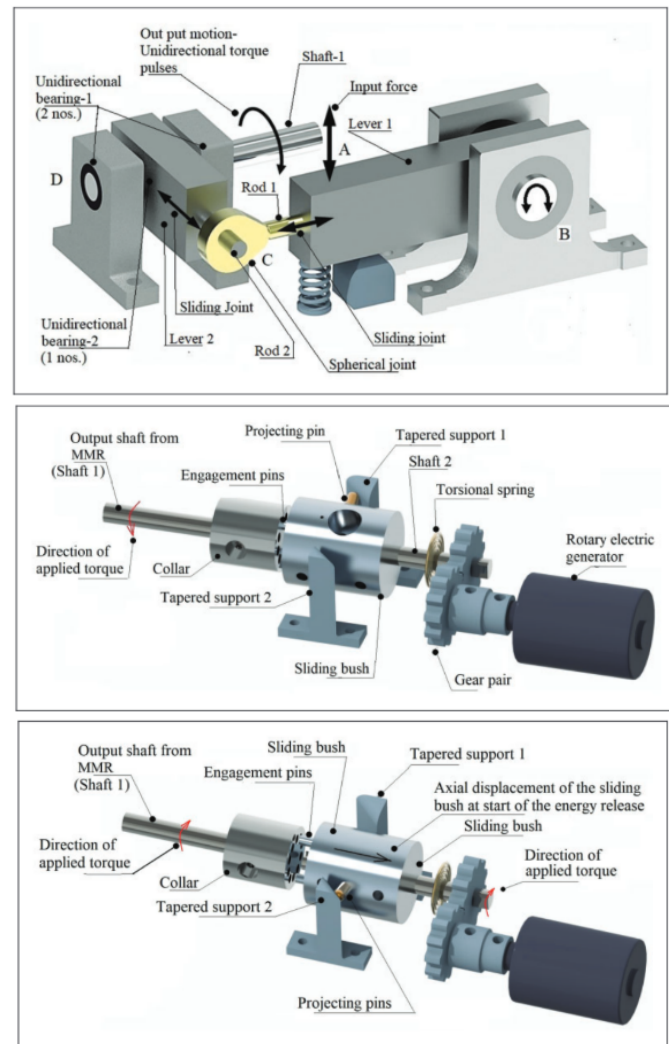


Fig. 21. Vibration energy harvester. MMR (top), working principle (middle and bottom). When oscillating force occurs due to vibrations, the reciprocating movement is captured and transmitted to a shaft. The energy is stored in the torsional spring, receiving angular deflection. The energy is stored up to a certain threshold, after which the energy is released to the electric generator through the gear train to generate electric power [27].

ton, hydraulic rectifier, hydraulic motor, and electromagnetic generator. The two ports of the cylinder are connected to the ports of the hydraulic motor through the hydraulic rectifier. The output of the hydraulic motor goes to the electromagnetic generator, connected with a shaft. A depiction of the design and working principle is shown in Figure 24. In response to excitation, oil flows through port 11, valve A, port 21, port 22, valve D, and port 12 consecutively. This causes the hydraulic motor to rotate clockwise. Reversed excitation lets the oil flow through port 12, valve C, port 21, port 22, valve B, and port 11 consecutively. This causes the hydraulic motor to rotate clockwise as well, determining the unidirectional rotation.

To conclude this section on rotary electromagnetic energy harvesting, Table III shows the energy harvesting capabilities of the proposed designs.

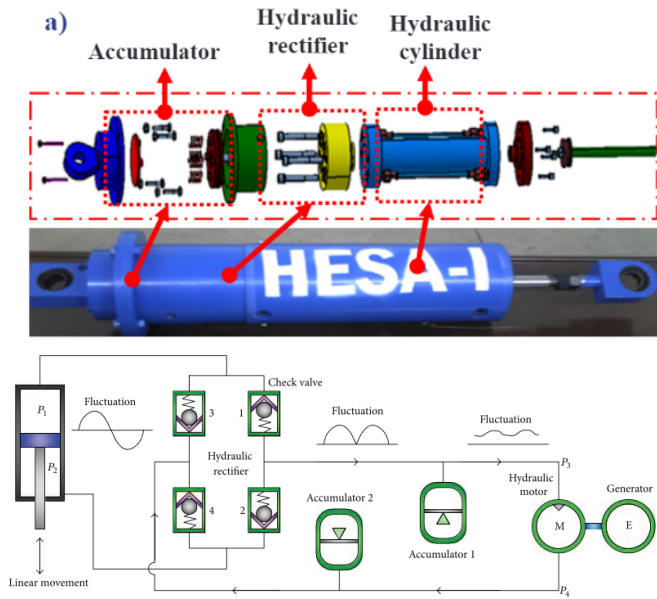


Fig. 22. Hydraulic harvesting shock absorber. Design (top) and working schematic (bottom). The main working is based on high pressure oil flowing into the hydraulic rectifier. After which, the oil goes through the accumulator which drives the hydraulic motor to generate electricity [28].

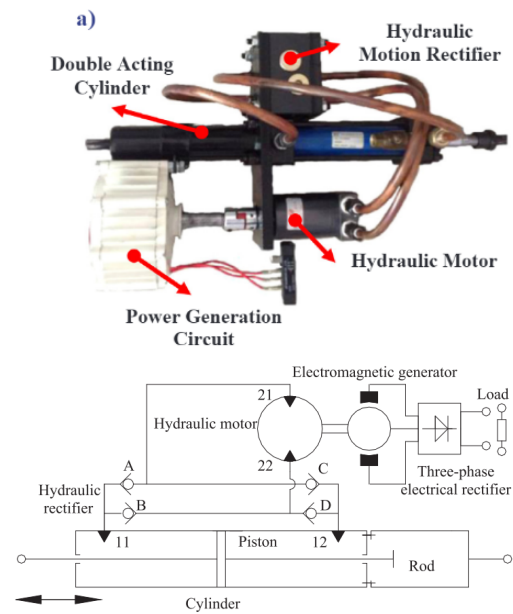


Fig. 24. Harvesting shock absorber with hydraulic rectifier. Prototype (top) and working schematic (bottom). The output of the hydraulic motor goes to the electromagnetic generator, connected with a shaft [30].

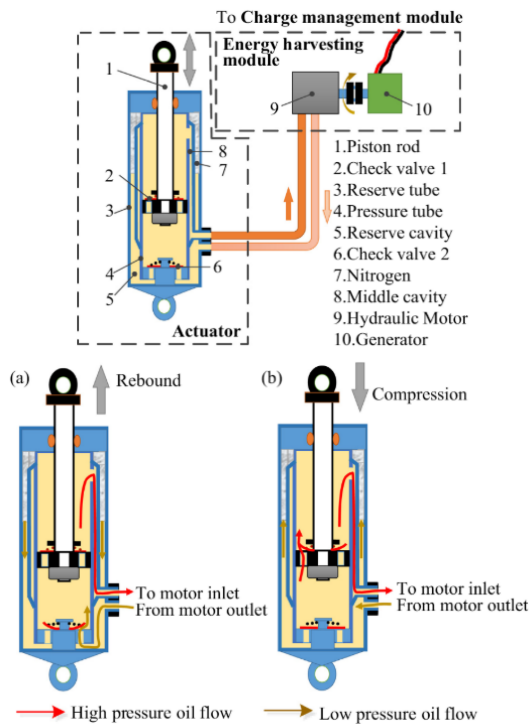


Fig. 23. Twin tube regenerative damper. Design (top) and working principle (bottom). Upward and downward movement both drive the motor in the same direction (unidirectional rotation) to generate power [29].

TABLE III
ENERGY HARVESTING CAPABILITIES - ROTARY ELECTROMAGNETIC

No.	Reference	Energy harvesting technology	Frequency (Hz)	Amplitude (mm)	Acceleration (m/s ²)	Power (mW)	Experiment	Comment
8	Li et al. [17]	Rack and pinion based energy harvester	3	5		62900 - 104300	Sinusoidal excitation	
9	Ali et al. [5]	Barrel cam based energy harvester	2	7.5		3850	Sinusoidal excitation	
10	Pan et al. [18]	Ball Screw based railroad energy harvester	2	3		19900	Sinusoidal excitation	
11	Zhang et al. [19]	Vibration rectifier based energy harvesting system	1	2.5	18	86670	Sinusoidal excitation	
12	Maravandi et al. [20]	Two-leg motion based energy harvester	1	5		540	Sinusoidal excitation	
13	Salman et al. [21]	Helical gears based energy harvester	2.5	5		270000	Sinusoidal excitation	
14	Gonzalez et al. [22]	Synchronous pulley and belt based harvester	2	10		2500	Sinusoidal excitation	
15	Bowen et al. [23]	Cable transmission based energy harvester	1	15		1400	Sinusoidal excitation	
16	Li et al. [24]	Helical gears based energy harvester	2.5	7		4252	Sinusoidal excitation	
17	Fan et al. [25]	Flexible motion rectifier in energy harvesting backpack	3		3 g	700	Running on treadmill at 7 km/h and 1.9 kg load	Running at 7 km/h equals 3 Hz frequency
18	Liu et al. [26]	Rack and pinion based energy harvesting backpack	1.1	25		2100	Sinusoidal excitation	
19	Satpute et al. [27]	Energy regulating vibration harvester	3-15	2		120 - 520	Sinusoidal excitation	Given average. Peak power 4.13 W
20	Fang et al. [28]	Hydraulic-electromagnetic based energy harvester	10	3		200000	Sinusoidal excitation	
21	Zhang et al. [29]	Twin-tube hydraulic pumping regenerative damper	1.655	50		200000	High speed shaker	
22	Li et al. [30]	Hydraulic motion rectifier based energy harvester	2	8		248800	Sinusoidal excitation	

B. Piezoelectric energy harvesting

Due to the possibility of maintaining simple and flexible mechanisms, piezoelectric energy harvesting has become another more common way of collecting vibration energy [31]. Zhang et al. [31] designed and analysed a multidirectional kinetic energy harvester. This system contains a kinetic energy harvesting module, an energy conversion module, and a power storage module. Vibrations are captured by an inertial block, which can rotate to capture vibrations in multiple directions. This is realised with a turntable that supports the whole capture mechanism. A piezoelectric beam (PZT material) with copper substrate is fixed at the end of the turntable. In addition, a deformation amplification mechanism is present. This is composed of a pendulum with magnet blocks and swing frame. The piezoelectric beam contains a magnet as well. When the pendulum swings close to the piezoelectric beam, deformation amplification is realised through magnetic repulsion. The kinetic energy is converted to electric energy and stored in supercapacitors. A depiction of the system is shown in Figure 25.

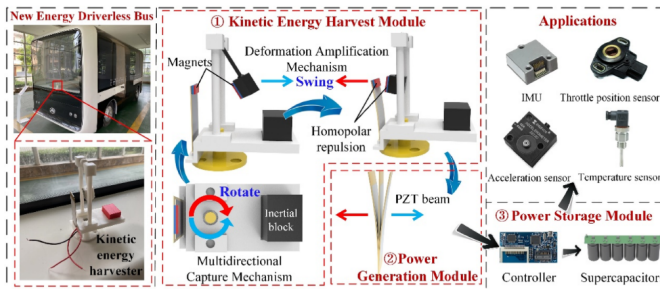


Fig. 25. Multidirectional pendulum piezoelectric energy harvester based on homopolar repulsion from magnets. Vibrations are captured by an inertial block, which can rotate to capture vibrations in multiple directions [31].

Zhong et al. [32] amplified vibrations with another method, namely a seesaw-type mechanism. This was done in order to enhance nonlinear energy harvesting [32]. The system is composed of primary cantilever beam with a U-shaped groove embedding a small cantilever beam (or internal beam). A mass is fixed at the end of the internal beam. A permanent magnet is fixed at the end of the primary beam and interacts with another external permanent magnet, forming a bistable structure. Mechanical energy is converted to electric energy with the use of a piezoelectric element (PZT) attached to the root of the primary beam. With induced vibrations, the motion of the internal beam constantly delivers energy to the primary beam. This accelerates the movement of the primary beam. The system is depicted in Figure 26.

Wang et al. [33] conducted a study on a bistable energy harvester as well. This system is based on 2 compressed springs. The bistability characteristic is achieved by exploiting the nonlinear force produced by the compressed springs [33]. The main structure is composed of a horizontal primary cantilever beam, four side beams, two vertical beams, two pre-compressed springs and a magnet. One end of the cantilever beam is fixed while the other end is connected

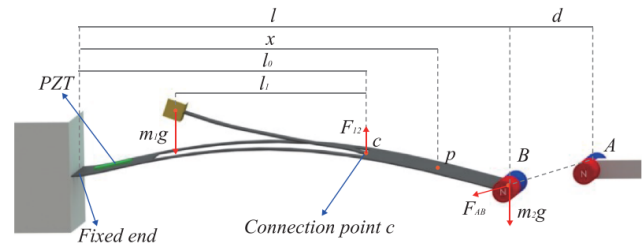


Fig. 26. Seesaw-type piezoelectric energy harvester, enhancing nonlinear energy harvesting. A bistable structure is introduced by placing a magnet at the end of the primary beam, which interacts with another permanent magnet [32].

to the springs. The end of the cantilever beam contains the magnet. The other ends of the compressed springs are connected to the middle part of the vertical beams. Four extra magnets are bolted to the ends of the vertical beams, at the inner sides. A piezoelectric film (PVDF) is bonded near the fixed end of the primary beam to harvest electrical energy. In the initial state without external excitation, the magnet at the free end of the cantilever beam is in unstable equilibrium. This is due to gravity, spring force, and force of the primary beam. When excited, the free end of the cantilever beam with magnet deviates. This causes the compressed springs to release their elastic energy into kinetic energy. This further forces the magnet away from unstable equilibrium. The magnets placed at the ends of the vertical beams apply repulsive forces and contribute to returning to initial unstable equilibrium position. The system has a total of three equilibrium positions (two stable and one unstable) [33]. An image of the system can be seen in Figure 27.

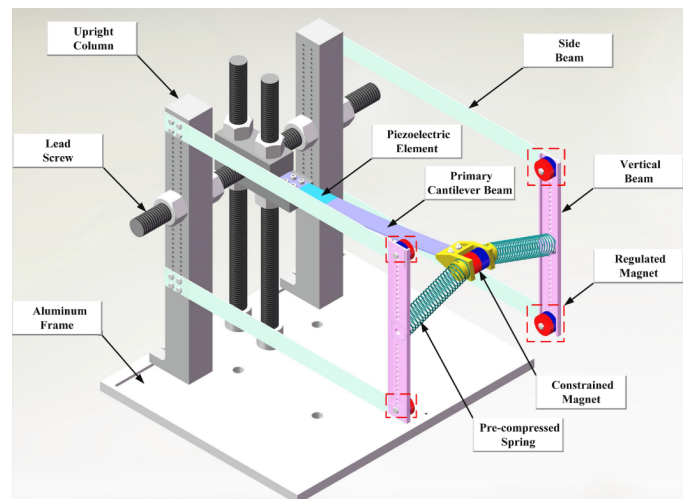


Fig. 27. Spring-based bistable energy harvester. The bistability characteristic is achieved by exploiting the nonlinear force produced by the compressed springs [33].

Ma et al. [34] proposed a piezoelectric compliant mechanism to harvest vibrational energy. This energy

harvester can operate at low frequency without a large proof mass and provides uniform strain. A unimorph beam is composed of top and bottom electroded piezoelectric material (PVDF) bonded to a substrate layer. One end of the beam is clamped. The other end is connected to the middle of a U-shaped link with compliant hinges. The proof mass is connected to the end of the U-shaped link. Therefore, the compliant mechanism at the tip can amplify the tip displacement to produce large motion of the proof mass and harvest electrical energy. The schematic and prototype are depicted in Figure 28.

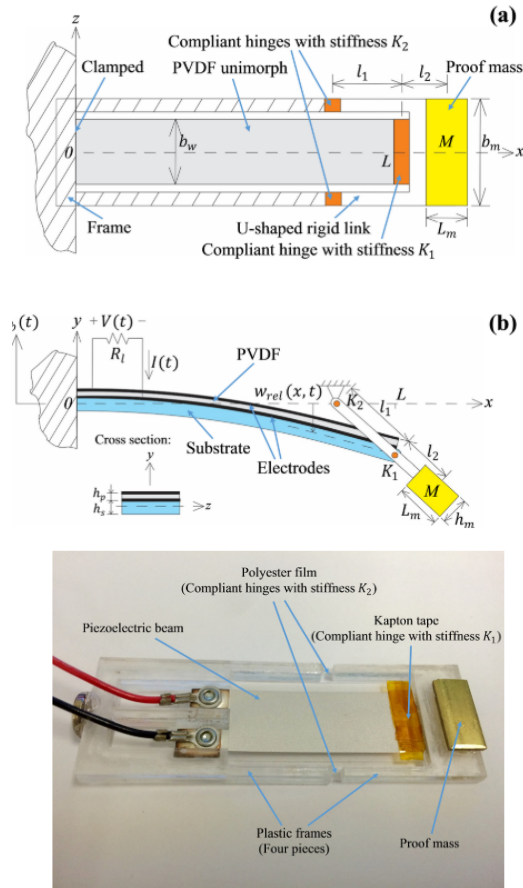


Fig. 28. Piezoelectric compliant energy harvester. Schematic (design (a) and model (b)) and prototype (bottom). The beam is composed of top and bottom electroded piezoelectric material. The proof mass at the end amplifies the displacement [34].

Inspired by the flight mechanism of the dipteran, Zhou et al. [35] proposed a bio-inspired energy harvester to capture ultralow-frequency vibration energy. The system is composed of an aluminum rod, two rigid rods, two flexible beams, and a proof mass. One end of the flexible beam is fixed to the base while the other end is connected to a rigid link with the use of a hinge. The other end of the rigid link is connected to the proof mass. The proof mass is guided along the axis of the aluminum rod. In addition, two piezoelectric patches (PZT-5H) are attached to the flexible beams to harvest electrical energy. When the proof mass oscillates, power is generated. The system is depicted in Figure 29.

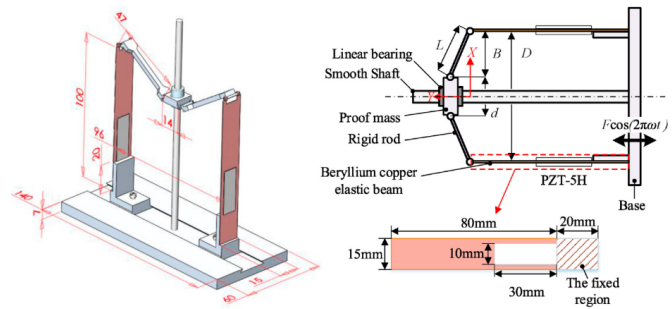


Fig. 29. Bio inspired piezoelectric vibration energy harvester schematics. This design is inspired by the flight mechanism of the dipteran [35].

Zhao et al. [36] designed a new type of ring piezoelectric energy harvester that uses magnetic forces. This harvester is used to capture and harvest vibration energy in vehicle suspension. The harvester is composed of a motion conversion component and an energy conversion component. The linear motion between vehicle and wheel is converted to rotary motion. This is achieved with a ball screw mechanism. The energy conversion mechanism is composed of an outer stator ring and an inner rotator ring. The stator ring holds rectangular magnetic slabs, all the same size. These slabs are uniformly mounted on the inner surface of the stator ring. Piezoelectric patches (PZT-4) are placed between the magnetic slabs and the stator ring. The rotator ring is connected to the ball screw mechanism. On the outer surface of the rotator, a set of magnetic slabs with the same size as the piezoelectric patches are placed along the circumferential direction. Therefore, when the rotator rotates, a (repelling) magnetic force is generated between stator and rotor. The magnetic force acts on the piezoelectric material along the polarization direction, harvesting electrical energy. The design is depicted in Figure 30.

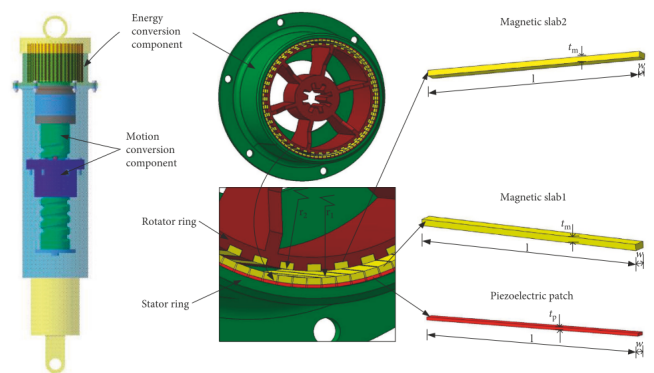


Fig. 30. Ring piezoelectric energy harvester. The energy conversion mechanism is composed of an outer stator ring and an inner rotator ring. The stator ring holds magnetic slabs and piezoelectric patches, the rotator ring holds magnetic slabs as well [36].

Shi et al. [37] proposed a piezoelectric electromagnetic vibration energy harvester to harvest the low-frequency vibrations from the human body. This system is based on a frequency-up conversion technique. The design is depicted

in Figure 31. There are four piezo-electromagnetic coupling cantilever beams installed along the circumferential direction of a shaft. Elements of macrofibercomposite (MFC), which is a piezoelectric actuator and sensor, are bonded on the surface of the cantilever beams to harvest electrical energy. Each cantilever beam contains a magnet on the free end, which functions as a mass block. In addition, four coils are placed under the magnets to harvest electromagnetic energy as well. A rotating mass block is added and functions as a pendulum to apply inertial motion. When the system is excited, energy is harvested through the piezoelectric elements and the electromagnetic elements. The working principle is shown in Figure 31 as well.

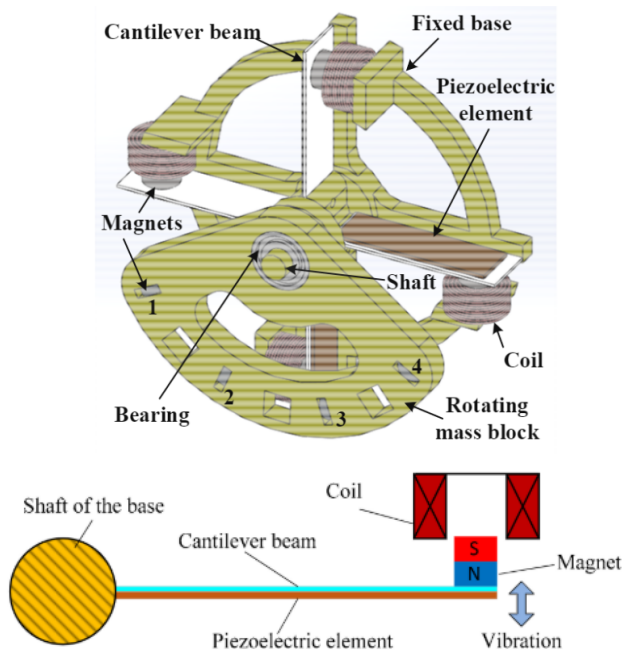


Fig. 31. Design of multi-directional piezo-electromagnetic vibration harvester (top) and working (bottom). The multidirectional characteristic comes from four cantilever beams being placed in the circumferential direction [37].

Shukla et al. [38] conducted a study on harvesting vibration energy from human body induced vibrations as well. In particular from the human waistline. A concept is derived where translational and oscillatory components of the walking motion are coupled to a pendulum mounted at the waist. Energy is harvested through striking and bending piezoelectric unimorphs (PVDF). These piezoelectric unimorphs are mounted on a stator. The piezoelectric elements are bent and released by stainless steel strikers, mounted on the rotor. Inertial masses are added and their position can be adjusted with slots. The rotor is mounted on a shaft. This system is called the PENDEXE (pendulum excited piezoelectric energy harvester) and is depicted in Figure 32.

Halim et al. [39] proposed a system to harvest human induced vibrations with the use of impact-driven flexible side walls. This system consists of a hollow cylindrical channel that contains a freely movable ball. At the ends of the channel, two rectangular flexible side walls are clamped. Each of

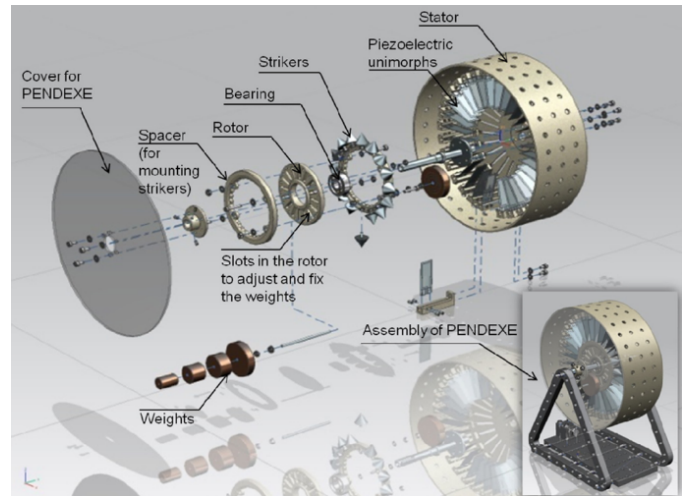


Fig. 32. Design of the pendulum excited piezoelectric harvester (PENDEXE). Energy is harvested through striking and bending piezoelectric unimorphs (PVDF) [38].

these flexible side walls contains a unimorph piezoelectric beam (PZT-5H4E), with a mass loaded at the free end of the unimorph. Therefore, each flexible side beam functions as the base of a unimorph piezoelectric beam. When excited, the freely movable metal ball vibrates through the channel and hits the flexible side walls. The impact force is transferred to the loaded mass at the free end of the unimorph. The unimorph will vibrate and cause strain in the piezoelectric elements to generate voltage. A depiction of the system can be found in Figure 33.

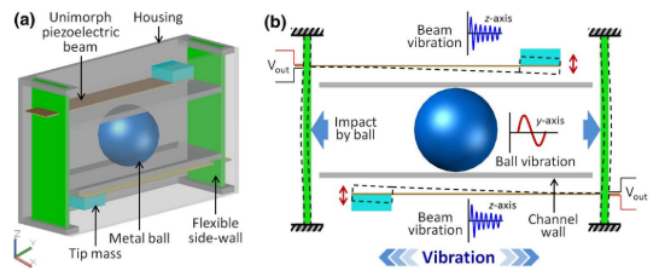


Fig. 33. Piezoelectric energy harvester using impact driven flexible side walls. (a) schematic and (b) working principle. At the instance of impact of the ball, vibrations are transferred to the unimorphs through the flexible side walls to harvest energy [39].

Zhang et al. [40] studied and analysed an arc-shaped piezoelectric energy harvester. As the name says, the main component of the system is an arc-shaped cantilever piezoelectric beam (PVDF) to harvest power. In addition, a load resistance, a tip magnet, and an external magnet are added to the system. The system is mounted on a structure that can be excited in the z direction, as depicted in Figure 34. The piezoelectric material covers the whole arc-shaped cantilevered beam to convert vibration energy into electric energy. The magnet's repulsive force creates a bistable structure. The amplitude of vibrations and therefore the harvested power increases.

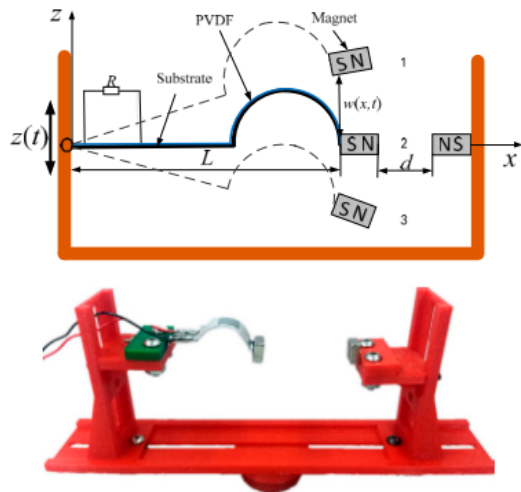


Fig. 34. Arc-shaped piezoelectric vibration energy harvester. Schematic (top) and prototype (bottom). The repulsive forces of the magnet creates a bistable structure [40].

Between these designs there are various piezoelectric materials used. These are listed in Table IV. Between different PZT materials, there is hard PZT and soft PZT. PZT stands for lead zirconate titanate. Hard PZT can withstand higher levels of electrical excitation and mechanical stress. Soft PZT features high sensitivity and permittivity. Soft PZT is however susceptible to self heating which can go beyond the maximum operating temperature [41]. PZT-4 is a series of hard PZT materials, PZT-5 is a series of soft PZT materials [42]. PZT in general has excellent piezoelectric properties. The disadvantage of PZT is its toxicity due to the presence of lead [41]. PVDF (Polyvinylidene fluoride) is a piezoelectric polymer, and offers some advantages over the PZT ceramics. They are more flexible (lower young's modulus) and can therefore be placed on curved surfaces, have low density, good stability, and are tough. The piezoelectric properties however are moderate [41]. Macro fiber composite (MFC) is a low profile actuator and sensor [43]. It consists of rectangular piezo ceramic rods sandwiched between layers of adhesive, electrodes, and polyimide film [43]. The electrodes are attached to the film in a pattern which transfers voltage. It offers high performance, flexibility and reliability.

TABLE IV
PIEZOELECTRIC MATERIAL

No.	Reference	Energy harvesting technology	Material
23	Zhang et al. [31]	Multidirectional harvester based on homopolar repulsion	PZT
24	Zhong et al. [32]	Seesaw-type vibration energy harvester	PZT
25	Wang et al. [33]	Bistable nonlinear vibration energy harvester	PVDF
26	Ma et al. [34]	Compliant based vibration harvester	PVDF
27	Zhou et al. [35]	Bio inspired bistable vibration harvester	PZT-5H
28	Zhao et al. [36]	Suspension based vibration harvester	PZT-4
29	Shi et al. [37]	Piezo-electromagnetic coupling based vibration harvester	MFC
30	Shukla et al. [38]	PENDEXE	PVDF
31	Halim et al. [39]	Impact driven flexible side walls based vibration harvester	PZT-5H4E
32	Zhang et al. [40]	Arc-shaped vibration harvester	PVDF

To conclude this section on piezoelectric vibration energy harvesting, Table V shows the energy harvesting capabilities of the proposed designs.

TABLE V
ENERGY HARVESTING CAPABILITIES - PIEZOELECTRIC

No.	Reference	Energy harvesting technology	Frequency (Hz)	Amplitude (mm)	Acceleration (m/s ²)	Power (mW)	Experiment	Comment
23	Zhang et al. [31]	Multidirectional harvester based on homopolar repulsion				1233	Swing held at 70 degrees and let to oscillate	Mass pendulum is 40g
24	Zhong et al. [32]	Seesaw-type vibration energy harvester	7.34	2		0.09	Simulation	
25	Wang et al. [33]	Bistable nonlinear vibration energy harvester	7	9		0.269	Vibration shaker, sine sweep excitation (4-12 Hz)	
26	Ma et al. [34]	Compliant based vibration harvester	5			0.0156	Vibration shaker, sine sweep excitation (0-20 Hz)	
27	Zhou et al. [35]	Bio inspired bistable vibration harvester	4		0.7 g	0.1431	Vibration shaker, sine sweep excitation (0-10 Hz)	
28	Zhao et al. [36]	Suspension based vibration harvester				332400	Simulation quarter car road, tested with different classes of road roughness	Roughness class D gives 332W peak power at 120 km/h
29	Shi et al. [37]	Piezo-electromagnetic coupling based vibration harvester	4.8		0.8 g	1.31	Multidirectional vibration and swing device, simulating the human arm	Energy harvesting through piezo-electromagnetic coupling
30	Shukla et al. [38]	PENDEXE	2	15	2.4	0.290	Linear voice coil actuator, sinusoidal oscillation	
31	Halim et al. [39]	Impact driven flexible side walls based vibration harvester	4.96		2 g	0.175	Hand shaking	
32	Zhang et al. [40]	Arc-shaped vibration harvester	14	2			Vibration shaker, sine sweep excitation (10-20 Hz)	External load resistance unknown to calculate power. Peak voltage 18 V

C. Hydraulic energy harvesting

As stated in [subsubsection I-B3](#), hydraulic energy harvesting is achieved with the use of hydraulic cylinders and accumulator(s). Shi et al. [44] proposed a hydraulic energy harvesting method that harvests energy from human walking induced backpack motion. The system contains 4 symmetrically deployed hydraulic cylinders, 2 springs, loads connected to a load plate, and an accumulator. These components are mounted to a backpack style frame. To enlarge the force generated in the vertical direction by the load, the hydraulic cylinders have an incline angle to the vertical. This schematic can be seen in [Figure 35](#). The energy harvesting system is carried on the back of the human body. The backpack style frame is made of high strength carbon fiber. When excited by walking, the backpack load oscillates up and down following the center of gravity of the human body. This kinetic energy is converted into hydraulic energy with the hydraulic cylinders, through the action of oil suction and discharge. Hydraulic oil flows through check valves, the solenoid valve, and flow meter into the accumulator for storage. The system is depicted in [Figure 35](#).

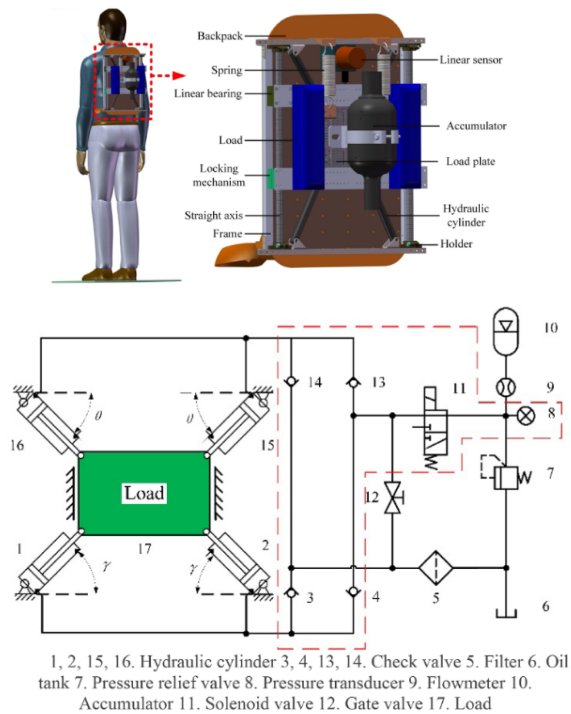


Fig. 35. Hydraulic system based energy harvesting backpack. Model (top) and schematic (bottom). Kinetic energy from the up and down oscillating backpack load is converted into hydraulic energy [44].

To conclude this section on hydraulic energy harvesting, [Table VI](#) shows the energy harvesting capabilities. After this, a final overview of all proposed designs is given in [Table VII](#).

TABLE VI
ENERGY HARVESTING CAPABILITIES - HYDRAULIC

No.	Reference	Energy harvesting technology	Frequency (Hz)	Amplitude (mm)	Acceleration (m/s ²)	Power (mW)	Experiment	Comment
33	Shi et al. [44]	Hydraulic vibration harvesting backpack		40		6200	Different backpack loads/walking speeds	Highest power output at 5.5 km/h and 15kg load

TABLE VII
ENERGY HARVESTING CAPABILITIES - OVERVIEW OF ALL PROPOSED DESIGNS

No.	Reference	Energy harvesting technology	Frequency (Hz)	Amplitude (mm)	Acceleration (m/s ²)	Power (mW)	Experiment	Comment
1	Wei et al. [8]	Electromagnetic actuator for vibration suppression	5.0	3.045		95.0	Sinusoidal excitation	
2	Mofidian et al. [10]	A dual-purpose vibration isolator energy harvester	12.5		1 g	0.115	Vibration shaker	
3	Halim et al. [11]	Human-limb driven electromagnetic energy harvester	5.17		2 g	2.15	Hand shaking	
4	Wang et al. [13]	Plane vibration-based electromagnetic energy harvester	4.5			0.270	Walking and jogging	
5	Chamanian et al. [14]	Wearable wireless sensor network with electromagnetic energy harvesting	2.65		0.15 g	0.127	Human waist motion	
6	Berdy et al. [15]	Magnetic levitation energy harvesting system	6.7		0.1 g	0.410	Vibration shaker	Power output limited by levitating magnet displacement limit
7	Abdelnaby et al. [16]	Energy harvesting using flextensional compliant mechanism	1.4	4		0.0120	Sinusoidal excitation	
8	Li et al. [17]	Rack and pinion based energy harvester	3	5		62900 - 104300	Sinusoidal excitation	
9	Ali et al. [5]	Barrel cam based energy harvester	2	7.5		3850	Sinusoidal excitation	
10	Pan et al. [18]	Ball Screw based railroad energy harvester	2	3		19900	Sinusoidal excitation	
11	Zhang et al. [19]	Vibration rectifier based energy harvesting system	1	2.5	18	86670	Sinusoidal excitation	
12	Maravandi et al. [20]	Two-leg motion based energy harvester	1	5		540	Sinusoidal excitation	
13	Salman et al. [21]	Helical gears based energy harvester	2.5	5		270000	Sinusoidal excitation	
14	Gonzalez et al. [22]	Synchronous pulley and belt based harvester	2	10		2500	Sinusoidal excitation	
15	Bowen et al. [23]	Cable transmission based energy harvester	1	15		1400	Sinusoidal excitation	
16	Li et al. [24]	Helical gears based energy harvester	2.5	7		4252	Sinusoidal excitation	
17	Fan et al. [25]	Flexible motion rectifier in energy harvesting backpack	3		3 g	700	Running on treadmill at 7 km/h and 1.9 kg load	Running at 7 km/h equals 3 Hz frequency
18	Liu et al. [26]	Rack and pinion based energy harvesting backpack	1.1	25		2100	Sinusoidal excitation	
19	Satpute et al. [27]	Energy regulating vibration harvester	3-15	2		120 - 520	Sinusoidal excitation	Given average. Peak power 4.13 W
20	Fang et al. [28]	Hydraulic-electromagnetic based energy harvester	10	3		200000	Sinusoidal excitation	
21	Zhang et al. [29]	Twin-tube hydraulic pumping regenerative damper	1.655	50		200000	High speed shaker	
22	Li et al. [30]	Hydraulic motion rectifier based energy harvester	2	8		248800	Sinusoidal excitation	
23	Zhang et al. [31]	Multidirectional harvester based on homopolar repulsion				1233	Swing held at 70 degrees and let to oscillate	Mass pendulum is 40g
24	Zhong et al. [32]	Seesaw-type vibration energy harvester	7.34	2		0.09	Simulation	
25	Wang et al. [33]	Bistable nonlinear vibration energy harvester	7	9		0.269	Vibration shaker, sine sweep excitation (4-12 Hz)	
26	Ma et al. [34]	Compliant based vibration harvester	5			0.0156	Vibration shaker, sine sweep excitation (0-20 Hz)	
27	Zhou et al. [35]	Bio inspired bistable vibration harvester	4		0.7 g	0.1431	Vibration shaker, sine sweep excitation (0-10 Hz)	
28	Zhao et al. [36]	Suspension based vibration harvester				332400	Simulation quarter car road, tested with different classes of road roughness	Roughness class D gives 332W at 120 km/h
29	Shi et al. [37]	Piezo-electromagnetic coupling based vibration harvester	4.8		0.8 g	1.31	Multidirectional vibration and swing device, simulating the human arm	Energy harvesting through piezo-electromagnetic coupling
30	Shukla et al. [38]	PENDEXE	2	15	2.4	0.290	Linear voice coil actuator, sinusoidal oscillation	
31	Halim et al. [39]	Impact driven flexible side walls based vibration harvester	4.96		2 g	0.175	Hand shaking	
32	Zhang et al. [40]	Arc-shaped vibration harvester	14	2			Vibration shaker, sine sweep excitation (10-20 Hz)	External load resistance unknown to calculate power. Peak voltage 18 V
33	Shi et al. [44]	Hydraulic vibration harvesting backpack		40		6200	Different backpack loads/walking speeds	Highest power output at 5.5 km/h and 15kg load

IV. DISCUSSION

This section will discuss interpretations and implications that can be made based on the results given in the preceding section. If a particular design is mentioned, it will be referred to according to the number given in the first column of Table VII.

A. Design advantages and limitations

Considering the structure of linear electromagnetic designs (1-8), it is easily integrated into most systems without the need of a transmission system. Therefore requiring less space. In addition, power is generated whilst some designs also pose as vibration dampers. When used as a suspension system in vehicles it will improve vehicle dynamics. It does however, have low conversion efficiency due to continuous change in direction (inertia).

Comparing with the rotary electromagnetic designs (8-22), energy harvesting systems with a transmission mechanism generally have a higher energy conversion than without. This is due to the fact that with transmission systems the kinetic energy transfer is more smooth. Considering the rack pinion based systems (8, 11, 18), ball screw system (10), barrel cam system (9), two-leg based system (12), and the helical gears systems (13, 16), these systems have low friction and backlash and therefore generally a higher conversion efficiency. This also means less power losses. To achieve this however, accurate system design is vital to reach the smoothest operation as possible. The cable or belt transmission systems (14, 15) however may experience slip when the torque is too high. This will reduce the generated power. That is why friction of the cable on the pulley must be taken into consideration to avoid slip.

Considering the hydraulic (transmission) based systems (20-22, 33), the potential power generation of these systems is high. Due to the change of volume these systems are very sensitive to small vibrations. In addition, these systems can transfer/absorb very large forces. It is however, not that efficient. Large amounts of power is lost during the hydraulic loop. In addition, there is a time delay in the opening and closing of the check valves in the rectifying circuit. This reduces the efficiency when the input frequency increases, leading to a reduction in energy recovery. Also, the pipelines require a lot more space than other energy harvesting systems would, are more complex to manufacture and have a risk of leaking during operation. If pipes or components leak oil, it might influence the pressure to reduce and introduce cavitation. This can create numerous pockets of oil bubbles throughout the oil [28], since the pressure is at an instance where the oil has the tendency to change into a gaseous state. Cavitation is the formation of bubbles within a liquid at low pressure. When the pressure increases again, the bubbles turn back into liquid. As this happens, shocks can occur as the bubbles 'pop', which causes noise and possible damage to the pipes.

Piezoelectric structures (23-32) have the advantage of simple architecture, flexible design, and easy fabrication. Therefore it is easier to produce task specific designs with this

material. Effective deformation however is relatively small, which limits the generated electricity (μW). Therefore, nearly all the presented piezoelectric designs (23-32) contain some sort of amplification mechanism to increase the effective strain or frequency.

B. Frequency and deformation amplification

There are some mechanisms that influence the input, to harvest more power. One way to influence the input is by amplifying the frequency. The idea of this; convert the low input frequency into a higher (resonant) frequency to harvest a larger amount of power. Since at a higher vibration frequency, more kinetic energy can be captured. Another method to influence the input is by deformation amplification; increase the amplitude of the input vibration to harvest a larger amount of power. These 2 methods both occur.

Energy harvesting mechanisms that use piezoelectric material generally use amplitude amplification techniques but some up-convert the frequency. These piezoelectric systems are systems 23-26, 29, 31 and 32. Amplitude amplification can be achieved in multiple ways. Adding a proof mass or exploiting magnetic repulsion are two methods used to spike up the amplitude. There is also a linear electromagnetic system that amplifies the vibrations using a compliant mechanism. This is system number 7.

Frequency up-conversion is achieved with a more novel way in system 3 and 31, which is based on mechanical impact. A moving metal ball impacts a beam and causes it to vibrate at higher frequency. Table VIII displays whether a system uses amplitude amplification or frequency up-conversion.

TABLE VIII
VIBRATION AMPLIFICATION

No.	Reference	Energy harvesting technology	Amplitude	Frequency
3	Halim et al. [11]	Human-limb driven electromagnetic energy harvester		x
7	Abdelnaby et al. [16]	Energy harvesting using flextensional compliant mechanism	x	
23	Zhang et al. [31]	Multidirectional harvester based on homopolar repulsion	x	
24	Zhong et al. [32]	Seesaw-type vibration harvester	x	
25	Wang et al. [33]	Bistable nonlinear vibration energy harvester	x	
26	Ma et al. [34]	Compliant based vibration harvester	x	
29	Shi et al. [37]	Piezo-electromagnetic coupling vibration harvester		x
31	Halim et al. [39]	Impact driven flexible side walls based vibration harvester		x
32	Zhang et al. [40]	Arc-shaped vibration harvester	x	

For the rotary electromagnetic systems, amplification of the input can occur in a later stage. Just before the motion is transmitted towards the generator. This is also where the linear motion has been converted to rotary motion. Therefore, when amplification of motion occurs, it is the rotation that experiences amplification. This is achieved through sets of gears that increase torque or speed. Most of the systems contain a planetary gearbox. These systems are listed in Table IX. Traditionally, a planetary gearbox functions to increase torque, but can also work to increase speed. Table IX also displays which systems increase torque and which systems increase rotational speed.

C. Power output

What can be seen in Table VII, is that there is a difference in power output between the presented designs within a category,

TABLE IX
ROTATION AMPLIFICATION

No.	Reference	Energy harvesting technology	Torque	Speed
8	Li et al. [17]	Rack and pinion based energy harvester	x	
11	Zhang et al. [19]	Vibration rectifier based energy harvesting system	x	
12	Maravandi et al. [20]	Two-leg motion based energy harvester	x	
13	Salman et al. [21]	Helical gears based energy harvester	x	
14	Gonzalez et al. [22]	Synchronous pulley and belt based energy harvester	x	
15	Bowen et al. [23]	Cable transmission based energy harvesting backpack		x
16	Li et al. [24]	Helical gears based energy harvester		x
18	Liu et al. [26]	Rack and pinion based energy harvesting backpack	x	
19	Satpute et al. [27]	Energy regulating vibration harvester	x	

and also between the different categories. The results given in this table are the peak power output results from the described experiments. Not all conducted studies provided a peak generated output power. If this was the case, the power output was calculated with the external resistance placed in the circuit. The output power can be calculated with the following formula: $P = V^2/R$. With the generated voltage (V) and external resistance (R).

D. Motion rectification

In section III some design descriptions discuss a form of motion rectification. Motion rectifiers convert the bidirectional vibrational motion into unidirectional motion (rotation). This can be achieved either mechanical or hydraulic. Unidirectional motion contains the systems that drive the electromagnetic generator unidirectional. This means that the transmission mechanism converts the bidirectional motion of vibrations into unidirectional motion. Bidirectional motion contains the systems that drive the electromagnetic generator bidirectionally. This means a transmission system does not convert the bidirectional motion of vibrations. By converting to unidirectional rotation, the reliability and efficiency of the energy harvester is enhanced as it reduces the impact force during transmission. Table X displays which systems from section III convert the bidirectional motion to unidirectional motion and distinguishes mechanical and hydraulic motion rectifiers.

TABLE X
MOTION RECTIFICATION

No.	Reference	Energy harvesting technology	Mechanical	Hydraulic
8	Li et al. [17]	Rack and pinion based energy harvester	x	
9	Ali et al. [5]	Barrel cam based energy harvester	x	
10	Pan et al. [18]	Ball Screw based railroad energy harvester	x	
11	Zhang et al. [19]	Vibration rectifier based energy harvesting system	x	
13	Salman et al. [21]	Helical gears based energy harvester	x	
16	Li et al. [24]	Helical gears based energy harvester	x	
17	Fan et al. [25]	Flexible motion rectifier in energy harvesting backpack	x	
18	Liu et al. [26]	Rack and pinion based energy harvesting backpack	x	
19	Satpute et al. [27]	Energy regulating vibration harvester	x	
20	Fang et al. [28]	Hydraulic-electromagnetic based energy harvester		x
21	Zhang et al. [29]	Twin-tube hydraulic pumping regenerative damper		x
22	Li et al. [30]	Hydraulic motion rectifier based energy harvester		x

E. Classification

With the knowledge gained from the results, one can categorize the harvesting systems even further. Or at least, provide more elaborate descriptions based on their working principles. From the study on the different energy harvesting systems, the main differentiation of the proposed designs is

based on the characteristic working principles. First it must be considered if either electromagnetic induction principle, piezoelectric material, or hydraulics are used. If the electromagnetic induction principle is utilised, classification depends on the characteristics of the transmission system if present. After which the following characteristics can be considered as well and all harvesters may be classified accordingly:

- Unidirectional or bidirectional motion
- Deformation amplification or frequency up-conversion

F. Piezoelectric material

When designing and analyzing piezoelectric vibration energy harvesters, a piezoelectric material is chosen. Multiple piezoelectric materials are utilised (as described in subsection III-B). These are listed in Table IV. There is a difference in characteristics between these materials and must therefore be taken into consideration since it will determine the dynamics of the system. It was expected that the harvesters containing PZT would perform better concerning the power output due to their excellent piezoelectric properties. The differences however are small. There is a trade off between piezoelectric power output and flexibility, which can be acted on. Two bistable vibration harvesters for instance (25 and 32), use the more flexible PVDF and are designed such that it has two stable equilibrium positions to enhance the power output. The power output can also be enhanced by introducing a larger number of piezoelectric unimorphs, as is done in the PENDEXE (30).

The cantilever based designs resonate at natural frequency. Resonance implies that the amplitude is increased, which therefore increases the power output. A downside to this is that the bandwidth is narrow. A shift from the resonant frequency (or natural frequency) will decrease the power output significantly. It also influences the design, since bigger size leads to lower resonant frequency. It is desired that energy harvesters are sensitive to low frequent vibrations in a broad spectrum. The characteristics of piezoelectric vibration harvesters make it harder to achieve this.

G. Limitations

As can be seen in Table VII, there is not one category for which the same experimental conditions apply to all designs. Mostly, sinusoidal excitation experiments are conducted to assess the power generation capabilities. It makes it however, more difficult to compare energy harvesting technology when experiments are not similar.

It is hard to achieve this, especially considering the piezoelectric designs. Most of the conducted experiments with piezoelectric materials experienced nonlinear behavior. That is why the capabilities are assessed on the power output, since each vibration harvester has its own dynamics and reacts differently to excitation.

Another limitation is found in the lack of information on power storage modules. Where some papers provide detailed descriptions on the charging circuit (including external resistances), some papers do not even mention a power storage device.

Lastly, to be able to draw a valid comparison in the harvested energy it is important that a fair comparison can be made. Initially the goal was to find the power density of every energy harvesting system and draw a comparison based on that. However, most papers did not describe the power density of a harvesting system. Another method would be to derive the power/mass ratio to compare the power output. Unfortunately most papers did not describe masses of the harvesting systems.

H. Recommendations

The studies analysed in this review discuss vibration energy harvesters and their energy harvesting capabilities in terms of power output. This only illustrates the performance for a short period of time. Future studies should contain durability tests to actually validate the working over longer periods of time and assess the reliability, durability and fatigue of the product.

Future work might also include research into developing a standard experimental model for vibration energy harvesting systems where they can make a valid and comparable assessment. Also, not all experiment descriptions provide the information to draw a valid comparison. The amplitude of the vibrations for instance is not described in every experiment. Therefore the acceleration is displayed instead to give some indication. In addition, to assess the conversion of kinetic energy to electrical energy, the efficiency must also be included to draw a valid comparison. A more elaborate table of the energy harvesting capabilities can be set up, which might also include a more in-depth classification based on [subsection IV-E](#).

V. CONCLUSION

The goal of this review was to present an overview of the most novel vibration energy harvesting systems from human and vehicular induced vibrations based on their energy harvesting mechanism. Using a systematic search method, a total number of 655 papers was narrowed down to 44 relevant papers. These documents discussed various energy harvesting mechanisms based on different principles. The analysis on different energy harvesting mechanisms shows the three main categories electromagnetic, piezoelectric and hydraulic energy harvesters. The electromagnetic harvesting systems can be further classified based on whether a transmission mechanism is used or not. The different energy harvesting systems found in literature are presented in accordance with these three categories. The results section contains the descriptions of these harvesting mechanisms and ends with an overview of the energy harvesting capabilities.

From the results it can be said that the rotary electromagnetic systems generally produce more power than linear electromagnetic and piezoelectric systems. The mechanisms containing hydraulics have the highest power output. However, high power output does not mean high efficiency. The dynamics of the harvesting mechanism determines the efficiency and power output of the system. This can be effected by for instance accurate system design, the use amplification mechanisms and motion rectification. Choosing a piezoelectric material also has its effects on the dynamics of piezoelectric vibration harvesters.

Also, the surrounding context of an application determines the harvesting mechanism. Energy harvesting shock absorbers (linear and rotary) pose as an energy regenerating alternative in automotive suspension systems, improving vehicle dynamics. Other described mechanisms show great potential in harvesting energy from human limb movement such as walking, running or hand shaking.

The goal to present an overview of the most novel vibration energy harvesting systems from human and vehicular induced vibrations is reached. Future studies should include a form of a durability test setup to assess the working of said mechanisms over longer periods of time. In addition, developing a standard experimental model in the future gives better insights and makes it easier to draw a valid comparison between vibration energy harvesters. This experimental model should contain clear experimental conditions and provide more elaborate results concerning the performance of the vibration harvesters.

ACKNOWLEDGEMENTS

I would like to thank my supervisor Gerwin Smit for his supervision and giving me the opportunity to pursue graduation in this research field. His guidance is much appreciated.

REFERENCES

- [1] A. Wickenheiser and E. Garcia, "Design of energy harvesting systems for harnessing vibrational motion from human and vehicular motion," George Washington Univ, Dept Mech & Aerosp Engr, Washington, DC 20052 USA, 2010.
- [2] M. A. A. Abdelkareem, L. Xu, M. K. A. Ali, A. Elagouz, J. Mi, S. J. Guo, Y. L. Liu, and L. Zuo, "Vibration energy harvesting in automotive suspension system: A detailed review," *Applied energy*, vol. 229, pp. 672–699, 2018.
- [3] H. Shi, Z. Y. Liu, and X. S. Mei, "Overview of Human Walking Induced Energy Harvesting Technologies and Its Possibility for Walking Robotics," *Energies*, no. 1.
- [4] M. A. Halim, H. Cho, M. Salauddin, and J. Y. Park, "A miniaturized electromagnetic vibration energy harvester using flux-guided magnet stacks for human-body-induced motion," *Sensors and actuators A-physical*, vol. 249, pp. 23–31, 2016.
- [5] A. Ali, L. F. Qi, T. S. Zhang, H. Li, A. Azam, and Z. T. Zhang, "Design of novel energy-harvesting regenerative shock absorber using barrel cam follower mechanism to power the auxiliaries of a driverless electric bus," *Sustainable energy technologies and assessments*, vol. 48, 2021.
- [6] K. T. Prajwal, K. Manickavasagam, and R. Suresh, "The european physical journal special topics A review on vibration energy harvesting technologies: analysis and technologies," *The European Physical Journal Special Topics*.
- [7] Z. Jin-Qiu, P. Zhi-Zhao, Z. Lei, and Z. Yu, "A review on energy-regenerative suspension systems for vehicles," *Lecture Notes in Engineering and Computer Science*, vol. 3 LNECS, pp. 1889–1892, 2013.
- [8] W. Wei, Q. Li, F. Xu, X. Zhang, J. Jin, J. Jin, and F. Sun, "Research on an electromagnetic actuator for vibration suppression and energy regeneration," *Actuators*, no. 2.
- [9] X. Y. Xiao, Y. N. Wang, X. He, Q. F. Li, and H. Li, "Design and Simulation Analysis of an Energy Regenerative Electromagnetic Shock Absorber for Vehicles," *Journal of applied science and engineering*, vol. 22, no. 4, pp. 625–636, 2019.
- [10] S. M. M. Mofidian and H. Bardaweel, "A dual-purpose vibration isolator energy harvester: Experiment and model," *Mechanical Systems and Signal Processing*, pp. 360–376.
- [11] M. A. Halim, J. Y. Park, and IEEE, "Optimization of a human-limb driven, frequency up-converting electromagnetic energy harvester for power enhancement," Kwangwoon Univ, Dept Elect Engr, Seoul 139701, South Korea PU - IEEE PI - New York PA - 345 E 47TH ST, New York, NY 10017 USA, pp. 1013–1016 WE – Conference Proceedings Citation In, 2015.
- [12] M. A. Halim, J. Y. Park, and IOP, "A miniaturized human-motion energy harvester using flux-guided magnet stacks," Kwangwoon Univ, Dept Elect Engr, 447-1 Wolgye Dong, Seoul 139701, South Korea, 2016.
- [13] S. Q. Wang and D. C. Li, "Design and analysis of a plane vibration-based electromagnetic generator using a magnetic spring and ferrofluid," *Journal of the korean physical society*, vol. 67, no. 5, pp. 818–822, 2015.
- [14] S. Chamanian, H. Ulsan, O. Zorlu, S. Baghaee, E. Uysal-Biyikoglu, and H. Kulah, "Wearable battery-less wireless sensor network with electromagnetic energy harvesting system," *Sensors and actuators A-physical*, vol. 249, pp. 77–84, 2016.
- [15] D. F. Berdy, D. J. Valentino, and D. Peroulis, "Kinetic energy harvesting from human walking and running using a magnetic levitation energy harvester," *Sensors and actuators A-physical*, vol. 222, pp. 262–271, 2015.
- [16] M. A. Abdelnaby and M. Arafa, "Energy harvesting using a flextensional compliant mechanism," *Journal of intelligent material systems and structures*, vol. 27, no. 19, pp. 2707–2718, 2016.
- [17] Z. Li, L. Zuo, J. Kuang, and G. Luhrs, "Energy-harvesting shock absorber with a mechanical motion rectifier," 2012.
- [18] Y. Pan, T. Lin, C. Liu, J. Yu, J. Y. Zuo, and L. Zuo, "A Compact Ball Screw Based Electromagnetic Energy Harvester for Railroad Application," Virginia Tech, Dept Mech Engr, Blacksburg, VA 24060 USA, 2018.
- [19] X. T. Zhang, H. Y. Pan, L. F. Qi, Z. T. Zhang, Y. P. Yuan, and Y. J. Liu, "A renewable energy harvesting system using a mechanical vibration rectifier (MVR) for railroads," *Applied energy*, vol. 204, no. 8th International Conference on Applied Energy (ICAE), pp. 1535–1543, 2017.
- [20] A. Maravandi and M. Moallem, "Regenerative Shock Absorber Using a Two-Leg Motion Conversion Mechanism," *IEEE-ASME transaction on mechatronics*, vol. 20, no. 6, pp. 2853–2861, 2015.
- [21] W. Salman, L. F. Qi, X. Zhu, H. Y. Pan, X. T. Zhang, S. Bano, Z. T. Zhang, and Y. P. Yuan, "A high-efficiency energy regenerative shock absorber using helical gears for powering low-wattage electrical device of electric vehicles," *ENERGY*, vol. 159, pp. 361–372, 2018.
- [22] A. Gonzalez, J. L. Olazagoitia, J. Vinolas, I. Ulacia, and M. Izquierdo, "An Innovative Energy Harvesting Shock Absorber System for Motor-bikes," *IEEE-ASME transaction on mechatronics*.
- [23] L. Bowen, J. Vinolas, J. L. Olazagoitia, and J. E. Otero, "An Innovative Energy Harvesting Shock Absorber System Using Cable Transmission," *IEEE-ASME transaction on mechatronics*, vol. 24, no. 2, pp. 689–699, 2019.
- [24] H. Li, P. Zheng, T. S. Zhang, Y. Q. Zou, Y. J. Pan, Z. T. Zhang, and A. Azam, "A high-efficiency energy regenerative shock absorber for powering auxiliary devices of new energy driverless buses," *Applied energy*, vol. 295, 2021.
- [25] K. Q. Fan, P. W. Xia, R. C. Li, J. Y. Guo, Q. X. Tan, and D. M. Wei, "An innovative energy harvesting backpack strategy through a flexible mechanical motion rectifier," *Energy conversion and management*, vol. 264, 2022.
- [26] M. Y. Liu, W. C. Tai, and L. Zuo, "Enhancing the performance of backpack energy harvester using nonlinear inerter-based two degrees of freedom design," *Smart materials and structures*, vol. 29, no. 2, 2020.
- [27] N. Satpute, L. Jugulkar, S. Jabade, G. Korwar, and S. Arawade, "Design and analysis of motion and energy regulating vibration harvester," *Proceedings of the institution of mechanical engineers part c-journal of mechanical engineering science*, vol. 236, no. 3, pp. 1391–1405, 2022.
- [28] Z. Fang, X. Guo, L. Xu, and H. Zhang, "Experimental Study of Damping and Energy Regeneration Characteristics of a Hydraulic Electromagnetic Shock Absorber," *Advances in Mechanical Engineering*.
- [29] Y. X. Zhang, H. Chen, K. H. Guo, X. J. Zhang, and S. E. Li, "Electro-hydraulic damper for energy harvesting suspension: Modeling, prototyping and experimental validation," *Applied energy*, vol. 199, pp. 1–12, 2017.
- [30] C. Li, R. Zhu, M. Liang, and S. Yang, "Integration of shock absorption and energy harvesting using a hydraulic rectifier," *Journal of Sound and Vibration*, no. 17, pp. 3904–3916.
- [31] T. Zhang, M. Tang, H. Li, J. Li, Y. Zou, Y. Pan, and Z. Zhang, "A Multidirectional Pendulum Kinetic Energy Harvester Based on Homopolar Repulsion for Low-Power Sensors in New Energy Driverless Buses," *International Journal of Precision Engineering and Manufacturing-Green Technology*, pp. 603–618.
- [32] X. Zhong, B. Wang, R. Li, Y. Wu, M. Ma, and H. Deng, "Energy conversion mechanisms of a seesaw-type energy harvester," *Journal of Physics D: Applied Physics J. Phys. D: Appl. Phys.*, p. 11.
- [33] Z. Wang, T. Li, Y. Du, Z. Yan, and T. Tan, "Nonlinear broadband piezoelectric vibration energy harvesting enhanced by inter-well modulation," *Energy Conversion and Management*, vol. 246, p. 114661, oct 2021.
- [34] X. K. Ma, A. Wilson, C. D. Rahn, and S. Trolrier-McKinstry, "Efficient Energy Harvesting Using Piezoelectric Compliant Mechanisms: Theory and Experiment," *Journal of vibration and acoustics-transactions of the asme*, vol. 138, no. 2, 2016.
- [35] J. X. Zhou, X. H. Zhao, K. Wang, Y. P. Chang, D. L. Xu, and G. L. Wen, "Bio-inspired bistable piezoelectric vibration energy harvester: Design and experimental investigation," *ENERGY*, vol. 228, 2021.
- [36] Z. Zhao, T. Wang, B. F. Zhang, and J. H. Shi, "Energy Harvesting from Vehicle Suspension System by Piezoelectric Harvester," *Mathematical problems in engineering*, vol. 2019, 2019.
- [37] G. Shi, J. F. Chen, Y. S. Peng, M. Shi, H. K. Xia, X. D. Wang, Y. D. Ye, and Y. H. Xia, "A Piezo-Electromagnetic Coupling Multi-Directional Vibration Energy Harvester Based on Frequency Up-Conversion Technique," *MICROMACHINES*, vol. 11, no. 1, 2020.
- [38] R. Shukla and A. J. Bell, "Pendexe: A novel energy harvesting concept for low frequency human waistline," *Sensors and actuators A-physical*, vol. 222, pp. 39–47, 2015.
- [39] M. A. Halim and J. Y. Park, "Piezoelectric energy harvester using impact-driven flexible side-walls for human-limb motion," *Microsystem technologies-micro-and-nanosystems-information storage and processing systems*, vol. 24, no. 5, pp. 2099–2107, 2018.

- [40] X. Zhang, W. Yang, M. Zuo, H. Tan, H. Fan, Q. Mao, and X. Wan, "An arc-shaped piezoelectric bistable vibration energy harvester: Modeling and experiments," *Sensors (Switzerland)*, vol. 18, no. 12, 2018.
- [41] H. Liang, G. Hao, and O. Z. Olszewski, "A review on vibration-based piezoelectric energy harvesting from the aspect of compliant mechanisms," *Sensors and Actuators A: Physical*, vol. 331, p. 112743, nov 2021.
- [42] P. Technology, C. Show, and A. Us, "Zibo Yuhai Electronic Ceramic Co., Ltd. Home > PZT Materials PZT Materials PZT-5 Series The PZT-5 series materials are all [soft]. They range in Curie temperatures from 165 ° C to 350 ° C . All these materi applications from hydrophones to ink jet pri," pp. 4–7.
- [43] S. Material, "Smart Material - Home of the MFC Benefits and Features : Flexible , durable and reliable Increased strain actuator efficiency Directional actuation and sensing Damage-tolerant Available as elongator (d33 mode) and contractor (d31 mode) Conforms to sur," pp. 2–5, 2022.
- [44] H. Shi, S. Luo, J. Xu, and X. S. Mei, "Hydraulic system based energy harvesting method from human walking induced backpack load motion," *Energy conversion and management*, vol. 229, 2021.